GEORGIA INSTITUTE OF TECHNOLOGY
OFFICE OF CONTRACT ADMINISTRATION

RESEARCH PROJECT INITIATION

Date: March 10, 1976

Project Title: Analysis of the Gas Core Actinide Transmutation Reactor (GCATR)

Project No: E-26-621

Principal Investigator: Dr. J. D. Clement/Dr. J. H. Rust

Sponsor: National Aeronautics and Space Administration

Agreement Period: From 3/1/76 Until 2/28/77

Type Agreement: Grant No. NSG 1288

Amount: $56,639 NASA
2,981 GIT (E-26-319)
$59,620 Total

Reports Required:
Final Technical Report

NOTE: Continuation of E-26-615

Sponsor Contact Person (s):

Administrative Matters
Thru OCA
Mr. Frank S. Kawalkiewicz
Grants Officer
National Aeronautics and
Space Administration
Langley Research Center
Hampton, Virginia 23665
(804) 827-3629

Technical Matters
Dr. Frank Hohl
Technical Officer
National Aeronautics and
Space Administration
Environmental & Space
Sciences Division
Langley Research Center
Hampton, Virginia 23665
(804) 827-2144

Assigned to: Nuclear Engineering

COPIES TO:

Principal Investigator	Library
School Director	Rich Electronic Computer Center
Dean of the College	Photographic Laboratory
Director, Research Administration	Project File
Director, Financial Affairs (2)	
Security-Reports-Property Office ✓	
Patent Coordinator	Other

RA-3 (9-75)

GEORGIA INSTITUTE OF TECHNOLOGY
OFFICE OF CONTRACT ADMINISTRATION

SPONSORED PROJECT TERMINATION

Date: May 23, 1979

Project Title: Analysis of the Gas Core Actinide Transmutation Reactor (GCATR)

Project No: E-26-621

Project Director: Dr. J. D. Clement

Sponsor: National Aeronautics and Space Administration; Langley Research Center

Effective Termination Date: 2/28/79

Clearance of Accounting Charges: 3/31/79

Grant/Contract Closeout Actions Remaining:

- _ Final Invoice and Closing Documents
- X Final Fiscal Report
- X Final Report of Inventions
- X Govt. Property Inventory & Related Certificate
- _ Classified Material Certificate
- _ Other _____

Assigned to: Nuclear Engineering (School/Laboratory)

COPIES TO:

Project Director
Division Chief (EES)
School/Laboratory Director
Dean/Director—EES
Accounting Office
Procurement Office
Security Coordinator (OCA)
Reports Coordinator (OCA)
Library, Technical Reports Section
Office of Computing Services
Director, Physical Plant
EES Information Office
Project File (OCA)
Project Code (GTRI)
Other _____

CA—4 (3/76)

SEMI-ANNUAL REPORT

NASA GRANT NSG-1288

ANALYSIS OF THE GAS CORE ACTINIDE TRANSMUTATION REACTOR (GCATR)

J. D. Clement and J. H. Rust

NASA Program Manager, F. Hohl

Prepared for the

National Aeronautics and Space Administration

by the

School of Nuclear Engineering
Georgia Institute of Technology
Atlanta, Georgia 30332

September 1, 1976

SEMI-ANNUAL REPORT

NASA GRANT NSG-1288

ANALYSIS OF THE GAS CORE ACTINIDE TRANSMUTATION REACTOR (GCATR)

J. D. Clement and J. H. Rust

NASA Program Manager, F. Hohl

Prepared for the

National Aeronautics and Space Administration

by the

School of Nuclear Engineering
Georgia Institute of Technology
Atlanta, Georgia 30332

September 1, 1976

ACKNOWLEDGMENTS

This work was supported by NASA Grant NSG-1288. The authors wish to express their appreciation to the program manager Dr. Frank Hohl for helpful suggestions during the performance of the research.

The following graduate students, supported by the grant, made significant contributions to the research project: Lyu Kim, Clyde Lightfoot, Frank Rives, Roy Waldo, and Pak Tai Wan.

In addition, the NASA research program was also used as a design project for the Nuclear Engineering design course in the academic curriculum. The following students were of great assistance in the research work:

Patrick Acree
Abderrahnane Belblidia
David Campbell
Benjamin Clark
Stephen Curtis
James Dullea
Robert Frost
Dan Griggs
William Horn
Douglas Moss
Richard Myers
Clyde Norman
John Osterholtz
Harry Patat
Wayne Reitz
Richard P. Saputa
Jeffrey A. Smith
John Snader
James Tahler
Patrick Wattson
Roy Ziering

TABLE OF CONTENTS

LIST OF TABLES

LIST ILLUSTRATIONS

ABSTRACT

The Georgia Institute of Technology, under the sponsorship of the National Aeronautics and Space Administration, has undertaken a research program entitled "Analysis of the Gas Core Actinide Transmutation Reactor, GCATR." The overall objective of the study is to investigate the feasibility, design, and optimization of the GCATR. This semi-annual report summarizes results from March 1, 1976 to August 31, 1976.

Update of Actinide Cross Sections and Sensitivity Analysis Using the ORIGEN Code

The ORIGEN computer program was implemented on Georgia Tech's Cyber 74 computer system. More recent and accurate values for the actinide cross sections were researched and used to update the ORIGEN cross section library. The latest cross sections were obtained from the Savannah River Laboratory and the Brookhaven National Library. In order to evaluate the effects of uncertainties in the nuclear data, the sensitivity of results based upon variation in the actinide cross sections were analyzed. The results are tabulated in the Report.

Calculations of the Actinide Burnup Potential in the GCATR

Before performing detailed calculations, the potential of the GCATR was explored by making comparative computations of the GCATR with LWR and LMFBR systems.

The comparisons, although based on simplifying assumptions, show that in some respects the GCATR system is superior to LWR and LMFBR transmutation systems. For example, the GCATR services 10 LWR's

in comparison to three for the LMFBR and one for the LWR. Over a 40 year span, the GCATR system provides 520,000 MWe-years in comparison to 192,000 MWe-years for the LMFBR and 40,000 MWe-years for the LWR. The GCATR system burns up 10.239 metric tons of actinides in 40 years as compared to 2.930 for the LMFBR and 0.423 for the LWR. The hazard reduction factor of the GCATR system is 5.85 in comparison to 5.25 for LMFBR and 4.11 for LWR transmutation systems.

Heat Transfer Analysis of Actinide Fuel Rods

A thermal-hydraulic analysis was made of actinide fuel rods in the form of oxides encapulated with a metal cladding. Reasonable design constraints, which limit the actinide rod thermal output, are 590 watts/cm for the linear heat rate and 662°C for the maximum cladding temperature. For the water coolant there will be a constraint on heat flux given by the DNB heat flux. The DNB ratio was not allowed to fall below 1.3.

Heat transfer calculations were made for three possible coolants--sodium, water, and helium. The burnup in the actinide fuel rods was limited to 150,000 MWD/t. These considerations led to maximum fast neutron fluxes in the actinide fuel rods of 4×10^{16} n/cm^2-sec for sodium and 10^{16} n/cm^2-sec for helium. Rod diameters, pitch-to-diameter ratios, and maximum and average volumetric heat generation rates were calculated and tabulated for the three coolants.

GCATR Reactor Design

General criteria for ATR reactor design and particular criteria for the GCATR are formulated and discussed. Calculations were made using

the MACH-I program for a three-region reactor containing core, actinide, and reflector regions. The core region contained the $^{233}UF_6$ gaseous fuel.

The initial objective of the reactor design analysis was to evaluate characteristics of several modifications of the reactor described and establish the optimal type. MACH-I calculations were performed for a spherical geometry. H_2O and D_2O were each used as the coolant and moderator. By applying a power limit of 2500 MWth to the reactor it was possible to calculate the maximum flux in the actinides. It was clear from these calculations that D_2O was far superior to H_2O in the reactor. Not enough calculations have been performed to determine whether the actinides should be placed in the center or on the outside of the core. A higher flux is obtainable in the center, but more actinides may be placed on the outside. The amount of moderation provided had a significant effect on the results as well. Since the only limit imposed on the flux was on the total number of fissions in the reactor per second, a more thermalized reactor would have a lower flux due to the larger thermal neutron cross fission section for the fuel. However, for a given neutron spectrum the smaller the critical mass the larger the neutron flux.

A major advantage of the GCATR was demonstrated in these calculations, since fluxes several orders of magnitude above those in conventional reactors were achieved. If the flux is to be high and still have a limited power output the critical mass should be as small as possible. However, if the maximum amount of actinides are to be exposed to a high flux the core should have a large size. This dictates as low a fuel density as possible. Hence, a GCATR is much better suited to this problem than a solid fuel reactor.

Further calculations indicated that a thicker graphite reflector was helpful and that replacing D_2O with graphite had a negligible effect. It was thus concluded that if D_2O were to be used as the coolant for this reactor, its use should be limited to cooling requirements and graphite used exclusively for the reflector.

Further calculations indicated that a soldium coolant would allow a much higher neutron flux than the D_2O coolant from a heat transfer point of view. In addition, a very fast reactor may indeed be preferable to a more thermal one because of the increased fission to capture ratio in the actinides. Future calculations will investigate these possibilities

Overall System Design

The GCATR is designed to transmute by fission the transuranium actinides from ten LWR's. This burnup capability exceeds that of either the LWR or LMFBR. Preliminary drawings are presented. The core is a right circular cylinder with approximate dimensions of a two-meter height and a one-meter diameter. Actinide fuel rods are arranged along the length of the core outside the liner. The fuel assemblies will require a coolant, such as sodium, helium, or high pressure water. The actinide fuel rod coolant will be at a pressure comparable to that of UF_6 so as to reduce the required thickness of the core liner wall. The reactor will need to be enclosed by a thick-walled pressure vessel which could be made of carbon steel with a stainless steel liner.

Because of its high burnup requirements, the GCATR will generate a considerable amount of thermal power which must be converted into electricity in order to economically justify the concept.

Because it was considered undesirable for UF_6 to have the possibility of interacting with water due to failure of a boiler tube, the UF_6 exchanges heat with a molten salt ($NaBF_4$) in an intermediate heat exchanger. $NaBF_4$ was developed as an intermediate coolant for the molten salt breeder reactor and would be inert with UF_6. Another desirable feature of $NaBF_4$ is that the boron present in the salt would eliminate criticality problems with UF_6 in the heat exchanger.

Preliminary calculations with the MACH-I diffusion code indicates that the power generated in the actinide fuel rods ranges from 20-36 percent of the plant output.

Multiple intermediate heat exchangers are employed on the plant so as to keep these heat exchangers compact and also improve upon the reliability and safety by redundancy of equipment. The heat load of these heat exchangers will be of the order of 500 Mw.

The $NaBF_4$ enters the intermediate heat exchanger at 400°C and exits at 510°C. It then enters a boiler where it exchanges heat to produce superheated steam at 100 bar pressure and 480°C. The steam is expanded through high and low pressure turbines to a pressure of 0.07 bar. Steam is extracted at optimal temperatures from three locations in the turbines for use in feedwater heaters. The overall efficiency of the plant is 36 percent.

I. INTRODUCTION

This semi-annual report summarizes results of work performed from March 1, 1976 to August 31, 1976, under NASA Research Grant NSG-1288 entitled "Analysis of the Gas Core Actinide Transmutation Reactor (GCATR)." Complete descriptions and details will be found in the Final Report.

The major tasks in the first six months were in the following areas:

1. Update of Actinide Cross Sections and Sensitivity Analysis Using the Origen Code
2. Calculations of the Actinide Burnup Potential in the GCATR
3. Heat Transfer Analysis of Actinide Fuel Rods
4. GCATR Reactor Design
5. Overall System Design.

These topics will be summarized in Chapters III through VII, respectively.

II. BACKGROUND

The technical background was reviewed in a paper included as Appendix A. The paper, by Clement, Rust, Schneider and Hohl, was presented at the Third Symposium on Uranium Plasmas at the Princeton University Conference, June 10-12, 1976.

III UPDATE OF ACTINIDE CROSS SECTIONS AND SENSITIVITY ANALYSIS USING THE ORIGEN CODE

Introduction

The value of any calculation depends upon the validity of the data on which it is based and the accuracy of the calculational scheme. In order to be confident of the results of GCATR calculations, a search was made for the most recent and accurate cross section data; then a sensitivity analysis of the ORIGEN results was performed with respect to the possible errors in the cross sections, so that the effect of inaccuracies in the cross section data could be determined.

Implementation of the ORIGEN Code

An integral part of the proposed program was the implementation of the isotope generation and depletion code ORIGEN.[1] The ORIGEN computer code is a collection of programs that: (1) constructs a set of linear, first-order, ordinary differential equations describing the rates of formation and destruction of the nuclides contained in the library; (2) solves the resulting set of equations for a given set of initial conditions and irradiation histories to obtain the isotopic compositions of discharged fuel components as a function of post irradiation time; and (3) uses the isotopic compositions and nuclear properties of individual nuclides to construct tables describing the radioactivities, thermal powers, potential inhalation and ingestion hazards and photon and neutron production rates in the discharged fuels. ORIGEN utilizes a vast library containing information on 813 isotopes whose cross sections were found in various references. This library contained nuclear data pertaining to four different

reactor types — HTGR, LWR, LMFBR, and MSBR. The nuclear data was varied according to the shape of a typical neutron spectrum for each reactor type.

In order to make ORIGEN more directly applicable to the GCATR and contain cross sections equivalent with the most current known today, ORIGEN was modified to allow for easy manipulation of all isotopes from Tl-207 through ES-253. These isotopes were chosen because most discrepancies with cross section values were found among this particular group of cross sections as pointed out by Raman. This option described allows the replacement of particular cross sections by updated values as they became available from the National Laboratories as well as the inclusion of actual spectrum-averaged effective cross sections describing the GCATR into the ORIGEN library. The cross section sensitivity study was greatly facilitated by the cross section manipulation option.

Status of Cross Section Data

A search was made for new cross sections because the ones in the ORIGEN[1] library were outdated. Three papers containing compilations [2][3][4] were investigated. Each listed thermal cross sections and resonance integrals for neutron capture and neutron induced fission. These are listed in Tables III-1 through III-4. Also, a computer tape was obtained from Brookhaven National Laboratory of the Evaluated Nuclear Data File.[5]

The ORIGEN library contains integral cross sections for every actinide isotope in the thermal, resonance, and fast energy ranges for use in LWR calculations. For LMFBR problems, it gives only a complete spectrum-averaged cross section for each type of reaction. Many of these cross

TABLE III-1

THERMAL NEUTRON CAPTURE CROSS SECTIONS

(all units are barns)

ISOTOPE	HALF-LIFE	BNL-325 (4)	ORIGEN (1)	BENJAMIN ETAL (2)	BENJAMIN (1975) (3)
Th 228	1.913 yr	123±15	120		
Th 229	7340 yr	54±6	0		
Th 230	7.7×10^4 yr	23.2±0.6	23		
Th 231	25.5 hr		0		
Th 232	1.41×10^{10} yr	7.40±0.08	7.4		
Th 233	22.2 min	1500±100	1500		
Th 234	24.1 d	1.8±0.5	0		
Pa 231	3.25×10^4 yr	210±20	200		210
Pa 232	1.32 d	760±100	0		
Pa 233	27.0 d	41±6	43		41
Pa 234m	1.17 min		0		
Pa 234g	6.67 hr		0		
U 232	72 yr	73.1±1.5	78		73.1
U 233	1.55×10^5 yr	47.7±2.0	49		
U 234	2.47×10^5 yr	100.2±1.5	95		100.2
U 235	7.13×10^8 yr	98.6±1.5	98		
U 236	2.34×10^7 yr	5.2±0.3	6		5.2
U 237	6.75 d	411±138	0		378
U 238	4.51×10^9 yr	2.70±0.02	2.73		
U 239	23.5 min	22±5	0		
U 240	14.1 hr		0		

TABLE III-1 (con't)

ISOTOPE	HALF-LIFE	BNL-325	ORIGEN	BENJAMIN ETAL	BENJAMIN (1975)
Np 234	4.40 d				
Np 235	396 d	1784±204			
Np 236	1.29×10^{8} yr		0		
Np 237	2.14×10^{6} yr	162±3	170		169
Np 238	2.12 d		0		
Np 239	2.35 d	45±20	60		
Np 240	7.3 min		0		
Np 240g			0		
Pu 236	2.85 yr		0		
Pu 237	45.6 d				
Pu 238	87.8 yr	547±20	500		559
Pu 239	2.44×10^{4} yr	268±3	632		
Pu 240	6540 yr	289.5±1.4	366		289.5
Pu 241	15 yr	368±10	550		362
Pu 242	3.87×10^{5} yr	18.5±0.4	18.5	18.7	18.5
Pu 243	4.96 hr	60±30	0	87.4	87.4
Pu 244	8.3×10^{7} yr	1.7±0.1	1.6		1.7
Pu 245	10.5 hr	150±30	277		
Am 241	433 yr	832±20	925		831.8
Am 242m	152 yr	1400±860	2000		
Am 242g	16 hr		0	0	
Am 243	7.37×10^{3} yr	79.3±2.0	105	75.5	77
Am 244m	26 min				
Am 244g	10.1 hr		0		
Cm 242	163 d	16.5	30		20

TABLE III-1 (con't)

ISOTOPE	HALF-LIFE	BNL-325	ORIGEN	BENJAMIN ETAL	BENJAMIN (1975)
Cm 243	28 yr	225±100	200		
Cm 244	17.9 yr	13.9±1.0	10	9.95	10.6
Cm 245	8.5×10^3 yr	345±20	343	371	383
Cm 246	4.76×10^3 yr	1.3±0.3	1.25	1.4	1.44
Cm 247	1.54×10^7 yr	60±30	60	58	58
Cm 248	3.5×10^5 yr	4±1	3.56	2.89	2.89
Cm 249	64 min	1.6±0.8	2.8		
Cm 250	1.7×10^4 yr		2.0		
Bk 249	311 d		1450	1600	1600
Bk 250	3.22 hr		350		
Cf 249	350.6 yr	465±25	450	480	481.4
Cf 250	13.1 yr	2030±200	1900	1701	1701
Cf 251	900 yr	2850±150	2850	2849	2849
Cf 252	2.63 yr	20.4±1.5	19.8	20.4	20.4
Cf 253	17.8 d	17.6±1.8	12.6	12.0	12.0
Cf 254	60.5 d		50		
Es 253	20.47 d	155±20	345	155	155
Es 254m	39.3 hr	1.3			
Es 254g	276 d	<40			

TABLE III-2

NEUTRON CAPTURE RESONANCE INTEGRALS

ISOTOPE	BNL-325 (4)	ORIGEN (1)	BENJAMIN ETAL (2)	BENJAMIN (1975) (3)
Th 228	1013	0		
Th 229	1000±175	0		
Th 230	1010±30	1000		
Th 231		0		
Th 232	85±3	83		
Th 233	400±100	386		
Th 234		0		
Pa 231	1500±100	480		1500
Pa 232		0		
Pa 233	895±30	920		895
Pa 234m		0		
Pa 234g		0		
U 232	280±15	280		280
U 233	140±6	147		
U 234	630±70	665		630
U 235	144±6	130		
U 236	365±20	210		365
U 237	290	0		1200
U 238	275±5	19.9		
U 239		10		
U 240		0		
Np 234		0		
Np 235		0		
Np 236		0		

TABLE III-2 (con't)

ISOTOPE	BNL-325	ORIGEN	BENJAMIN ETAL	BENJAMIN (1975)
Np 237	660±50	756		660
Np 238		0		
Np 239		415		
Np 240m		0		
Np 240g		0		
Pu 236		0		
Pu 237		0		
Pu 238	141±15	150		164
Pu 239	200±20	130		
Pu 240	8013±960	2000		8013
Pu 241	162±8	139		162
Pu 242	1130±30	1280	1280	1275
Pu 243		0	264	264.0
Pu 244	43±4	0		42.5
Pu 245	220±40	0		
Am 241	1477±140	2150		1538
Am 242m	7000±2000	0		
Am 242g		0		
Am 243	1820±70	1500	2159	1927
Am 244m		0		
Am 244g		0		
Cm 242	150±40	0		150
Cm 243	2345±470	500		
Cm 244	650±50	650	585	585
Cm 245	101±8	120	104	104

TABLE III-2 (con't)

ISOTOPE	BNL-325	ORIGEN	BENJAMIN ETAL	BENJAMIN (1975)
Cm 246	121±7	121	119	117.0
Cm 247	800±400	500	500	500
Cm 248	275±75	170	251	251
Cm 249		0		
Cm 250		0		
Bk 249		1240	4000	4000
Bk 250		0		
Cf 249	760±35	1.46	777	625
Cf 250		11,600	11,600	11,500
Cf 251	1600±300	1600	1600	1590
Cf 252	43.5±3.0	44	43.5	43.4
Cf 253		0	12.0	12.1
Cf 254		1650		
Es 253	7300±390	0	7300	7308
Es 254m		0		
Es 254g		0		

TABLE III-3

THERMAL FISSION CROSS SECTIONS

ISOTOPE	BNL-325 (4)	ORIGEN (1)	BENJAMIN ETAL (2)	BENJAMIN (1975) (3)
Th 228	<0.3	0		
Th 229	30.5±3.0	32		
Th 230	<0.0012	0		
Th 231		0		
Th 232	0.039±0.004mb			
Th 233	15±2	0		
Th 234	<0.01	0		
Pa 231	.010±.005	0		0.01
Pa 232	700±100	0		
Pa 233	<0.1	0		<1
Pa 234m	<500	0		
Pa 234g	<5000	0		
U 232	75.2±4.7	77		75.2
U 233	531.1±1.3	525		
U 234	<0.65	0		<0.65
U 235	682.2±1.3	520		
U 236		0		
U 237	<0.35	0		<0.35
U 238		0		
U 239	14±3	0		
U 240		0		

TABLE III-3 (con't)

ISOTOPE	BNL-325	ORIGEN	BENJAMIN ETAL	BENJAMIN (1975)
Np 234	900±300	0		
Np 235		0		
Np 236	2500±150	0		
Np 237	.019±.003	0.019		0.019
Np 238	2070±30	1600		2070
Np 239	1	0		
Np 240m		0		
Np 240g		0		
Pu 236	165±20	170		162
Pu 237	2400±300			2200
Pu 238	16.5±0.5	1715		17.3
Pu 239	742.5±3.0	1520		
Pu 240	.030±.045	0		0.030
Pu 241	1009±8	1480		1015
Pu 242	0.2	0.035	0	
Pu 243	196±16	0	180	180
Pu 244		0		
Pu 245		0		
Am 241	3.15±0.10	3.13	3.1	3.14
Am 242m	6600±300	6000	6000	7600
Am 242g	2900±1000	2900	2900	2100
Am 243	<0.07	0.45		
Am 244m	1600±300			
Am 244g	2300±300	2300		

TABLE III- 3(con't)

ISOTOPE	BNL-325	ORIGEN	BENJAMIN ETAL	BENJAMIN (1975)
Cm 242	<5	5		<5
Cm 243	600±50	600		690
Cm 244	1.2±0.1	1.20	1.5	1.1
Cm 245	2020±40	1727	2098	2161
Cm 246	0.17±0.10	0	0.17	0.17
Cm 247	90±10	120	72.3	72.3
Cm 248	0.34±0.07	0	0.11	0.34
Cm 249		50		
Cm 250		0		
Bk 249		0		
Bk 250	960±150	3000		
Cf 249	1660±50	1690		1665
Cf 250	<350	0		
Cf 251	4300±300	3750	4801	4801
Cf 252	32±4	32	32.0	32.0
Cf 253	1300±240	1300	1100	1100
Cf 254		0		
Es 253		0		
Es 254m	1840±80			1840
Es 254g	2900±110			2900

TABLE III-4

FISSION RESONANCE INTEGRALS

ISOTOPE	BNL-325 (4)	ORIGEN (1)	BENJAMIN ETAL (2)	BENJAMIN (1975) (3)
Th 228		0		
Th 229	464±70	0		
Th 230		0		
Th 231		0		
Th 232		0		
Th 233		0		
Th 234		0		
Pa 231		0		
Pa 232		0		
Pa 233		0		
Pa 234m		0		
Pa 234g		0		
U 232	320±40	320		320
U 233	764±13	746		
U 234		0		
U 235	275±5	240		
U 236		0		
U 237		0		
U 238		0		
U 239		0		
U 240		0		

TABLE III-4 (con't)

ISOTOPE	BNL-325	ORIGEN	BENJAMIN ETAL	BENJAMIN (1975)
Np 234		0		
Np 235		0		
Np 236		0		
Np 237		0		
Np 238	880±70	0		880
Np 239		0		
Np 240m		0		
Np 240g		0		
Pu 236		0		
Pu 237		0		
Pu 238	24±4	25		25
Pu 239	301±10	300		
Pu 240		0		
Pu 241	570±15	537		570
Pu 242	5	0.6	4.74	4.7
Pu 243		0	541	542
Pu 244		0		
Pu 245		0		
Am 241	21±2	0		21
Am 242m	1570±110	0		1570
Am 242g		0		<300
Am 243		1.5	3.4	3.34
Am 244m		0		
Am 244g		0		

TABLE III-4 (con't)

ISOTOPE	BNL-325	ORIGEN	BENJAMIN ETAL	BENJAMIN (1975)
Cm 242		0		
Cm 243	1860±400	1850		1860
Cm 244	12.5±2.5	12.5	17.1	17.9
Cm 245	750±150	1140	766	766
Cm 246	10±0.4	0	10	9.94
Cm 247	880±100	1060	761	766
Cm 248	13.2±0.8	0	14.7	14.7
Cm 249		0		
Cm 250		0		
Bk 249		0		
Bk 250		0		
Cf 249	2114±70	2920	1863	1610
Cf 250		0		
Cf 251	5900±1000	5400	5400	5380
Cf 252	110±30	110	110	111
Cf 253		0	2000	2000
Cf 254		0		
Es 253		0		
Es 254m		0		
Es 254g	2190±90	0		2200

sections have since become better known. Cross sections that had not been well known when the library was created had been entered as zeros. Much data has since been obtained so that these values can now be assigned.

One of the sources investigated was "A Consistent Set of Transplutonium Multigroup Cross Sections,"[2] by R. W. Benjamin, et al. It lists thermal cross sections and resonance integrals for neutron capture and fission for a number of isotopes. Benjamin also wrote "Status of Measured Neutron Cross Sections of Transactinium Isotopes for Thermal Reactors."[3] In it is listed cross sections for a large number of isotopes and a discussion of the current need for cross section measurement of those isotopes.

The most useful source was "Neutron Cross Sections."[4] This is a very complete compilation of cross section data for every isotope and includes maximum errors for each cross section. These errors were useful as input for the cross section sensitivity analysis because upper and lower limits for each cross section could be substituted for the values in ORIGEN. For these reasons, this source was chosen to update the ORIGEN library.

Differential cross section data was found in "DLC-2D/100G, 100 Group Neutron Cross Section Data Based on ENDF/B."[5] It was obtained from Brookhaven National Laboratory on computer tape and contains ENDF/B3 data with the addition of U-233 and fluorine. This 100 group set was generated from nuclear data in either point by point or parametric representation by the PSR-13/SUPERTOG[6] code. A data retrieval code, DLC2RP,[7] was used to obtain a group by group printout of this data and to prepare it for imput to a reactor physics code. This data was not used in the sensitivity analysis but has been prepared for input into ANISN,[8]

a one-dimensional discrete ordinates transport theory code, which will perform criticality calculations for the GCATR.

Later, Brookhaven National Laboratory will release the Second Volume of "Neutron Cross Sections."[9] This volume will contain graphs of cross sections versus energy for a wide energy range and should become useful as a source of fast cross section data.

Cross Section Update

The cross sections from BNL-325 (shown in Tables III-1 through III-4) were substituted for those in the ORIGEN library for every isotope heavier than, and including, Th-228. These cross sections were more recent and more complete than those in the ORIGEN library. They were also accompanied by the listings of the maximum possible errors in each cross section. These errors were employed in the sensitivity analysis as described in the next section.

Cross Section Sensitivity Analysis

1. Description of Analysis Procedure.

In order to determine the possible effects of uncertainties in the nuclear data, the sensitivity of ORIGEN results to variations in the actinide cross sections was analysed. The specific results analysed were the actinide concentrations in the transmuter core. The general procedure was as follows:

(1) The concentrations (in gram-atoms per metric ton of fresh fuel) of each actinide in the spent fuel of a normal PWR cycle were calculated.

(2) It was assumed that 99.5% of the uranium and plutonium is reprocessed out of the spent fuel at 150 days after discharge from the PWR.

(3) The resulting actinide concentrations were determined at 215 days after reprocessing (365 days after discharge from the PWR).

(4) The concentrations of actinides in a PWR transmuter discharge were calculated, assuming that the actinides from step three are placed in another PWR that is also loaded with one metric ton of fresh fuel. This was chosen as the base case.

(5) Step four was repeated, changing the cross sections for fission or capture of one isotope from the base case. This step was repeated for each isotope studied.

(6) The isotopic concentrations from each run were then compared to those of the base case to determine the difference due to the cross sections. The results are tabulated later in this report.

Steps one, two, and three were done by one ORIGEN calculation. In steps four and five, one ORIGEN run was needed for each case explored. A schematic of the run scheme is shown in Figure III-1.

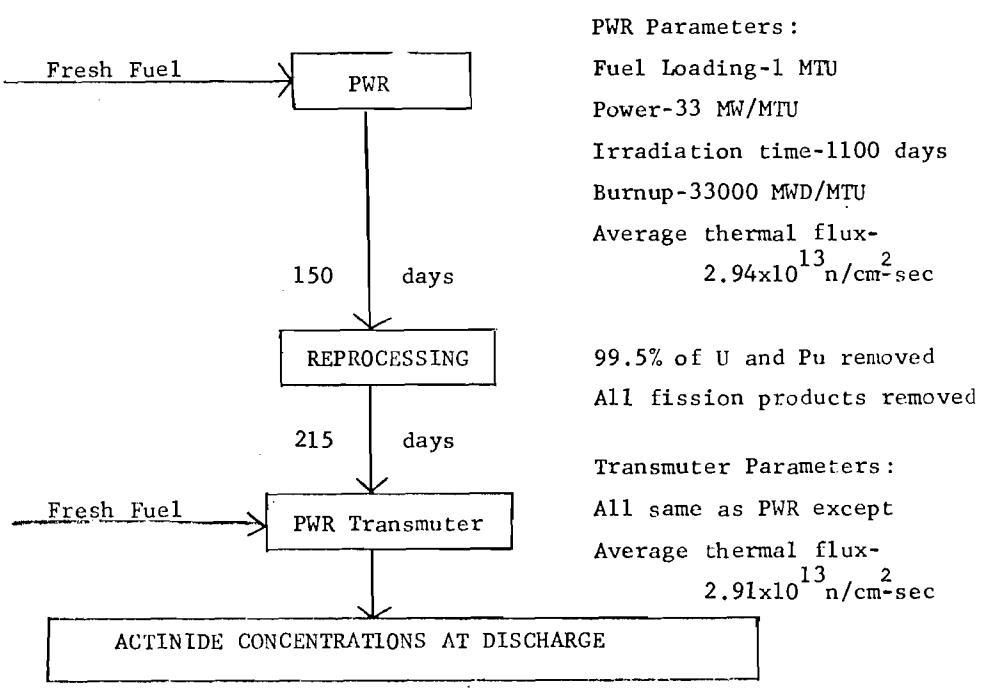

Figure III-1

Sensitivity Analysis Run Scheme With Reactor Parameters

The input parameters for the PWR and the PWR transmuter calculations were the same except that the transmuter had the actinides from the PWR in its core at beginning-of-life. The fresh fuel for each reactor consisted of 3.30% U-235, 96.67% U-238, and 0.027% U-234 for a total of one metric ton of uranium fuel.

Each reactor was run for 1100 days at 33 MW/MTU for a total burnup of 33,000 MWD/MTU. At 150 days after discharge from the PWR, ORIGEN calculated the removal of 100% of the fission products and 99.5% of the uranium and plutonium from the spent fuel. The actinide concentrations at 215 days after reprocessing (365 days after discharge from the PWR) were then calculated and input to the transmuter calculations. The actinide concentrations at discharge from the transmuter were calculated and recorded. These results formed the base case.

Subsequent ORIGEN calculations were duplicates of the base case except that the input cross sections for fission or capture for one isotope were changed to the upper limit values specified by BNL-325. It is important to note that all other parameters were held constant. Table III-5 is a list of the sensitivity runs performed.

2. Discussion of Sensitivity Analysis Results

The basis of comparison between cases was chosen to be the actinide concentrations of several important isotopes at discharge from the transmuter. Since three americium and three curium isotopes were studied by Boccola et al[10] in a somewhat similar study, these were focused upon. Neptunium-237 was also chosen because it is the actinide (excepting uranium and plutonium isotopes) which has the highest concentration at discharge and over a long decay period (10^7 years).

TABLE III-5

List of ORIGEN Sensitivity Runs

Run	Isotope	Reaction
1	BASE CASE	All average cross sections
2	Np-237	CAPTURE
3	Pu-241	"
4	Pu-242	"
5	Am-241	"
6	Am-242m	"
7	Am-243	"
8	Cm-242	"
9	Cm-243	"
10	Cm-244	"
11	Np-237	FISSION
12	Am-241	"
13	Am-242m	"
14	Am-243	"
15	Cm-242	"
16	Cm-243	"
17	Cm-244	"

TABLE III-6

ACTINIDE CONCENTRATIONS VS. SENSITIVITY ANALYSIS RUNS
AT DISCHARGE AFTER REMOVAL OF 99.5% of U and Pu
TRANSMUTATION

UNITS ARE GRAM-ATOMS PER MTU IN FRESH FUEL

Isotope / Base	NP 237	Am 241	AM242A	AM 243	CM 242	CM 243	CM 244	TOTAL(*)
BASE	4.53E+00	2.68E-01	1.18E-02	3.45E-01	2.85E-02	1.46E-03	3.14E-01	2.62E+01
1237(C)	4.41E+00	2.69E-01	1.18E-02	3.45E-01	2.85E-02	1.46E-03	3.14E-01	2.61E+01
1241(C)	4.53E+00	2.67E-01	1.17E-02	3.53E-01	2.84E-02	1.46E-03	3.17E-01	2.62E+01
1242(C)	4.53+00	2.67E-02	1.17E-02	3.53E-01	2.84E-02	1.46E-03	3.17E-01	2.62E+01
1241(C)	4.53E+00	2.62E-01	1.19E-02	3.45E-01	2.88E 02	1.48E-03	3.14E-01	2.62E+01
1242M(C)	4.53E+00	2.68E-01	1.18E-02	3.46E-01	2.84E-02	1.46E-03	3.14E-01	2.62E+01
1243(C)	4.53E+00	2.68E-01	1.18E-02	3.39E-01	2.85E-02	1.46E-03	3.18E-01	2.62E+01
1242(C)	4.53E+0	2.68E-01	1.18E-02	3.45E-01	2.82E-02	1.82E-03	3.15E-01	2.62E+01
1243(C)	4.53E+00	2.68E-01	1.18E-02	3.45E-01	2.85E-02	1.33E-03	3.14E-01	2.62E+01
1244(C)	4.53E+00	2.68E-01	1.18E-02	3.45E-01	2.85E-02	1.46E-03	3.07E-01	2.62E+01
1237(F)	4.53E+00	2.68E-01	1.18E-02	3.45E-01	2.85E-02	1.46E-03	3.14E-01	2.62E+01
1241(F)	4.53E+00	2.68E-01	1.18E-02	3.45E-01	2.84E-02	1.46E-03	3.14E-01	2.62E+01
1242M(F)	4.53E+00	2.68E-01	1.18E-02	3.45E-01	2.84E-02	1.46E-03	3.14E-01	2.62E+01
1243(F)	4.53E+00	2.68E-01	1.18E-02	3.45E-01	2.85E-02	1.46E-03	3.14E-01	2.62E+01
1242(F)	4.53E+00	2.68E-01	1.18E-02	3.45E-01	2.85E-02	1.46E-03	3.14E-01	2.62E+01
1243(F)	4.53E+00	2.68E-01	1.18E-02	3.45E-01	2.85E-02	1.36E-03	3.14E-01	2.62E+01
1244(F)	4.53E+00	2.68E-01	1.18E-02	3.45E-01	2.85E-02	1.46E-03	3.14E-01	2.62E+01

(*) TOTAL OF ALL ACTINIDES AND THEIR DAUGHTERS

TABLE III-7

ACTINIDE PRODUCTION SENSITIVITIES
RELATIVE TO CAPTURE CROSS SECTIONS

REFERENCE NUCLIDE	ADJUSTED NUCLIDE	CHANGE IN σ_c	CHANGE IN I_c	RESULTING CHANGE IN CONCENTRATION
Np-237	Np-237	+ 1.85%	+ 7.58%	- 2.65%
Am-241	Pu-241	+ 2.72%	+ 4.94%	- 0.37%
	Am-241	+ 2.40%	+ 9.46%	- 2.24%
Am-242m	Pu-241	+ 2.72%	+ 4.94%	- 0.85%
	Pu-242	+ 2.16%	+ 2.65%	- 0.85%
	Am-241	+ 2.40%	+ 9.46%	+ 0.85%
	Am-242m	+61.43%	+28.57%	0.00%
Am-243	Pu-241	+ 2.72%	+ 4.94%	+ 2.32%
	Pu-242	+ 2.16%	+ 2.65%	+ 2.32%
	Am-241	+ 2.40%	+ 9.46%	0.00%
	Am-242m	+61.43%	+28.57%	+ 0.29%
	Am-243	+ 2.52%	+ 3.85%	- 1.74%
Cm-242	Am-241	+ 2.40%	+ 9.46%	+ 1.05%
	Am-242m	+61.43%	+28.57%	- 0.35%
	Cm-242	+21.21%	+26.67%	- 1.05%
Cm-243	Am-241	+ 2.40%	+ 9.46%	+ 1.37%
	Am-242m	+61.43%	+28.57%	0.00%
	Am-243	+ 2.52%	+ 3.85%	0.00%
	Cm-242	+21.21%	+26.67%	+24.26%
	Cm-243	+44.44%	+20.00%	- 8.90%

ACTINIDE PRODUCTION SENSITIVITIES

RELATIVE TO CAPTURE CROSS SECTIONS (cont.)

REFERENCE NUCLIDE	ADJUSTED NUCLIDE	CHANGE IN σ_c	CHANGE IN I_c	RESULTING CHANGE IN CONCENTRATION
Cm-244	Am-242m	+61.43%	+28.57%	0.00%
	Am-243	+ 2.52%	+ 3.85%	+ 1.27
	Cm-242	+21.21%	+26.67%	+ 0.32%
	Cm-243	+44.44%	+20.00%	0.00%
	Cm-244	+ 7.19%	+ 7.69%	- 2.23%

TABLE III-8

ACTINIDE PRODUCTION SENSITIVITIES

RELATIVE TO FISSION CROSS SECTIONS

REFERENCE NUCLIDE	ADJUSTED NUCLIDE	CHANGE IN σ_f	CHANGE IN I_f	RESULTING CHANGE IN CONCENTRATION
Np-237	Np-237	+15.79%	0.00%	0.00%
Am-241	Am-241	+ 3.17%	+ 9.52%	0.00%
Am-242m	Am-241	+ 3.17%	+ 9.52%	0.00%
	Am-242m	+18.75%	+ 7.01%	0.00%
Am-243	Am-241	+ 3.17%	+ 9.52%	0.00%
	Am-242m	+18.75%	+ 7.01%	0.00%
	Am-243	0.00%	+126.67%	0.00%
Cm-242	Am-241	+ 3.17%	+ 9.52%	- 0.35%
	Am-242m	+18.75%	+ 7.01%	- 0.35%
	Cm-242	+20.00%	0.00%	0.00%
Cm-243	Am-242m	+18.75%	+ 7.01%	0.00%
	Am-243	0.00%	+126.67%	0.00%
	Cm-242	+20.00%	0.00%	0.00%
	Cm-243	+ 8.33%	+ 21.51%	- 6.85%
Cm-244	Am-242m	+18.75%	+ 7.01%	0.00%
	Am-243	0.00%	+126.67%	0.00%
	Cm-242	+20.00%	0.00%	0.00%
	Cm-243	+ 8.33%	+ 21.51%	0.00%
	Cm-244	+ 8.33%	+ 20.00%	0.00%

The discharge concentrations for each of these isotopes in every case studied are listed in Table III-6. Note that the total amount of actinides is the same for all but the case in which the capture cross sections of Np-237 were changed, and this change was only 0.38%. This indicates that the maximum possible error in the total actinide concentrations due to error in the cross sections of one isotope is very small.

The concentrations listed in Table III-6 were used to create Tables III-7 and III-8. These tables list the change in concentration of these isotopes due to changes in their cross sections or their precursors. In each table, the first column is the nuclide whose concentration is studied. The second column is the nuclide whose cross sections were altered. The next two columns show the percent change in the cross sections of the nuclide listed in column two. The final column lists the resulting change in concentration at discharge of the isotope in the first column.

Generally, an increase in either capture or fission cross sections caused a decrease in the concentration of the adjusted nuclide due to increased removal of that nuclide. The exact change in concentration is difficult to estimate directly because the creation rate of the nuclide is as important as the destruction rate. In fact, if the creation rate is much greater than the destruction rate, the effect of the cross section change is very small. This is the case for most actinides in the transmuter.

The factors affecting the creation rate are as follows:

(1) the amount of precursors present,

(2) cross sections of the precursors,

(3) the transmuter flux.

The factors affecting the destruction rate are:

(1) the amount of the reference nuclide present,

(2) cross sections of the reference nuclide present,

(3) the transmuter flux.

The flux is the same in both cases. Therefore, the ratio of the presursor to reference nuclide concentrations and cross sections gives an indication of the possible effect of varying the cross sections of the reference nuclide. For example, the greatest cross section adjustment was performed for capture by Am-242m. Despite a 61.43% and 28.57% capture increase in the thermal and resonance regions respectively, the total amount of Am-242m remained essentially unchanged (<0.005%). Referring to Table III-6 one sees that the Am-241 to Am-242m concentration ratio is about 20:1. The Am-241 to Am-242 cross section ratio is about 1:2, leaving an apparent production-destruction ratio of 10:1. The decay scheme must also be taken into effect, however. Figure III-2 is a schematic of the U-238 buildup chain. It shows that about 80% of the Am-242m destruction rate is due to fission. This reduces the effect of a change in the capture cross sections for Am-242m to a negligible amount.

At the other extreme, the concentration of Cm-243 was greatly sensitive to changes in the capture cross sections of Cm-242. This occurs because essentially all of the Cm-242 that is destroyed becomes Cm-243 (see Figure III-2).

These two cases are the extremes. All the other results can be explained by similar reasoning. From Tables III-7 and III-8, it is shown that with few exceptions, the actinide isotopic concentrations are changed by a small amount (<2.5%) and that the total actinide amount is never significantly altered by an error in the cross sections of one isotope.

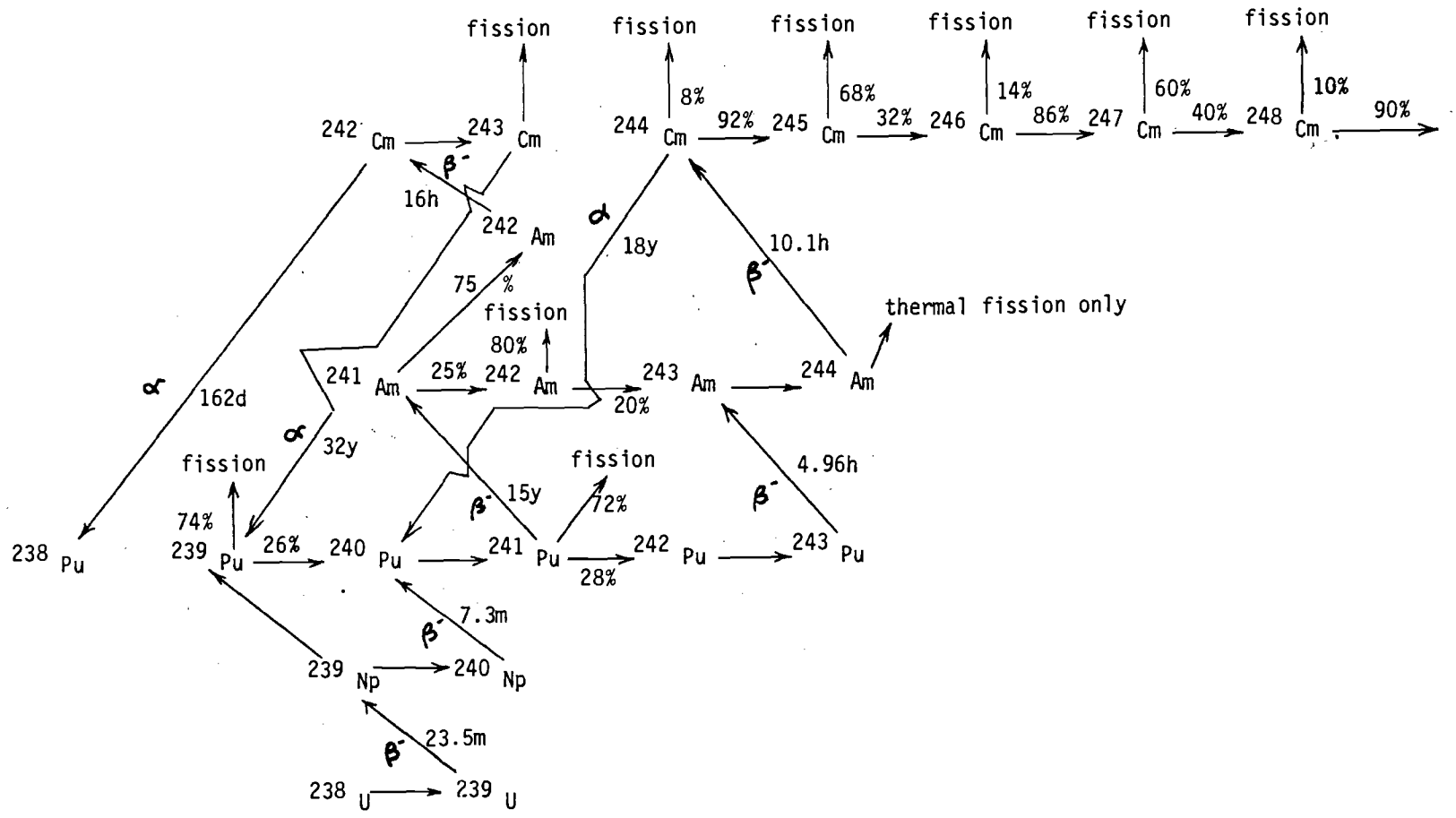

Fig. III-2 ^{238} Buildup Chain

TABLE III-9

ACTINIDE PRODUCTION SENSITIVITIES RELATIVE TO NUCLEAR DATA

Nuclide (Q)	Precursors and nucl. itself (i)	Nuclear datum (q_i)		
		$\sigma_{th}(n,\gamma)$	R.I. (n,γ)	$\lambda(\beta-)$
Am-241	Pu-240	14.35	40.67	
	Pu-241	-0.98	-0.64	96.65
	Am-241	-6.84	-8.24	
Am-242-m	Am-241	37.42	45.08	
	Am-242-m	-10.88	-	
Am-243	Pu-241	39.12	47.08	0.38
	Pu-242	2.36	84.75	
	Pu-243			0.11
	Am-241	0.37	0.44	
	Am-242-m	0.59	-	
	Am-243	-1.00	-7.47	
Cm-242	Am-241	29.31	83.03	
	Am-242			0.55
	Cm-242	-0.17	-	-36.66 (a
Cm-243	Am-242			18.51
	Cm-242	99.86	-	
	Cm-243	-1.12	-1.46	-0.50 (a
Cm-244	Pu-243			0.18
	Am-242-m	0.37	-	
	Am-242			-0.15
	Am-243	10.21	75.63	
	Cm-244	-0.01	-	

Comparison of Sensitivity Analysis Results to Those of Bocola[10]

Bocola, et al[10], performed a sensitivity analysis similar to that previously discussed. In this analysis, the sensitivity of the nuclide concentrations were determined relative to the thermal capture cross sections, capture resonance integrals and decay constants. The Bocola results are reproduced exactly from that paper and listed in Table III-9. Before making this comparison, the following basic differences between this analysis and the Georgia Tech analysis should be pointed out:

1. The Bocola analysis is applicable to a single cycle of LWR fuel whereas the Georgia Tech analysis was done for recycled actinides in a LWR transmutation reactor.
2. The Bocola analysis was done by a perturbation method, in which the cross section of the reference nuclide was perturbed 20%. The Georgia Tech analysis was accomplished by substituting the maximum possible value of the cross section in place of the original cross section. The maximum value was determined by BNL-325[4]. The method used in the Georgia Tech analysis is an exact method, whereas perturbation theory is an approximation that is only applicable for small perturbations. The use of realistic values for the change in cross sections lends more credibility to the Georgia Tech analysis.
3. The Bocola analysis did not include the sensitivities relative to fission cross sections. Therefore, the results may only be compared with respect to capture sensitivities.

4. Since the original concentrations of nuclides and cross section changes are so different for the two studies, the only useful comparison that can be made is whether each cross section change caused a positive or negative change in the nuclide concentration.

Comparing the format of Tables III-7 and III-9, the headings of Table III-9 could be listed from left to right as:

1. Reference Nuclide
2. Adjusted Nuclide
3. Sensitivity of reference nuclide concentration with respect to σ_γ, I_γ, and λ.

The sensitivities listed were obtained from the following formula:

$$S = \frac{\delta Q/Q}{\delta q/q} \tag{3.1}$$

where S = sensitivity

$\delta Q/Q$ = percent change in concentration

$\delta q/q$ = 20.

Comparing the tables it is seen that the signs of each sensitivity match the change in concentration calculation in the Georgia Tech analysis. In some cases, there was no change in the concentration of the reference nuclide in the Georgia Tech analysis, but this is due to the different conditions under which the analysis was run.

References for Chapter III

1. Bell, M. J., "ORIGEN--The ORNL Isotope Generation and Depletion Code," Oak Ridge National Laboratory, Oak Ridge, Tennessee, (May, 1973).

2. Benjamin, R. W., Vandervelde, U. D., Garrell, F. C., McBrosson, F. J., "A Consistent Set of Transpulutonium Multigroup Cross Sections," (1975).

3. Benjamin, R. W., "Status of Measured Neutron Cross Sections of Transactinium Isotopes for Thermal Reactors," Savannah River Laboratory, Aiken, South Carolina, (November 1975).

4. Mughabaghab, S. F., Garber, D. I., "Neutron Cross Sections, Third Edition, Volume One," Brookhaven National Laboratory, Upton, N. Y., (June, 1973).

5. Wright, R. Q., et al, "100G:100 Group Neutron Cross Section Data Based on ENDF/B," Radiation Shielding Information Center, Oak Ridge, Tennessee, (1972).

6. Wright, R. Q., Greene, N. M., Lucius, J. L., Craven, C. W., Jr., "SUPERTOG: A Program to Generate Fine Group Constants and P_n Scattering Matrices from ENDF/B," Oak Ridge National Laboratory, Oak Ridge, Tennessee, (1972).

7. Wright, R. Q., "User's Manual for DLC-2 Data Retrieval Program," informal notes, (July, 1972).

8. Engle, W. W., Jr., "A User's Manual for ANISN," Oak Ridge Gaseous Diffusion Plant, Oak Ridge, Tennessee, (March, 1967).

9. Garber, D. J. and Kinsey, R. R., "Neutron Cross Sections, Third Edition, Volume 2, Curves, Brookhaven National Laboratory, Upton, N. Y., (to be released in 1976).

10. Bocola, W., et al, "Considerations on Nuclear Transmutation for the Elimination of Actinides," C.M.E.N.-C.S.N. Casaccia, Rome, Italy, (1975).

IV. CALCULATIONS OF THE ACTINIDE BURNUP POTENTIAL IN THE GCATR

Before performing detailed calculations, it seemed desirable to explore the potential attractiveness of the GCATR concept making some simplifying approximations and assumptions.

Accordingly, calculations were made using the ORIGEN[1] code for the actinide mass balance in the GCATR. For these calculations, the following assumptions were made:

1. The GCATR services 10 LWR's. The actinide wastes from the LWR's are processed in a reprocessing facility, in which 99.9% of the uranium and plutonium and 100% of the fission products are removed. The reprocessed actinides are then placed in the GCATR core.
2. Reprocessing occurs 160 days after discharge from either the GCATR or LWR's.
3. The GCATR operates on a two-year cycle. Its own wastes are recycled through the reprocessing facility and back into the GCATR.
4. The GCATR uses 100% enriched U-233 fuel in the form of UF_6 gas.
5. The flux in the GCATR core is 1.36×10^{16} neutron per cm^2 per sec. The flux in the actinides in the GCATR is 7.78×10^{15} neutrons per cm^2 per second.

The mass of actinides in the GCATR is shown in Table IV-1 for the entire 40 year life of the reactor. The core region and actinide regions are kept separate, representing the separation of the GCATR core and actinides blanket. The "out" columns list the remaining balance after end of cycle. The difference in these figures is the mass of the fission products produced during the cycle. The "after reprocessing" columns

TABLE IV-1

GCATR ACTINIDE FLOW SCHEME

NOTE: (1) Units are metric tons of actinides (including U and Pu).

(2) In reprocessing, 99.9% of U and Pu are removed.

	CORE			ACTINIDES		
CYCLE	IN	OUT	AFTER REPROCESSING	IN	OUT	AFTER REPROCESSING
1	2.312	0.278	1.096×10^{-3}	1.293	1.108	0.382
2	2.312	0.278	1.096×10^{-3}	1.293	1.108	0.382
3	2.312	0.278	1.096×10^{-3}	1.576	1.404	0.603
4	2.312	0.278	1.096×10^{-3}	1.676	1.404	0.603
5	2.312	0.278	1.096×10^{-3}	1.898	1.574	0.732
6	2.312	0.278	1.096×10^{-3}	1.898	1.574	0.732
7	2.312	0.278	1.096×10^{-3}	2.026	1.672	0.086
8	2.312	0.278	1.096×10^{-3}	2.026	1.672	0.086
9	2.312	0.278	1.096×10^{-3}	2.099	1.729	0.849
10	2.312	0.278	1.096×10^{-3}	2.099	1.729	0.849
11	2.312	0.278	1.096×10^{-3}	2.142	1.762	0.874
12	2.312	0.278	1.096×10^{-3}	2.142	1.762	0.874
13	2.312	0.278	1.096×10^{-3}	2.167	1.781	0.889
14	2.312	0.278	1.096×10^{-3}	2.167	1.781	0.889
15	2.312	0.278	1.096×10^{-3}	2.182	1.793	0.898
16	2.312	0.278	1.096×10^{-3}	2.182	1.793	0.898
17	2.312	0.278	1.096×10^{-3}	2.191	1.800	0.903
18	2.312	0.278	1.096×10^{-3}	2.191	1.800	0.903
19	2.312	0.278	1.096×10^{-3}	2.196	1.804	0.906
20	2.312	0.278	1.096×10^{-3}	2.196	1.804	0.906

show the mass of actinides from that cycle that remain after 99.9% of the uranium and plutonium have been removed.

The results in Table IV-1 were determined by running the ORIGEN code, which calculates the buildup and depletion of each isotope given initial concentrations and reactor conditions. Equilibrium is not yet reached after 40 years with the proposed recycle scheme, due to the two year GCATR cycle. The equilibrium amount of actinides in the GCATR is 2.203 MTA at beginning of life and 1.809 MTA at end of cycle. This results in 0.910 MTA after reprocessing

Table IV-2 is a comparison of the reduction of actinide inventory by three proposed schemes. The first is the Claiborne scheme in which the wastes from one LWR are recycled back into the LWR itself. The second is the Beaman[2] scheme which uses an LMFBR to service three LWR's. The third is the Georgia Tech Gas Core GCATR to service ten LWR's. The corresponding actinide inventories in the GCATR scheme are higher because the system is much larger. The GCATR, however, burns far more actinides than the LMFBR and LWR systems. The important parameter for comparison is the hazard reduction factor, in which the GCATR is superior. This factor is the ratio of the amount produced to the amount remaining. It is the inverse of the percentage of remaining actinides for which the GCATR leaves 16.98%, the LMFBR leaves 19.05%, and the LWR leaves 24.33%.

The comparison, although based upon some simplified approximations, shows that the GCATR is attractive in comparison with the LMFBR and LWR. The GCATR services 10 LWR's for a total of 520,000 MWe years as compared to a total of 3LWR's and 192,000 MWe years for the LMFBR. The hazard

TABLE IV 2. COMPARISON OF ACTINIDE REDUCTION BY LMFBR, GCATR, AND LWR TRANSMUTATION OVER 40 YEAR LIFE. THE ACTINIDE AMOUNTS DO NOT INCLUDE U AND Pu.

	LWR (CLAIBORNE)[3]	LMFBR (BEAMAN)[2]	GCATR (GA. TECH)
SYSTEM	1 LWR	1 LMFBR AND 3 LWR'S	1 GCATR AND 10 LWR'S
POWER PRODUCTION	40,000 MWE YEARS	192,000 MWE YEARS	~520,000 MWE YEARS
ACTINIDE PRODUCTION	559 KGA	3620 KGA	12,352 KGA
AMOUNT REMAINING AT END-OF-LIFE	102 (IN LWR - NEAR EQUILIBRIUM) 34 (IN REPROCESSING) 136 KGA TOTAL	113 (NEWLY PRODUCED) 351 (EQUILIBRIUM IN LMFBR) 226 (INREPROCESSING) 690 KGA TOTAL	618 (NEWLY PRODUCED) 877 (IN GCATR - NEAR EQUILIBRIUM) 618 (IN REPROCESSING) 2113 KGA TOTAL
AMOUNT BURNED UP	423 KGA	2930 KGA	10,239 KGA
REDUCTION FACTOR	4.11	5.25	5.85

reduction factor of the GCATR System is 5.85, as compared to values of 5.25 and 4.11 for the LMFBR and LWR, respectively. The GCATR system burns up 10.239 metric tons of actinids in 40 years as compared to 2.930 and 0.423 for the LMFBR and GCTAR, respectively. These comparisons are graphically illustrated in Figures IV-1 through IV-3.

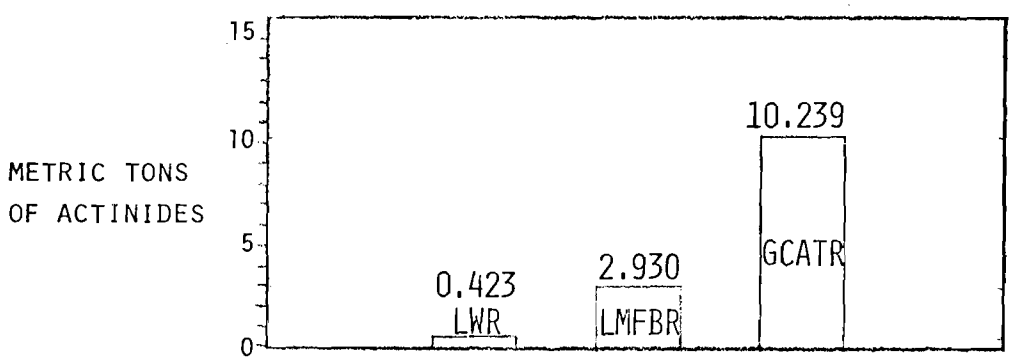

FIGURE IV-1. METRIC TONS OF ACTINIDES BURNED UP IN 40 YEARS BY LWR, LMFBR AND GA. TECH GCATR.

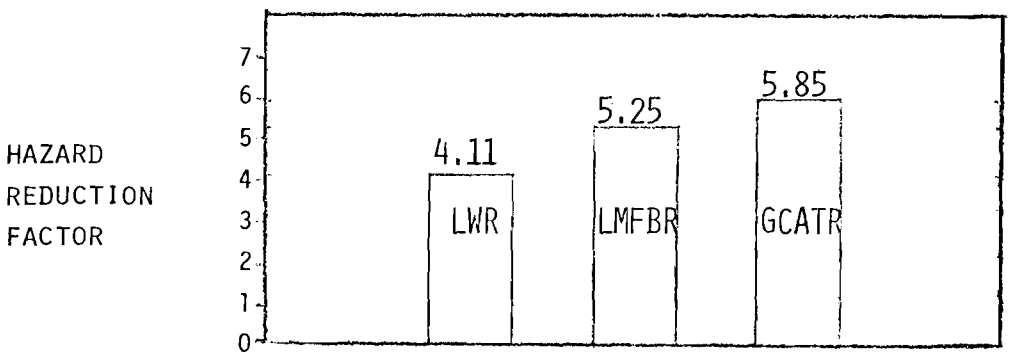

FIGURE IV-2. HAZARD REDUCTION FACTORS OF LWR, LMFBR AND GA. TECH GCATR OVER 40 YEAR LIFE.

(Hazard Reduction Factor = Actinides Produced ÷ Actinides Remaining at End of 40 Year Life)

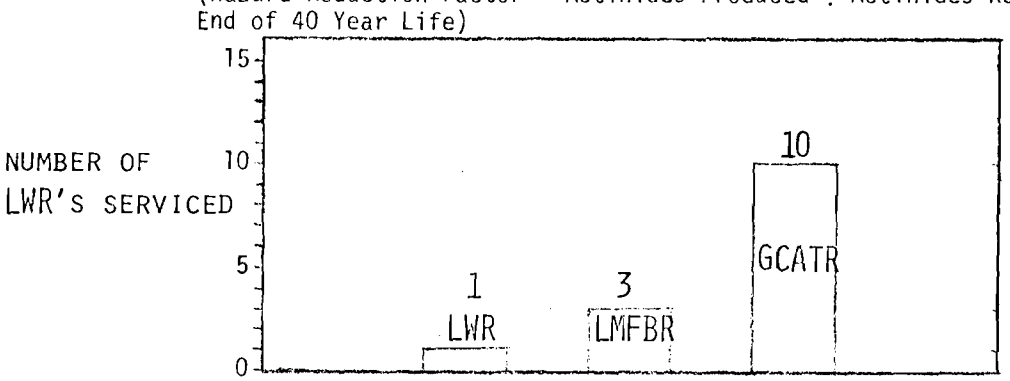

FIGURE IV-3. NUMBER OF LWR'S SERVICED BY LWR, LMFBR AND GA. TECH GCATR SYSTEMS.

References for Chapter IV

1. Bell, M. J., "ORIGEN — The ORNL Isotope Generation and Depletion Code," ORNL-4628, May, 1973.

2. Beaman, S. L., and Aitken, E. A., "Feasibility Studies of Actinide Recycle in LMFBR's as a Waste Management Alternative."

3. Clairborne, H. D., "Neutron Induced Transmutation of High-Level Radioactive Waste," ORNL-TM-3964, December, 1972.

V. HEAT TRANSFER ANALYSIS OF ACTINIDE FUEL RODS

The transuranium actinides (neptunium, plutonium, americium, curium, etc.) will not exist in a gaseous state at reasonable temperatures; consequently, it will be necessary to introduce these elements into the GCATR in a solid form. It is thought that the most reasonable approach for placing actinides in an actinide transmutation reactor is in the form of rods encapsulated with a metal cladding. The actinide fuel rods would be in the form of oxides and would be similar to the fuel rods used in present nuclear power plants. These rods would have to be cooled by a suitable coolant and would have the same design constraints that exist for fuel elements used in power reactors. A discussion of the design constraints follows:

1. Thermal outputs of the actinide fuel rods are limited because excessive temperatures may cause undesirable phase changes, fuel melting, or too high a level of stored energy in the fuel from a safety viewpoint.
2. Thermal outputs of the actinide fuel rods may be limited because of excessive temperatures in the cladding. Maximum cladding temperatures will be limited by loss of cladding creep.
3. Thermal outputs of the actinide fuel rods may be limited because the heat flux at the cladding-coolant interface may exceed the departure from nucleate boiling (DNB) heat flux.

There is a scarcity of thermal-physical property data on the oxides of transplutonium actinides. There is no data on the behavior of mixtures. It appears that the densities of all actinide oxides are about the same, being of the order of 11 grams/cc.[1] In addition, the known melting

points of actinide oxides are high, being of the order of 2400°C or higher. Consequently, since little is known about the transplutonium actinide oxides and a sizable fraction of the actinide fuel rods will be uranium oxide, it is assumed that the melting point and thermal conductivity of actinide oxide mixture is the same as UO_2.

For any type of fuel rod, the maximum fuel temperature is proportional to the maximum linear heat rate (watts/cm) of that fuel rod. For conditions in pressurized water reactors, the linear heat rate to cause centerline melting of UO_2 fuel pellets is of the order of 720 watts/cm. Consequently, the early design of pressurized water reactors limited maximum linear heat rates to about 590 watts/cm. More recently maximum linear heat rates have been reduced to about 500 watts/cm because higher linear heat rates allowed too high a level of stored energy in the fuel from the standpoint of the consequences of a loss of coolant accident.

With actinide fuel rods the maximum allowable linear heat rate is established at 590 watts/cm. This is a level which was considered the maximum for water-cooled nuclear power plants prior to 1973 and should not be considered conservative. The melting point for the mixture of actinide oxides may be below 2400°C and, consequently, a lower linear heat rate may be required to prevent centerline melting.

Actinide fuel pellets will be clad with a 300 series stainless steel. The design criteria for the Clinch River Breeder Reactor Core is that maximum stainless steel cladding midwall temperatures not exceed 662°C[2]. Therefore, this criteria will be applied to the cladding for the actinide fuel rods.

Departure from nucleate boiling (DNB) is a possibility whenever a liquid is used as a reactor coolant. For sodium as a coolant, the maximum cladding temperature constraint will preclude the possibility of coolant

boiling during normal reactor operation. Consequently, DNB will not be considered for use of sodium as a coolant. For high pressure water as a coolant, the maximum cladding temperature constraint is at temperatures far in excess of those necessary to produce DNB. Therefore, with a water coolant there will be a constraint on heat flux given by the DNB heat flux. In order to allow a margin of safety in the operation of nuclear reactors, the predicted DNB heat flux divided by the operating heat flux (called the DNB ratio) is not allowed to fall below some prescribed value such as 1.3. For the analysis of water-cooled actinide fuel rods the predicted DNB heat flux will be calculated with the Westinghouse (W-3) correlation which is an accepted standard in the nuclear power industry [3]. The DNB ratio will not be allowed to fall below 1.3.

Table V-1 summarizes the thermal design constraints imposed upon the actinide fuel rods.

TABLE V-1

SUMMARY OF THERMAL CONSTRAINTS ON ACTINIDE FUEL RODS

Linear Heat Rate:	590 watts/cm
Maximum Cladding Temperature:	662°C
Maximum Heat Flux: (applied to water coolant)	Westinghouse (W-3) DNB Heat Flux Divided by 1.3

As previously mentioned the actinide fuel rods need to be cooled by a suitable coolant which can withstand a reactor environment. The coolants selected for consideration are those currently in use in nuclear power plants—pressurized water, helium, and sodium. The specified coolant channel velocities, pressures, and inlet and outlet temperatures for these

coolants, which are somewhat typical of operating power reactors, are given in Table V-2.

TABLE V-2

COOLANT CONDITIONS FOR ACTINIDE FUEL RODS

Coolant	Inlet Velocity	Pressure	Inlet Temperature	Outlet Temperature
Water	8.2 m/sec	156 Bar	294°C	327°C
Helium	82 m/sec	100 Bar	370°C	537°C
Sodium	9.8 m/sec	100 Bar	370°C	537°C

A high burnup rate in the actinide fuel rods is desirable so as to shorten the time required for transforming the actinide by the fission process. The ultimate burnup rate will be limited by the heat transfer limitations discussed at the start of this chapter.

The volumetric heat generation rate in actinide fuel rods, which is proportional to the burnup rate, is given by

$$q''' = \sum_{i=1}^{n} K_i N_i \int_{o}^{\infty} \phi(E)\, \sigma_{f_i}(E)dE + E_c \tag{5.1}$$

where

q''' = volumetric heat generation rate, Mev/cm^3-sec

K_i = short range energy released from fission of i th fuel material, Mev/fission

N_i = atom density of i th fuel material, atoms/cm^3

$\phi(E)$ = neutron flux per unit energy, n/cm^2-sec-Mev

$\sigma_{f_i}(E)$ = energy dependent fission cross section of i th fuel material, cm^2

E_c = gamma volumetric heat generation rate, Mev/cm^3-sec

The value of K_i is not known for all the transplutonium actinides, but it should probably be close to that of uranium or plutonium. In addition, the spatial distribution of E_c should be similar to that of the neutron flux and this term can then be incorporated into K_i. For uranium the total recoverable energy release per fission is of the order of 200 Mev/fission. Consequently, by fission cross sections and the total neutron flux, Eq. 5.1 can be simplified to

$$q''' = 200\, \Phi \sum_{i=1}^{n} N_i\, \bar{\sigma}_{f_i}, \quad \text{Mev/cm}^3\text{-sec} \tag{5.2}$$

where $\bar{\sigma}_{f_i}$ is the spectrum-averaged fission cross section of the i th fuel material. From the limitations on q''', the maximum neutron flux permissible in actinide fuel rods can be determined from Eq. 5.2.

For actinide fuel rods of radius r_o cm. encapsulated in stainless steel tubes with a thickness and radial gap between fuel and cladding of ΔC cm., the linear heat rate is given by

$$q' = \pi\, r_o^2\, q''' \tag{5.3}$$

where

q' = linear heat rate, watts/cm

q''' = volumetric heat generation rate, watts/cm^3

The heat flux at the cladding outer surface is given by

$$q''_w = \frac{r_o^2\, q'''}{2\,(r_o + \Delta C)} \tag{5.4}$$

where q_w'' is the heat flux in watts/cm^2.

Inspection of Eq. 5.3 shows that the volumetric heat generation rate is inversely proportional to the the square of the fuel radius. Therefore, for a fixed upper limit for the linear heat rate, the maximum volumetric heat generation rate is found for the smallest possible fuel radius, r_o. From a design point of view there will be a minimum fuel radius for which it is practical to fabricate fuel rods. This minimum radius is assumed to be 0.127 cm.

By examining Eq. 5.4 it is seen that the volumetric heat generation rate is approximately inversely proportional to the fuel radius. Therefore, the maximum volumetric heat generation rate for a fixed heat flux is found for the smallest fuel radius. The minimum fuel radius is determined from a practical fabrication point of view and will be set at 0.127 cm.

From the arguments in the preceding paragraphs it is apparent that the maximum volumetric heat generation rate is achieved with the minimum fuel radius of 0.127 cm. Whether the limiting thermal constraint is due to a maximum linear heat rate (q'), heat flux (q_w''), or cladding temperature will require further analysis of the three reactor coolants and their associated flow conditions. The fuel pellets are assumed to be 0.254 cm. in diameter clad with a 300 series stainless steel of 0.033 cm. thickness with a diametral clearance between the fuel and cladding of 0.015 cm. This results in a fuel rod outside diameter of 0.335 cm. The volumetric heat generation rate in the fuel rods is assumed to have a cosine distribution along the rod axis and the rods are assumed to have an active length of 180 cm.

The thermal design constraints are listed in Table V-1. In order to determine the maximum cladding temperature it is necessary to calculate the heat-transfer coefficients for the various coolants. For a water coolant, the maximum cladding temperature will not be a constraint because the coolant would have gone through a departure from nucleate boiling (DNB) at cladding temperatures far below the 662°C limit. Therefore, it is necessary to calculate heat-transfer coefficients for sodium and helium.

For sodium the heat-transfer coefficient is given by[4]

$$h = \frac{k}{D_e}\left[6.66 + 3.126(P/D) + 1.184(P/D)^2 + 0.0155\left(\frac{\rho v D_e C_p}{k}\bar{\psi}\right)^{0.86}\right] \tag{5.5}$$

where

h = heat-transfer coefficient

k = sodium thermal conductivity

D_e = flow channel equivalent diameter

D = fuel rod diameter

P = rod pitch, spacing between fuel rod centers

ρ = sodium density

v = sodium velocity

C = sodium heat capacity

$\bar{\psi}$ = average ratio of eddy diffusivities

The average ratio of eddy diffusivities is calculated by

$$\bar{\psi} = 1 - \frac{1.82}{N_{Pr}\left(\epsilon_M/\nu\right)_{Max}^{1.4}} \tag{5.6}$$

where

N_{Pr} = sodium Prandtl number

$(\epsilon_M/\nu)_{Max}$ = maximum eddy diffusivity for momentum transfer given graphically in Ref. 4.

The heat-transfer coefficient for helium can be calculated with the Dittus-Boelter equation[5]

$$h = \frac{k}{D_e}\left[0.023\left(\frac{\rho v D_e}{\mu}\right)^{0.8}\left(\frac{C_p \mu}{k}\right)^{0.4}\right] \tag{5.7}$$

where μ is the helium viscosity.

The departure from nucleate boiling heat flux is calculated with an empirical correlation developed by Tong[3]

$$\frac{q''_{DNB,\ EU}}{10^6} = \left\{(2.022 - 0.0004302p) + (0.1722 - 0.0000984p) \times \exp[(18.77 - 0.004129p)\chi]\right\} \tag{5.8}$$

$$\times\ [(0.1484 - 1.596\chi + 0.1729\chi|\chi|)G/10^6 + 1.037]$$

$$\times\ [1.157 - 0.869\chi] \times [0.2664 + 0.8357 \exp(-3.151De)]$$

$$\times\ [0.8258 + 0.000794\ (h_{sat} - h_{in})],$$

where

$q''_{DNB,\ EU}$ = equivalent uniform channel DNB heat flux, Btu/hr-ft^2

p = pressure, psia

χ = quality

G = mass velocity, lb$_m$/ft^2-hr

h = enthalpy, Btu/lb_m

D_e = channel equivalent diameter, in.

For non-uniform axial heat flux distributions Eq. 5.8 is modified by employing a correction factor F such that

$$q''_{DNB,N} = q''_{DNB,EU}/F \tag{5.9}$$

where $q''_{DNB,N}$ = DNB heat flux for the non-uniformly heated channel

$q''_{DNB,EU}$ = equivalent uniform DNB flux from Eq. 5.8

and

$$F = \frac{C \int_0^{\ell_{DNB}} q''(z) \exp[-C(\ell_{DNB,N} - z]dz}{q''_{local} [1 - \exp(-C\ell_{DNB,EU})]} \tag{5.10}$$

where

$$C = 0.44 \frac{(1 - \chi_{DNB})^{7.9}}{(G/10^6)^{1.72}} \text{ in.}^{-1}$$

ℓ_{DNB} = axial location at which DNB occurs, in.

The fuel rod thermal-hydraulic analysis will have a variety of uncertainties due to manufacturing tolerances, physical property variations, maldistribution of flow, uncertainty in the correlations, and uncertainty in the fuel heating distribution. The effects of these uncertainties on the thermal-hydraulic performance of fuel rods is accounted for by applying hot channel/hot spot factors to computations based upon nominal conditions in the fuel assembly. Because of the similarity of the actinide fuel rods and

flow conditions to liquid metal-cooled fast breeder reactors, the hot channel/hot spot factors used in the analysis are the same as those used in the analysis of the Clinch River Breeder Reactor Plant[2]. Table V-3 gives values selected.

TABLE V-3

ACTINIDE FUEL ROD HOT CHANNEL/HOT SPOT FACTORS

Axial Nuclear*	Coolant	Film	Heat Flux
(F_Z^N)	$F_{\Delta h}$	$F_{\Delta t}$	F_q
1.57	1.232	1.168	1.081

The solution for the fuel rod geometry and volumetric heat generation rates requires simultaneous application of the thermal constraints listed in Table V-1. For sodium as a coolant the limiting constraint is a maximum linear heat rate of 590 watts/cm to prevent fuel melting. The limiting thermal constraint with helium is on the heat flux to prevent the cladding temperature from exceeding 662°C. With water, the limiting thermal constraint is departure from nucleate boiling.

Table V-4 lists the results of the heat transfer calculations for the three coolants.

---

*This is from the assumed cosine distribution for the axial dependence of the neutron flux.

TABLE V-4

RESULTS OF THERMAL ANALYSES OF ACTINIDE

FUEL RODS FOR VARIOUS COOLANTS

	Rod Diameter (cm)	P/D	q' (Max) (watts/cm)	q''_w (Avg) (watts/cm^2)	q''_w (Max) (watts/cm^2)	q''' (Avg) (watts/cm^3)	q''' (Max) (watts/cm^3)
Sodium	0.335	2.21	590	330	560	6,835	11,600
Helium	0.335	2.05	152	85	145	1,780	3,000
Water	0.335	2.00	415	232	394	4,800	8,150

P/D = fuel element pitch-to-diameter ratio; q' (Max) = maximum linear heat rate; q''_w (Avg) = average wall heat flux; q''_w (Max) = maximum wall heat flux; q''' (Avg) = average volumetric heat generation rate; q''' (Max) = maximum volumetric heat generation rate.

One result of great importance is the average volumetric heat generation rate in the fuel rod which is proportional to the maximum average fuel rod burnup rate. Fuel burnup is usually expressed in terms of megawatt-days per tonne of fuel (MWD/t). Maximum burnups proposed in advanced power reactors

such as the Clinch River Breeder Reactor Plant is 150,000 MWD/t[2]. For the average volumetric heat generation rates shown on Table V-4, the time required to achieve these burnups is 202 days with the sodium coolant, 775 days with the helium coolant, and 288 days with the water coolant. The Clinch River Breeder Reactor will require 1100 days to achieve 150,000 MWD/t burnup, so the burnup rate in the actinide fuel rods could be five times as fast as the conventional fuel in an LMFBR.

By taking the maximum volumetric heat generation rates in Table V-4 and applying this data to Eq. 5.2 it is possible to determine the maximum allowable neutron flux in the actinide fuel rods. For spent LWR fuels with a burnup of 33,000 MWD/t in which all fission products and 99.9 percent of the uranium and plutonium have been removed, the maximum neutron fluxes for a fast reactor spectrum are shown in Table V-5 for sodium and helium coolants.

TABLE V-5

MAXIMUM NEUTRON FLUXES IN ACTINIDE FUEL RODS

Coolant	Neutron Flux, n/cm^2-sec
Sodium	4×10^{16}
Helium	10^{16}

The maximum neutron flux in actinide fuel rods with a sodium coolant is about 10 times the maximum neutron flux in LMFBR's. Therefore, it is desirable to be able to construct reactors which are capable of generating

neutron fluxes at this high level. Gas core reactors may be able to generate this high a neutron flux because of their smaller fuel loadings.

References for Chapter V

1. Kirk and Othmer, Encyclopedia of Chemical Technology, Vol. 1, 2nd ed., John Wiley & Sons (1963).

2. Cavelli, M. D., and R. A., Markley, "Preliminary Thermal Hydraulic Design and Predicted Performance of the Clinch Breeder Reactor Core," 75-HT-71, presented at AIChE-ASME Heat Transfer Conference, San Francisco (August 11-13, 1975).

3. Tong, L. S., "Prediction of Departure From Nucleate Boiling for an Axially Non-Uniform Heat Flux Distribution," J. Nuclear Energy, 6, 21 (1967).

4. Dwyer, O. E., and R. N. Lyon, "Liquid Metal Heat Transfer," Proc. 3rd U. N. Intern. Conf. Peaceful Uses of Atomic Energy Geneva, 8, pp 182-189 (1965).

5. Dittus, F. W., and L. M. K., Boelter, University California Pub. Eng., 2, 443 (1930).

VI. REACTOR DESIGN

Any actinide transmutation reactor must satisfy the following general criteria:[1]

a) The transmutation process must not use more energy than was originally produced in the formation of the actinides.

b) The transmutation process must not create more actinides in its operation than it burns.

c) The transmutation process must be rapid enough to burn actinides at a significant rate compared to their creation in the nuclear industry.

Any gas core transmuter developed by this project must satisfy, in addition, the following criteria:

a) UF_6 will be used as the reactor fuel.

b) The reactor must generate a very high neutron flux in order to obtain a significant actinide fission rate.

c) The reactor must produce the neutron spectrum which provides the largest possible net destruction of actinides.

It is necessary to design the gas core actinide transmuter in conjunction with computer design codes. These codes make it possible to optimize the actinide burnup with the constraints of several economic, thermodynamic, and neutronic limitations. The code ORIGEN[2] may be used to determine the actinide burnup with time and the hazard reduction achieved by a specific type of reactor. However ORIGEN requires as input the neutron flux and spectrum in the actinide region of the reactor to do these calculations.

There are several design codes available which may be used to provide this information. To date this project has worked with MCC (Multigroup Constant Code), THERMOS, ANISN, and MACH-I. For the initial scoping calculations it was found that MACH-I[3] was by far the most useful. While the other codes provided higher accuracy, MACH-I provided sufficient accuracy for the initial design decisions and was much easier to employ. Because MACH-I was only a 26-group diffusion code its computer storage requirements were much smaller than with the transport codes.

An Actinide Transmuter Reactor can be visualized as a three-region reactor containing core, actinide, and reflector regions. The core region contained the $^{233}UF_6$ gaseous fuel. ^{233}U was employed to minimize actinide formation in the operation of the reactor itself. Previous work[4] has shown that 540°C and 100 bar are suitable conditions for such a reactor from thermodynamic and pressure considerations so these conditions were assumed for the UF_6 gas. This corresponded to a density of 0.69 gm/cm^3 and a uranium atom density of 1.20×10^{21} $atom/cm^3$.

Because no actinide compound is gaseous at reasonable temperatures the actinides were assumed to be in the form of oxide rods with properties similar to UO_2 fuel rods. Since a high neutron flux was required to cause a significant fissioning of the actinides, heat generation was a serious concern. Therefore, this region also included coolant.

The last simple region was the reflector. In those cases where moderation was desired, a moderating coolant and reflector were employed. In the actual calculations performed, a separate thin region was included between the core and actinides which was the Hastelloy liner for the

core. In addition, the actual calculations had two reflector regions, the inner one being either D_2O or H_2O and the outer one being graphite.

Within this framework several reactors were possible. The amount of moderator included in the actinide region and reflector could be changed causing the reactor to be fast, intermediate, or thermal. Various coolants and reflector materials were possible. In addition, one could place the actinides at the center of the reactor with the UF_6 region in a torus around it instead of placing the actinides outside a central UF_6 region.

The initial objective of the reactor design analysis is to evaluate the characteristics of several modifications of the reactor described and establish the optimal type. MACH-I calculations were performed in a spherical geometry on a reactor with the fuel in the center. H_2O and D_2O were each used as the coolant and moderator in both types. Figure VI-1 shows a sample reactor configuration.

By applying a power output limit of 2500 MW(th) to the reactor it was possible to calculate the maximum flux in the actinides. The results of sample calculations are shown in Table VI-1. It was clear from these calculations that D_2O was far superior to H_2O in the reactor. Not enough calculations had been done yet to determine whether the actinides should be placed in the center or on the outside. A higher flux is obtainable in the center, but more actinides may be placed on the outside. The amount of moderation provided had a significant effect on the results as well. Since the only limit imposed on the flux was on the total number of fissions in the reactor per second, a more thermal reactor would have a lower flux due to the larger thermal cross section

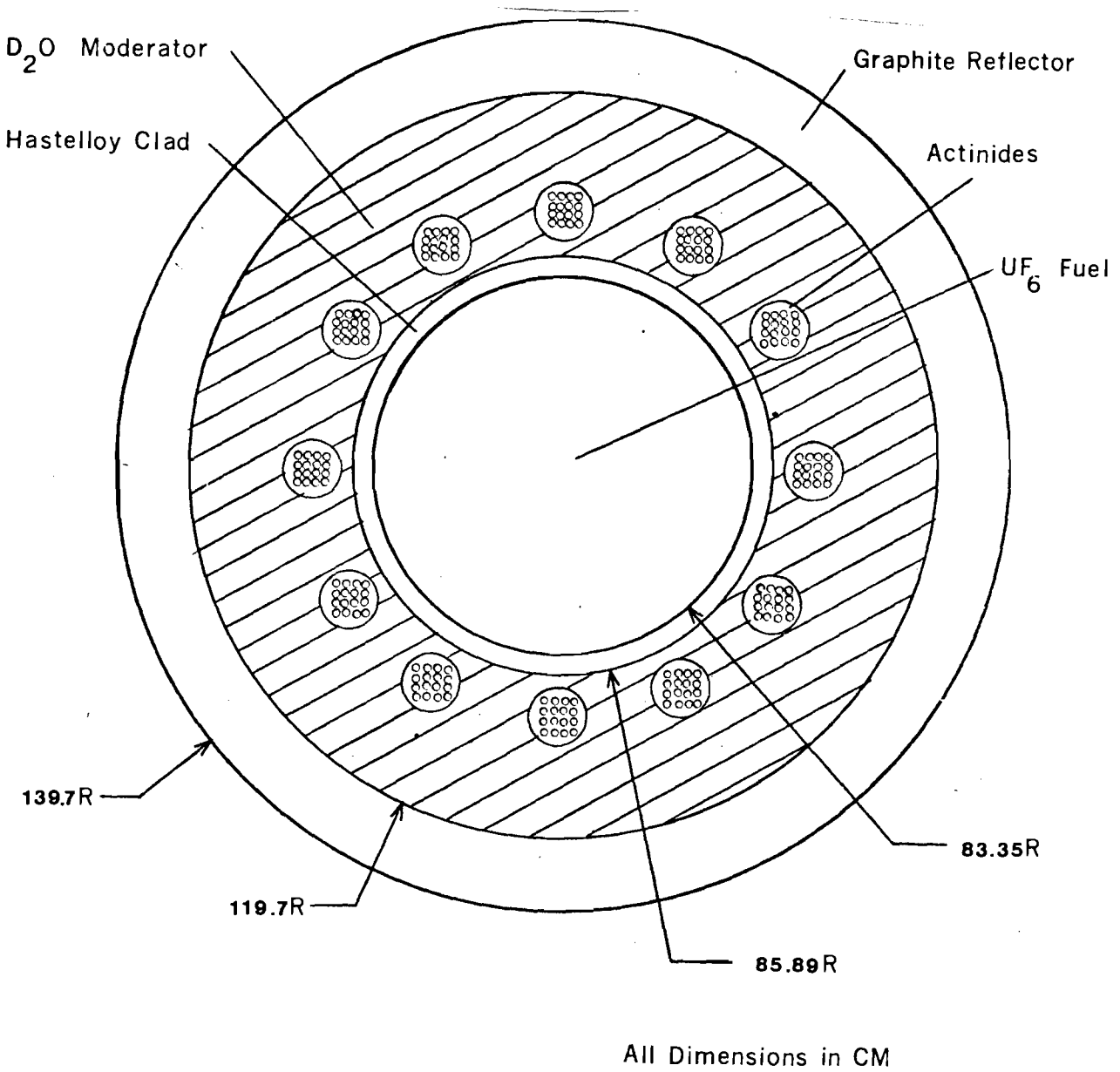

Fig. VI-1 Plan View of Typical Gas Core Actinide Transmutation Reactor

TABLE VI-1

CRITICAL PARAMETERS FOR GCATR: ACTINIDES IN REFLECTOR, D_2O MODERATED

I. Average Flux

	$\bar{\phi}_{Fast}$	$\bar{\phi}_{Epithermal}$	$\phi_{Thermal}$	ϕ_{Total}
Region 1 Fuel	4.0871×10^{15}	5.1147×10^{15}	5.139×10^{7}	9.20×10^{15}
Region 3 Actinides	1.3096×10^{15}	3.8019×10^{15}	4.8237×10^{13}	5.15×10^{15}

II. Radius and Volume

	1	2	3	4	5
Outer Radius, cm.^{3}	83.346	85.886	99.696	119.70	139.70
Volume, cm.^{3}	2.4252×10^6	2.2855×10^5	1.4870×10^6	3.0326×10^6	4.236×10^6

III. Critical Mass, kg.

U^{233}	UF_6
1050.8	1564.9

for fission in the fuel. For a given spectrum, however, it can be said that the smaller the critical mass the larger the flux may be.

A major advantage of the Gas Core Transmuter was demonstrated in these calculations, since fluxes several orders of magnitude above those in conventional reactors were achieved. If the flux is to be high and still have a limited power output the critical mass should be as small as possible. However, if the maximum amount of actinides are to be exposed to a high flux the core should have a large size. This dictates as low a fuel density as possible. Hence, a Gas Core Reactor is much more suited to this problem than is a solid fuel reactor. In addition, the Gas Core Reactor has a fast spectrum and a high flux.

Further calculations indicated that a thicker graphite reflector was valuable and that replacing D_2O with graphite had a negligible effect. It was thus concluded that if D_2O were to be used as the coolant for this reactor its use should be limited to cooling requirements and graphite used exclusively for the reflector.

Calculations in Chapter V indicated that a sodium coolant would allow a much higher flux than D_2O coolant from a heat transfer point of view. In addition, a very fast reactor may indeed be preferable to a more thermal one because of the increased fission to capture ratio. Future calculations will investigate these possibilities.

References for Chapter VI

1. Bloemke, J. O., "Technical Alternatives Document," Oak Ridge National Laboratory, Oak Ridge, Tennessee (1976).

2. Bell, M. J., ORIGEN--The ORNL Isotope Generation and Depletion Code, Oak Ridge National Laboratory, Oak Ridge, Tennessee (1973).

3. Menely, D. A., et al, "MACH-I, A One-Dimensional Diffusion Theory Package," ANL-7223 (1966).

4. Clement, J. D., and Rust, J. H., "Analysis of UF_6 Breeder Reactor Power Plants," Final Report, NASA, MSG-1168, Georgia Institute of Technology (1976).

VII. OVERALL SYSTEM DESIGN

The GCATR will be designed to transmute by fission the transuranium actinides from ten light water reactors (LWR's). Figure VII-1 illustrates the fuel cycle for the GCATR. As discussed in Chapter IV., the actinide burnup capability of the GCATR is far in excess of that capable by either LWR's or LMFBR's.

Figure VII-2 and VII-3 illustrate elevation and plan views of a typical GCATR. UF_6 at 100 bar pressure enters the reactor at 482°C and is heated by fissioning to 593°C. The core is a right cylinder with approximate dimensions of a two-meter height and a one-meter diameter. A Hastelloy-N or Monel 404 liner of 1.27 cm thickness will be used to isolate the UF_6 from the rest of the reactor.

Actinide fuel rods, discussed in Chapter V., will be arranged in fuel assemblies for placement along the length of the core outside the liner. These fuel assemblies will require a coolant which can be sodium, helium, or high pressure water. Figure VII-2 indicates sodium is the coolant.

The actinide fuel rod coolant will be at a pressure comparable to that of UF_6 so as to reduce the required thickness of the core liner wall. The reactor will need to be enclosed by a thick-walled pressure vessel which could be made of carbon steel with a stainless steel liner.

Because of its high burnup requirements, the GCATR will generate a considerable amount of thermal power which must be converted into electricity in order to economically justify the concept. Figure VII-4 illustrates the power plant schematic diagram.

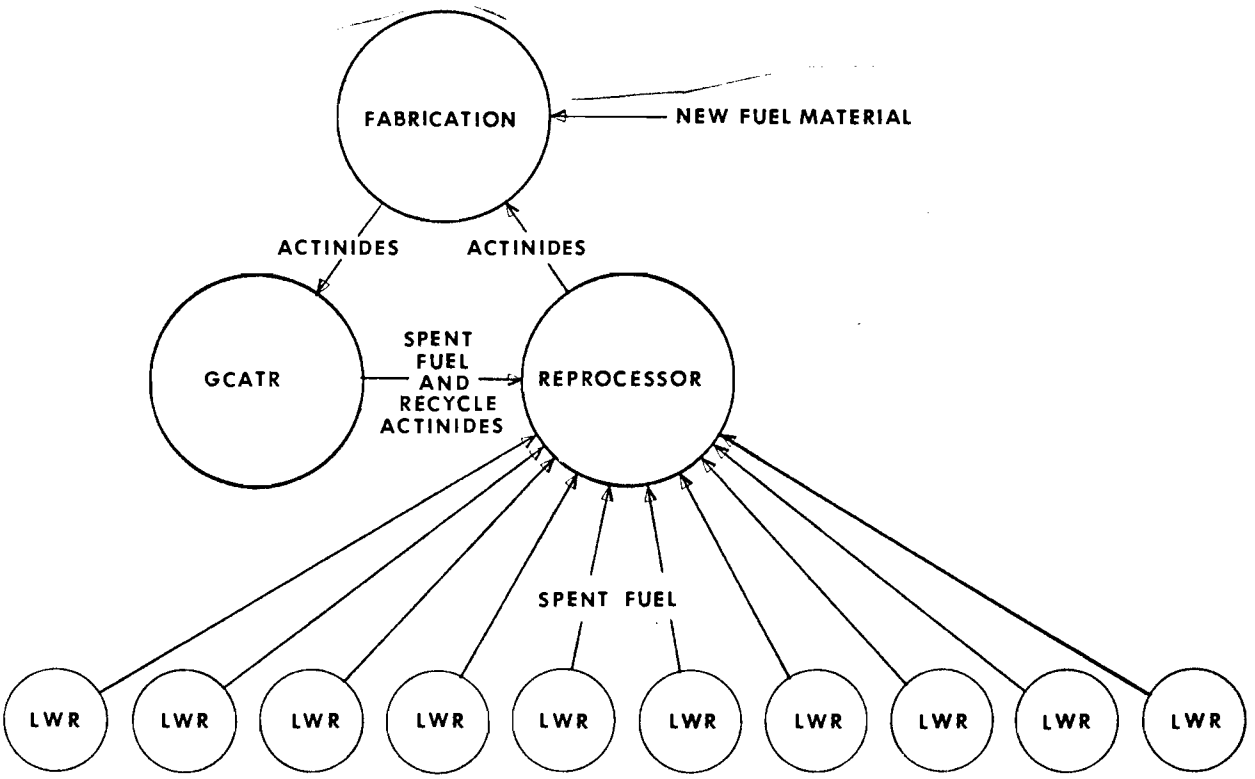

Fig. VII-1 Proposed Fuel Cycle for Gas Core Actinide Transmutation Reactor

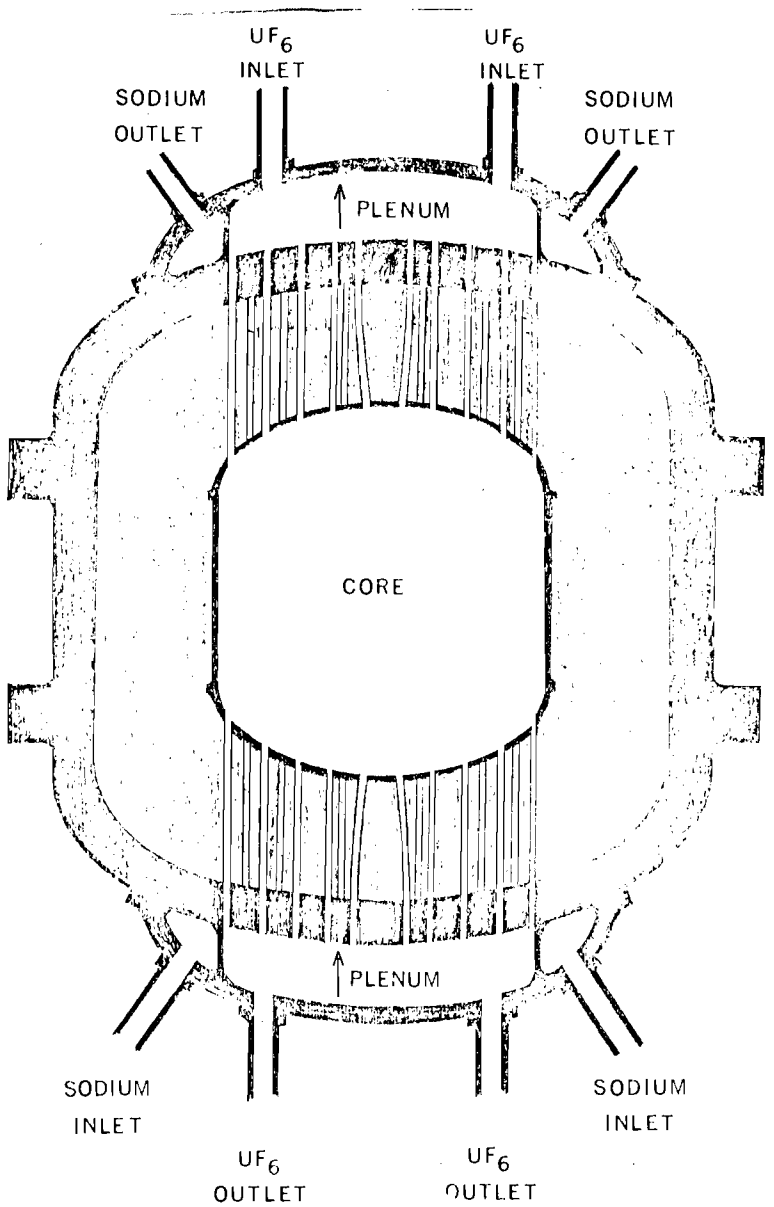

Fig. VII-2 Elevation View of Gas Core Actinide Transmutation Reactor

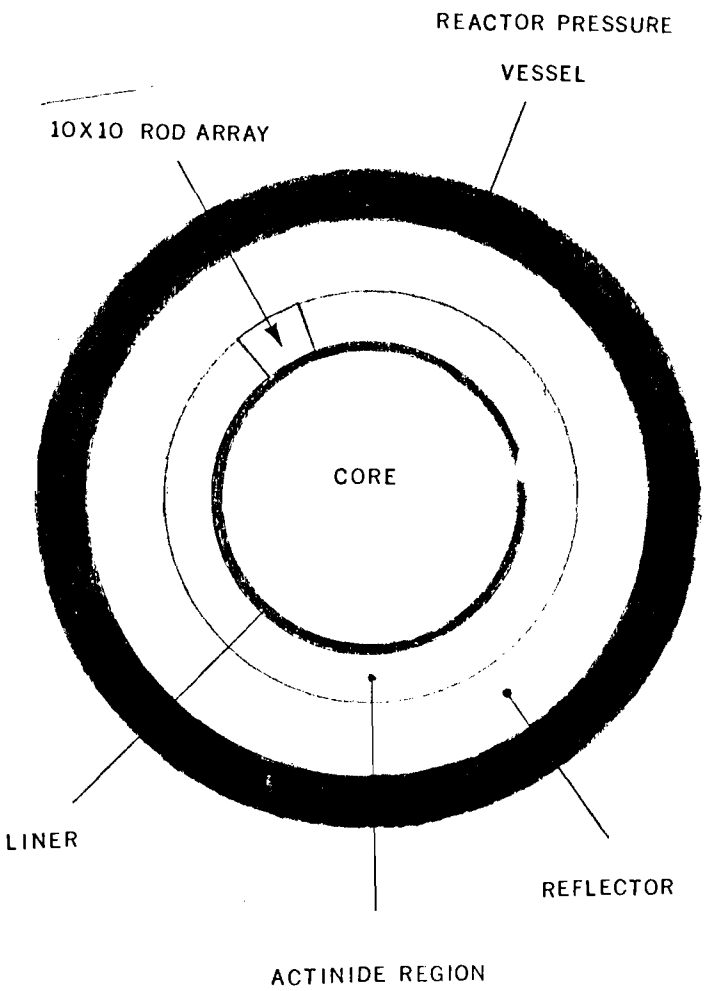

Fig. VII-3 Plan View of Gas Core Actinide Transmutation Reactor

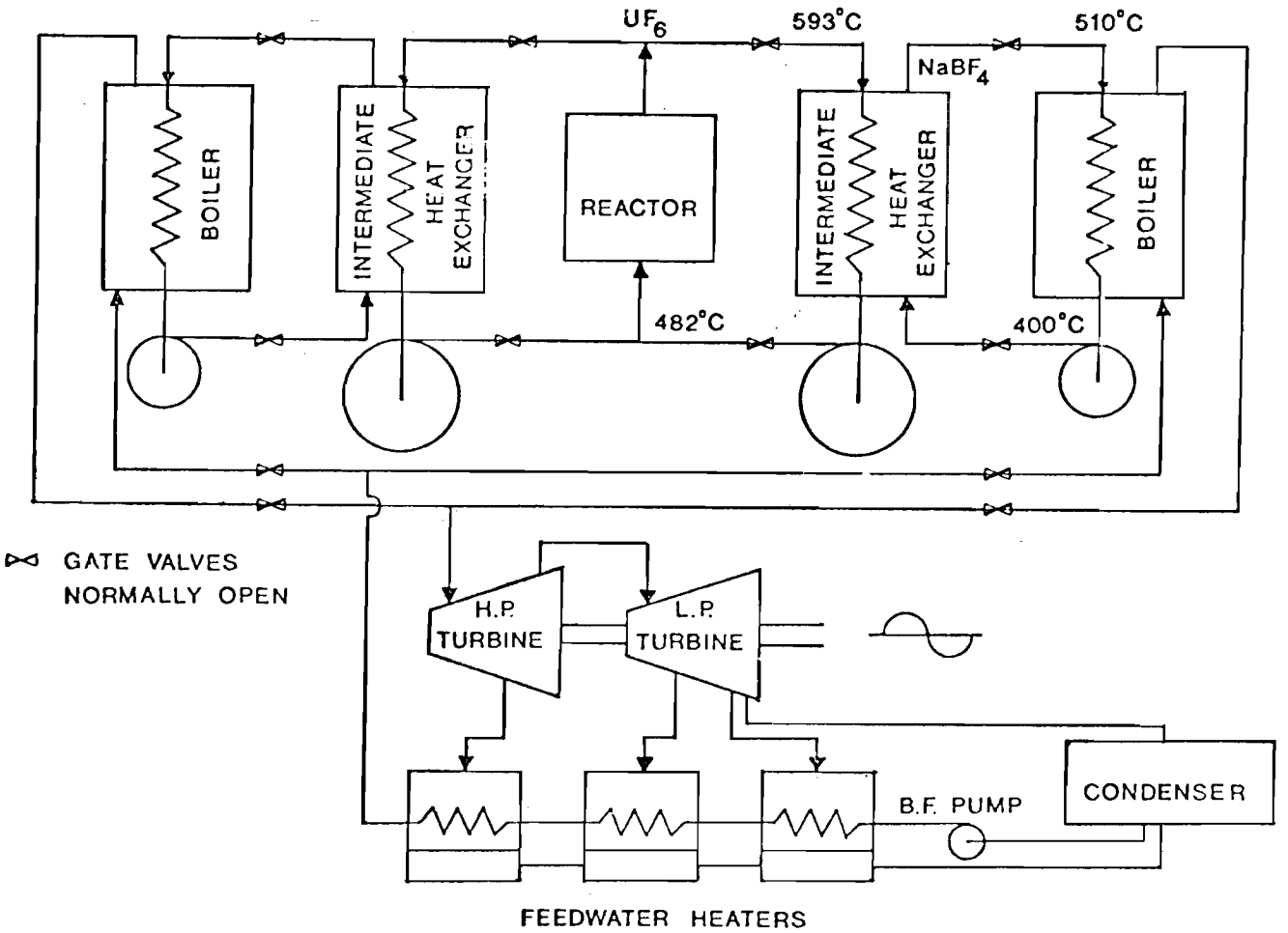

Fig. VII-4 Gas Core Actinide Transmutation Reactor Plant Schematic

Because it was considered undesirable for UF_6 to have the possibility of interacting with water due to failure of a boiler tube, the UF_6 exchanges heat with a molten salt ($NaBF_4$) in an intermediate heat exchanger. $NaBF_4$ was developed as an intermediate coolant for the molten salt breeder reactor and would be inert with UF_6. Another desirable feature of $NaBF_4$ is that the boron present in the salt would eliminate criticality problems with UF_6 in the heat exchanger.

Not shown on Figure VII-4 are flow paths for the coolant used to cool the actinide fuel rods. This coolant, which will be either sodium, helium, or water, will remove a considerable amount of reactor heat. Preliminary calculations with the MACH-I diffusion code indicates that the power generated in the actinide fuel rods ranges from 20-36 percent of the plant output.

Multiple intermediate heat exchangers are employed on the plant so as to keep these heat exchangers compact and also improve upon the reliability and safety by redundancy of equipment. The heat load of these heat exchangers will be of the order of 500 Mw so the plant shown in Figure VII-4 corresponds to 1000 Mw thermal power plant. Plants with higher power generation will have more intermediate heat exchangers.

The $NaBF_4$ enters the intermediate heat exchanger at 400°C and exits at 510°C. It then enters a boiler where it exchanges heat to produce superheated steam at 100 bar pressure and 480°C. The steam is expanded through high and low pressure turbines to a pressure of 0.07 bar. The efficiency of the high pressure turbine is assumed to be 85 percent and that of the low pressure turbine 80 percent. Steam is extracted at optimal temperatures from three locations in the turbines for use in feedwater heaters. The overall efficiency of the plant is 36 percent.

APPENDIX A

GEORGIA INSTITUTE OF TECHNOLOGY RESEARCH ON THE GAS CORE ACTINIDE TRANSMUTATION REACTOR (GCATR)

J. D. Clement, J. H. Rust, and A. Schneider
Georgia Institute of Technology
Atlanta, Georgia 30332

and

F. Hohl
National Aeronautics and Space Administration
Langley, Virginia 23665

Paper presented at the Third Symposium on Uranium Plasmas, Princeton University Conference, Princeton, New Jersey, June 10-12, 1976.

GEORGIA INSTITUTE OF TECHNOLOGY RESEARCH ON THE GAS CORE ACTINIDE TRANSMUTATION REACTOR (GCATR)*

J. D. Clement, J. H. Rust, and A. Schneider
Georgia Institute of Technology
Atlanta, Georgia 30332

and

F. Hohl
National Aeronautics and Space Administration
Langley, Virginia 23665

Abstract

The Gas Core Actinide Transmutation Reactor (GCATR) offers several advantages including (1) the gaseous state of the fuel may reduce problems of processing and recycling fuel and wastes, (2) high neutron fluxes are achievable, (3) the possibility of using a molten salt in the blanket may also simplify the reprocessing problem and permit breeding, (4) the spectrum can be varied from fast to thermal by increasing the moderation in the blanket so that the trade-off of critical mass versus actinide and fission product burnup can be studied for optimization, and (5) the U^{233}-Th cycle, which can be used, appears superior to the U^{235}-Pu cycle in regard to actinide burnup.

The program at Georgia Tech is a study of the feasibility, design, and optimization of the GCATR. The program is designed to take advantage of initial results and to continue work carried out by Georgia Tech on the Gas Core Breeder Reactor under NASA Grant-1168. In addition, the program will complement NASA's program of developing UF_6-fueled cavity reactors for power, nuclear pumped lasers, and other advanced technology applications.

The program comprises:

(1) General Studies -- Parametric survey calculations will be performed to examine the effect of reactor spectrum and flux level on the actinide transmutation for GCATR conditions. The sensitivity of the results to neutron cross sections will be assessed. Specifically, the parametric calculations of the actinide transmutation will include the mass, isotope composition, fission and capture rates, reactivity effects, and neutron activity of the recycled actinides.

(2) GCATR Design Studies -- This task is a major thrust of the proposed research program. Several subtasks are considered: optimization criteria studies of the blanket and fuel reprocessing, the actinide insertion and recirculation system, and the system integration.

The total cost of the GCATR in a nuclear waste management system will be evaluated and compared to the cost of alternate strategies presently being considered.

This paper presents a brief review of the background of the GCATR and ongoing research which has just been initiated at the Georgia Institute of Technology.

*Research sponsored by N.A.S.A.

I. Introduction

The high level radioactive wastes generated in the operation of nuclear power plants contain both fission products and actinide elements produced by the non-fission capture of fissile and fertile isotopes. The fission products, atoms of medium atomic weight formed by the fission of uranium or plutonium, consist mainly of short term (30 years or less half-life) isotopes, including Sr^{90} and Cs^{137}. Tc^{99} and I^{129} are long-lived fission products. The actinide components of radioactive wastes, including isotopes of Np, Am, Cm, and Pu and others are all very toxic and most have extremely long half-lives. The amount of long-lived radioactive material expected to be produced is substantial. Smith[1] has estimated that in 1977, 150 kg of Am^{243}, 150 kg of Am^{241}, and 15 kg of Cm^{244} will be produced. The actinides cause waste management difficulties at two stages in the fuel cycle. Some are carried over with the fission products during fuel reprocessing, but also some dilute plutonium wastes will appear from fuel manufacturing plants. Thus at the entrance to the waste facility are found a mixture of transuranic actinides combined with shorter-lived and temporarily more hazardous fission products.

The safe disposition of the radioactive wastes is one of the most pressing problems of the nuclear industry. Any viable plan must meet the three requirements of

(1) technical soundness
(2) reasonable economics
(3) public acceptance.

II. Background

The strategies which have been suggested for high-level nuclear waste management encompass

(1) terrestrial disposal (geologic, seabed, ice sheet)
(2) extraterrestrial disposal, and
(3) nuclear transmutation,

or some combination of these methods, such as terrestrial burial of the short-lived fission products and extraterrestrial disposal or nuclear induced transmutation of the long-lived actinides. Papers discussing all of these methods were presented at the Waste Management Symposium in December 1974.[2] The technical soundness of terrestrial disposal is a controversial topic, and also public acceptance is questionable. Extraterrestrial disposal is costly. Hence, there is increasing interest in

nuclear transmutation as a potential solution to the nuclear waste disposal problem. Figure 1 summarizes the nuclear waste management schemes which are under consideration.

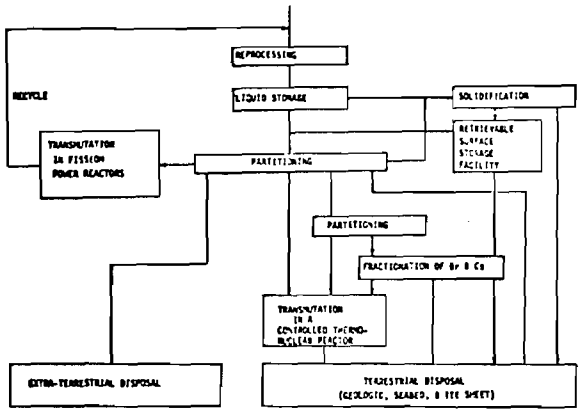

Fig. 1 Schematic representation of schemes for nuclear waste management

The first published suggestion for the use of neutron-induced transmutation of fission products was made in 1964 by Steinberg et al.,[3] who concerned themselves only with the transmutation of Kr^{85}, Sr^{90}, and Cs^{137}. Their calculations assumed that the krypton and cesium fission product wastes had been enriched to 90% in Kr^{85} and Cs^{137}. This was necessary due to the relatively small thermal neutron cross sections of these two nuclides and their small concentration with respect to their stable isotopes found in spent fuel. The Sr^{90} analysis was based on the presence of Sr^{90} and Sr^{89} which has a half-life of 53 days. If the strontium wastes are allowed to decay for one year before being returned to the reactor, then all the Sr^{89} portion will decay to Y^{89} (stable) which can be chemically separated from the Sr^{90}. However, even with these modifications to the waste isotopic composition, Steinberg et al, indicate that a thermal neutron flux of 10^{16} n/cm^2-sec is required before the halving time of Sr^{90} can be reduced from the normal half-life of 28.1 years to 1 year. A flux of 10^{17} n/cm^2-sec was indicated to be necessary before the halving time could be reduced from the natural half-life of 33 years to 1 year. The halving time describes the "total" time spent in a reactor for the inventory of a particular isotope to be reduced to half its value.

In another work, Steinberg and Gregory[4] considered the possibility of fission product burnup (specifically Cs^{137} and Sr^{90}) in a spallation reactor facility. In this scheme a nuclear power reactor is used to "drive" a high-energy proton accelerator with the resultant (p,xn) spallation reactions of the proton beam with the target producing the extreme fluxes of 10^{17} n/cm^2-sec necessary for fission product burnup. However, in addition to economic disadvantages this concept faces serious mechanical and material design problems.

Claiborne[5,6,7] was the first investigator to report detailed calculations of actinide recycling in light water reactors. Claiborne studied actinide recycling in light water reactors (LWR) operating on 3.3% U^{235}-U^{238} fuel cycle. He concluded that it was not practical to burn the fission products because the neutron fluxes were too low and "developing special burner reactors with required neutron fluxes of 10^{17} n/cm^2-sec or in thermonuclear nuclear reactor blankets is beyond the limits of current technology."[5]

For purposes of comparison, Claiborne[5] expressed radioactive waste hazards in terms of the total water required to dilute a nuclide or mixture of nuclides to its RCG (Radiation Concentration Guide Value, also known as the Maximum Permissible Concentration, MPC). Using this criterion, the waste from a PWR spent-fuel reprocessing plant is dominated by fission products for about the first 400 years. After the first 400 years the actinides and their daughters are the dominant factor. The americium and curium components of the actinide waste are the main hazards for the first 10,000 years, after which the long-lived Np^{237} and its daughters become the controlling factor. These data assume that 99.5% of the U and Pu has been removed from the waste.

Claiborne indicates that, if 99.5% of the U and Pu is extracted, then a significant reduction in the waste hazard can be achieved by also removing 99.5% of the other actinides, mainly americium, curium, and neptunium.

For the purpose of calculations, Claiborne assumes that recycling takes place in a typical PWR fueled with 3.3% enriched U and operated with a burnup of 33,000 MWd/metric tonne of uranium. The burnup was assumed continuous at a specific power of 30 MW/metric tonne over a three year period. The calculations also ignored intermittant operation and control rods and assumed that the neutron flux was uniform throughout a region. The recycled actinides were added uniformly to the 3.3% enriched fuel. The actual calculations were performed by a modified version of the nuclide generation and depletion code ORIGEN.[8] The calculations are based on three energy groups (thermal, 1/E energy distribution in the resonance region, and a fast group) with three principal regions in the reactor. Each region was in the reactor for three years while being cycled from the outside to the center so that the innermost region is removed each year.

The "standard" that was used for comparing the effect of the actinide recycle on the actinide waste hazard was the waste obtained after removing either 99.5% or 99.9% of the U and Pu at 150 days after discharge and sending the remaining quantities to waste along with all the other actinides, and all actinide daughters generated since discharge from the reactor. The results of Claiborne's calculations are presented in the form of a hazard reduction factor which he defines as "the ratio of the water required for dilution of the waste to the RCG for the standard case to that required to dilute the waste after each successive irradiation cycle."

The contributions of the actinides, fission products, and structural materials to the total waste hazard are shown in Table 1. Table 2 shows the effect of recycling the actinides in terms of the hazard reduction factor for two cases of actinide extraction efficiency. Note that the values decrease asymptotically with increasing recycles. This is due to the buildup of actinides in the system until decay and burnup equal production, after about 20 cycles. Figures 2 and 3 compare the effect of recycling in a LWR versus no-recycle for the short and long time hazards.

Table 1 Relative contribution of actinides and their daughters to the hazard measure of the waste and of each actinide and its daughters to actinide waste with 99.5% of U + Pu extracted[5]

Nuclides to Waste	Water required for dilution to the RCG[a] (% of total water required for the mixture) for decay times (yr) of: 10^2	5×10^2	10^4	10^5	10^6
	All Components of Waste:[b]				
Actinides	0.3	94	94	98	99
Fission Products	99+	5	6	2	1
Structural	0.04	1	0.2	0.03	4×10^{-4}
	Actinide Waste:[b]				
Americium	51	56	24	8	8
Curium	41	37	59	9	1
Neptunium	0.2	0.3	12	80	89
0.5% U + 0.5% Pu	8	7.7	5	3	1
Other	5×10^{-3}	1×10^{-3}	5×10^{-2}	6×10^{-3}	nil

[a]Using CFR RCGs and recommended default values for the unlisted nuclides.[8]

[b]Round-off may cause column not to total 100.

Table 2 Effect of recycle of actinides other than U and Pu on the hazard measure of waste from PWR spent fuel processing[5]

Recycle No.	Water required for dilution to RCG[a], ratio of standard to recycle[b] case (hazard reduction factor) for decay times (yr) of: 10^2	10^3	10^4	10^5	10^6
	Actinide Extraction Efficiency, 99.5%:				
0	12	15	18	28	52
1	9.3	12	13	20	46
2	8.2	10	11	18	44
3	7.6	8.4	9.3	17	43
4	7.2	7.4	8.3	17	42
5	6.8	6.6	7.5	17	42
10	5.8	4.7	5.8	17	42
20	5.1	3.8	4.9	17	42
30	5.0	3.6	4.6	17	42
	Actinide Extraction Efficiency, 99.9%:				
0	58	73	89	137	256
1	44	59	64	96	224
2	38	48	52	87	213
3	36	40	44	84	210
4	33	35	39	83	209
5	32	31	36	83	208
10	27	22	27	83	207
20	--	18	22	82	206
30	--	17	21	82	206

Using CFR RCGs and recommended default values for the unlisted nuclides.[8]

Chemical processing assumed at 150 days after reactor discharge; one cycle represents 3 years of reactor operation.

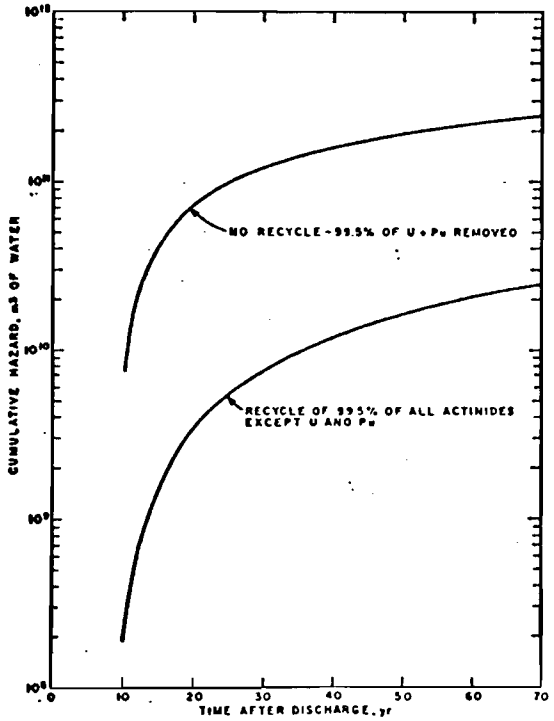

Fig. 2 Short-term cumulative hazard of actinide waste from 60-year operation of a typical PWR[5]

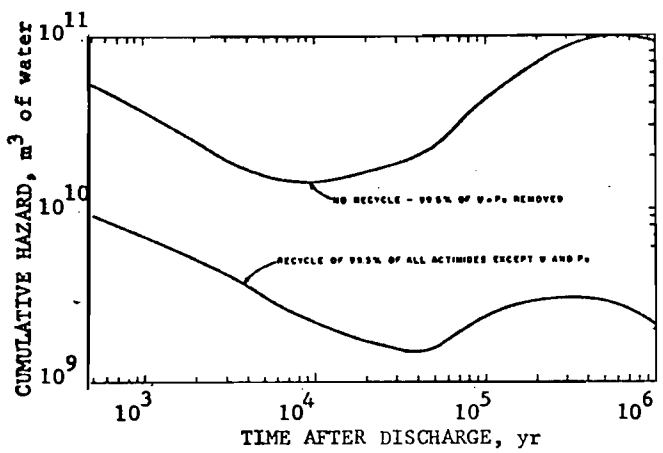

Fig. 3 Long-term cumulative hazard of actinide waste from 60-year operation of a typical PWR[5]

For the PWR examined, the decrease in the average neutron multiplication was only 0.8%. By increasing the fissile enrichment by only 2% (from 3.3 to 3.4% enrichment) the loss in reactivity can be compensated for.

The recycling of reactor actinide waste will increase radiation problems associated with chemical processing and fuel fabrication because of the increased radioactivity of the reactor feed and discharge streams. However, the increased actinide inventory in a reactor will probably have little effect on the potential danger in design basis accidents because the actinides are not volatile and, therefore, will not be significantly dispersed into the environment by any credible reactor accident.

Claiborne also states that the recycle of actinides in LMFBR's should produce even higher hazard reduction factors because of the better fission-to-capture ratio of the actinides in the presence of a fast flux. He also states that the recycling of actinides is well suited for fluid fuel reactors, such as the MSBR, because of the on-stream continuous reprocessing.

A technical group at Battelle Northwest Laboratories[9] extended Claiborne's work to provide a detailed review of the alternative method for long term radioactive waste management. Section 9 of their report was devoted to Transmutation Processing and covered four categories: (1) accelerators, (2) thermonuclear explosives, (3) fission reactors, and (4) fusion reactors. The study identified recycling in thermal power reactors as a promising method and went on to state, "consideration should also be given to evaluating the merit of having special purpose reactors optimized for destroying actinides."[9]

As reported in a review paper by Raman,[10] evaluations made by Raman, Nestor, and Dobbs[11] show that actinide inventories can be reduced further by recycling in a U^{233}-Th^{232} fueled reactor. This is made possible because neutron captures by the fertile Th^{232} produce the fissile U^{233}. Neutron capture by U^{233} results in higher U isotopes until U^{237} is reached. Plutonium and transplutonium isotopes are generated to a far lesser extent in a U^{233}-Th^{232} reactor than in a U^{235}-U^{238} reactor. Raman also stressed the need for more accurate cross section measurements.

The recycling of actinides in fast reactors has also been studied.[12,13,14,15] Greater actinide burnup is achievable in a fast reactor than in a thermal reactor because the fission-to-capture ratio is generally higher as shown in Table 3. In a 1973 review paper in Science, Kubo and Rose[16] suggested that recycling of actinides in an LMFBR has several advantages over recycling in a thermal reactor including the possibility that extreme chemical separations may not be required because fewer actinides are produced in a fast spectrum.

Paternoster, Ohanian, Schneider, Thom, and Schwenk[17,18,19] have studied the use of the gas core reactor for transmutation of fission products and actinide wastes. The fuel was UF_6 enriched to 6% in U^{235}. The four meter diameter core was surrounded by a reflector-moderator of D_2O with a thickness of 0.5 meter. The initial mass was 140 kg of $U^{235}F_6$. Adjustable control rods were located in the outer graphite reflector and the radioactive wastes were loaded in target ports. Figure 4 shows results of calculations, comparing both actinide and fission product waste in current LWR's with the gaseous fuel power reactor. Notice that after 800-1000 days, the actinide wastes in the gaseous core reactor are an order of magnitude less than those in a LWR.

In a study sponsored by NASA, Clement, Rust, and Williams[20,21] analyzed a gas core breeder reactor using a U^{233}-Th^{232} fuel cycle. One- and two-dimensional calculations were carried out for a UF_6 fueled core surrounded by a molten salt blanket. Figure 5 shows a diagram of the reactor. The medium fission energy in the core was found to be 300 keV, and there was some spectrum softening in the blanket.

Table 3 Fission-to-capture ratios of actinides in fast and thermal reactors[10]

Isotope	Half-Life Years	Fast Spectrum	Thermal Spectrum
Np^{237}	2.14×10^{6}	0.213	1.26×10^{-4}
Am^{241}	433	0.115	4.48×10^{-3}
Am^{242m}	152	4.85	1.12
Am^{243}	7370	0.309	4.87×10^{-4}
Cm^{244}	17.9	1.25	0.068

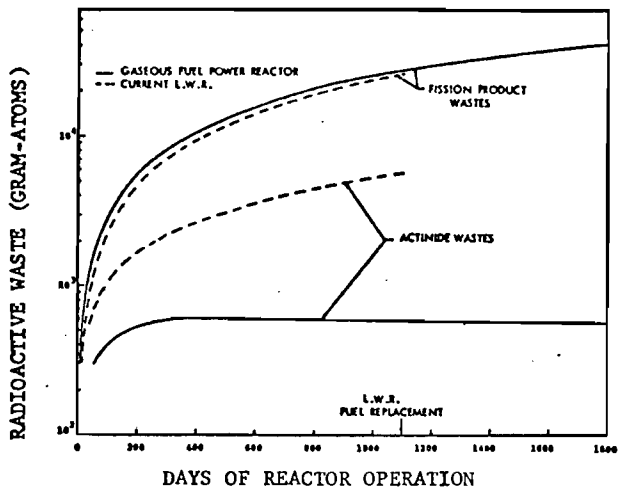

Fig. 4 Radioactive waste production of 3425 MW(t) fission power reactors[19]

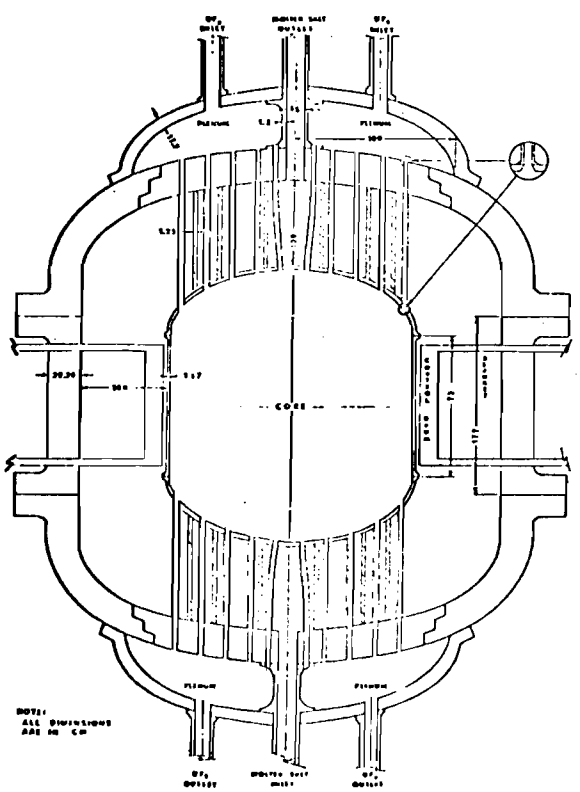

Fig. 5 UF_6 gas-core reactor

Table 4 is a brief summary of some important dates in the history of the GCATR. As previously stated, the burnup of fission products requires thermal neutron fluxes of the order of 10^{17} n/cm^2-sec. In the United States, the two reactors with the highest neutron fluxes are the ORNL High Flux Isotope Reactor (HFIR)[22] and the SRL High Flux Reactor (HFR)[23] which have maximum neutron fluxes of 3×10^{15} and 5×10^{15} n/cm^2-sec, respectively. Both of these reactors employ solid fuels and have essentially reached the upper limit in neutron fluxes because of heat transfer limitations. In addition, when operating at these neutron fluxes the refueling intervals are of the order of two weeks. The gas core reactor does not have the in-core heat transfer limitations posed by solid core reactors employing a coolant and, consequently, higher neutron fluxes should be achievable. In addition, reactor shutdown for refueling is not necessary because new fuel can be continuously added to the UF_6 during reactor operation. Therefore, a gas core reactor may be the only practical reactor for consideration of fission product burnup if such a scheme of waste disposal is considered desirable.

Table 4 Some dates in the history of GCATR

1960-73	- NASA sponsored research on gas-core reactor for rocket propulsion
1964	- Steinberg first suggests neutron-induced transmutation
1972	- Claiborne's studies of actinide recycling in LWR's
1973	- documentation of ORIGEN program
1974	- recycling studies in LWR's, LMFBR's, HTGR's by Croff, Raman, et al.
1974	- suggestion of GCATR by Paternoster, Ohanian, Schneider (University of Florida) and Thom (NASA)
1974-75	- UF_6 breeder reactor study at Georgia Tech sponsored by NASA
1976	- GCATR study at Georgia Tech sponsored by NASA

Table 5 summarizes some of the advantages of the GCATR which appear to make it an attractive candidate for actinide transmutation.

Table 5 Some advantages of the gas-core reactor

(1) The gaseous state of the fuel significantly reduces problems of processing and recycling fuel and wastes.

(2) High neutron fluxes are achievable.

(3) The possibility of using a molten salt in the blanket may also simplify the reprocessing problem and permit breeding.

(4) The spectrum can be varied from fast to thermal by increasing the moderation in the blanket so that the trade-off of critical mass versus actinide and fission product burnup can be studied for optimization.

(5) The U^{233}-Th cycle, which can be used, is superior to the U^{235}-Pu cycle in regard to actinide burnup.

III. GCATR Research Program

The overall objective of the NASA sponsored program is to study the feasibility, design, and optimization of a GCATR. The program involves three interrelated and concurrent tasks, as listed in Table 6.

Table 6 NASA sponsored GCATR research at Georgia Tech

General Studies
Update cross-sections
Sensitivity analysis
Parametric survey
Reactor and System Design
Design criteria
Reactor subsystem
(a) $^{233}UF_6$
(b) plasma core
Fuel and actinide insertion and recycling
Economic Analysis
Comparison of GCATR with other strategies

TASK 1 General Studies

Raman[9] has pointed out the need for more accurate cross section data and the necessity of assessing the sensitivity of the calculational results to the uncertainties in cross sections. This task will include the following subtasks:

A. Literature Survey and Cross Section Tabulation--A literature survey will be carried out and the best available cross sections of the fission products and actinides will be tabulated. Improved values will be used as they become available.

B. Implementation of a Versatile Depletion Program--ORIGEN[8] or a similar computer code will be implemented or developed. A depletion code which solves the equations of radioactive growth and decay and neutron transmutation for large numbers of isotopes is required. ORIGEN has been used previously for LWR's, LMFBR's, MSBR's, and HTGR's, and may also be suitable for the GCATR.

C. Parametric Survey Calculations--Parametric survey calculations will be performed to examine the effort of reactor spectrum, and flux level on the actinide transmutation for GCATR conditions. The sensitivity of the results to neutron cross sections will be assessed. These studies will be related to the nuclear analysis work of TASK 2. Specifically, the parametric calculations of the actinide transmutation will include the mass, isotope composition, fission and capture rates, reactivity effects, and neutron activity of the recycled actinides. Table 7 summarizes the most important parameters to te investigated.

Table 7 Most important parameters to be investigated

(1) The mass and composition of the actinides being recycled
(2) The rate at which the recycled actinides are fissioned and transmuted in the reactor
(3) The effect of the recycled actinides on fission reactor criticality and reactivity
(4) The effect of the recycled actinides on the out-of-reactor nuclear fuel cycle (i.e., fabrication, shipping, reprocessing, actinide inventory, etc.)

TASK 2 GCATR Design Studies

This task is a major thrust of the proposed research program. Four subtasks are considered:

A. Optimization Criteria Studies
B. Design Studies of the Reactor Subsystem
C. Design Studies of the Blanket and Fuel Reprocessing and Actinide Insertion and Recirculation System
D. System Integration

In subtask A, Optimization Criteria Studies, consideration will be given to understanding the trade-offs that are made to achieve a given result. For example, is the GCATR to be used only for actinide burnup? Should we also include breeding (U^{233}-Th) or fission product transmutation? If we reduce the mean neutron energy to achieve faster fission product burnup, how much do we sacrifice in actinide burnup? Should the reactor also be used to produce power? If so, how much power? What are the optimization criteria?

In subtask B, Design Studies of the Reactor Subsystem, a multidisciplinary approach similar to that in Refs. 20, 21 will be carried out involving:

(1) Materials
(2) Nuclear Analysis
(3) Thermodynamics and Heat Transfer
(4) Mechanical Design.

Results of this task will be used iteratively with the parametric study described in TASK 1. In previous work[20,21] one-dimensional and two-dimensional survey calculations were carried out for a UF_6-fueled core surrounded by a molten salt blanket, and a preliminary mechanical design was developed. This work will be extended to include the insertion of fission products and actinides in various locations in the reactor. The effect of other reactor component changes such as using different reflector materials (carbon, beryllium, deuterium oxide) or modifying the molten salt reflector by the addition of moderator will also be evaluated. Best available cross section data from TASK 1 will be utilized. A preliminary reactor design will be developed taking into account thermal and mechanical design considerations.

In subtask C, a preliminary design of the UF_6 and blanket reprocessing system (if molten salt) will be prepared and performance of the systems analyzed. Equilibrium fuel and blanket compositions including fission products and actinides will be computed. These results will provide necessary

information on equilibrium core and blanket compositions for use in the nuclear analyses.

Subtask D, System Integration, involves putting all the sub-components together in a workable system taking account of criticality, shielding, and economic considerations.

TASK 3 Comparison of the GCATR with Other Nuclear Waste Management Strategies

The cost of the GCATR shall be evaluated in terms of mills/kwhre. The cost can be broken down into the components:

(1) solid and liquid storage
(2) shipping
(3) interim retrievable storage separations
(4) separation
(5) disposal or elimination in GCATR

The total cost of the management system will be computed and compared to the cost of alternate strategies presently being considered.

As of June 1976, the research program has been underway for only two months. Table 8 summarizes the status of the program at this time.

Table 8 Summary of Georgia Tech GCATR research program to date

General Studies
1. Actinide cross sections have been updated
2. ORIGEN has been implemented and modified
3. Some sensitivity results and parametric studies have been obtained

Reactor Studies
1. Series of nuclear design codes have been implemented
2. Several configurations of $^{233}UF_6$ reactor are being analyzed

IV. References

1. Smith, J. A., "Proceedings of the Californium-252 Symposium," USAEC Report CONF-681032, p. 179 (1969)

2. "Waste Management Symposium," Nuclear Technology, 24 (December 1974)

3. Steinberg, M., Molzak, G., and Menovita, B., "Neutron Burning of Long-Lived Fission Products for Waste Disposal," BNL-8558, Brookhaven National Laboratory (September 1964)

4. Gregory, M. V. and Steinberg, M., "A Nuclear Transmutation System for Disposal of Long-Lived Fission Product Waste in an Expanding Nuclear Power Economy," BNL-1195 (November 1967)

5. Claiborne, H. C., "Neutron Induced Transmutation of High-Level Radioactive Wastes," ORNL-TM-3964 (December 1972)

6. Claiborne, H. C., "Effect of Actinide Removal on the Long-Term Hazard of High-Level Waste," ORNL Report TM-4724 (1975)

7. Bond, W. D., Claiborne, H. C., and Levze, R. E., "Methods for Removal of Actinides from High Level Wastes," Nuclear Technology, 24, 362-370 (December 1974)

8. Bell, M. J., "ORIGEN--The ORNL Isotope Generation and Depletion Code," ORNL-4628, Oak Ridge National Laboratory (May 1973)

9. Schneider, K. J. and Plat, A. M., "High-Level Radioactive Waste Management Alternatives," BNWL Report 1900 (1974)

10. Raman, S., "Some Activities in the United States Concerning the Physics Aspects of Actinide Waste Recycling," Review Paper from ORNL (1975)

11. Raman, S., Nestor, C. W., Jr., and Dabbs, J. W. T., "The U^{233}-Th^{232} Reactor as a Burner for Actinide Wastes," Proc. of the Conf. on Nuclear Cross Sections and Technology, Washington, D. C. (March 1975)

12. Breen, R., "Elimination of Actinides with LMFBR Recycle," Westinghouse Advanced Reactors Division, private communication reported in Ref. 10

13. Beaman, S. L., "Actinide Recycle Evaluations," General Electric Energy Systems and Technology Division, private communication reported in Ref. 10

14. Croff, A. G., "Parameter Studies Concerning Actinide Transmutation in Power Reactors," Transactions of the American Nuclear Society, 22, 345 (November 1975)

15. Davidson, J. W. and Draper, E. L., Jr., "Costs for Partitioning Strategies in High-Level Waste Management," Transactions of the American Nuclear Society, 22, 348 (November 1975)

16. Kubo, A. S. and Rose, D. J., "On Disposal of Nuclear Waste," Science, 182, No. 4118, 1205-1211 (December 1973)

17. Paternoster, R., Ohanian, M. J., Schneider, R. T. and Thom, K., "Nuclear Waste Disposal Utilizing a Gaseous Core Reactor," Transactions of the American Nuclear Society, 19, 203 (October 1974)

18. Paternoster, R. R., "Nuclear Waste Disposal Utilizing a Gaseous Core Reactor," Master's Thesis, University of Florida (1974)

19. Schwenk, F. C. and Thom, K. T., "Gaseous Fuel Nuclear Reactor Research," Paper presented at the Oklahoma State University Conference on Frontiers of Power Technology (October 1974)

20. Clement, J. D., Rust, J. H., and Williams, J. R., "Analysis of UF_6 Breeder Reactor Power Plants," Semi-annual Report NASA Grant NSG-1168 (October 1975)

21. Rust, J. H. and Clement, J. D., "UF_6 Breeder Reactor Power Plants for Electric Power Generation," Proc. Third Symposium on Uranium Plasmas, Princeton University Conference, June 10-12, 1976

22. Binford, F. T., et al., "The High-Flux Isotope Reactor," ORNL-3572 (Rev. 2) (May 1968)

23. Crandall, J. L., "The Savannah River High Flux Demonstration," USAEC Report DP-999 (1965)

E-26-621

SEMI-ANNUAL REPORT

NASA GRANT NSG-1288

SUPPLEMENT NO. 1

ANALYSIS OF THE GAS CORE ACTINIDE TRANSMUTATION REACTOR (GCATR)

J. D. Clement and J. H. Rust

NASA Program Manager, F. Hohl

Prepared for the

National Aeronautics and Space Administration

by the

School of Nuclear Engineering
Georgia Institute of Technology
Atlanta, Georgia 30332

September 1, 1977

SEMI-ANNUAL REPORT

NASA GRANT NSG-1288

SUPPLEMENT NO. 1

ANALYSIS OF THE GAS CORE ACTINIDE TRANSMUTATION REACTOR (GCATR)

J. D. Clement and J. H. Rust

NASA Program Manager, F. Hohl

Prepared for the

National Aeronautics and Space Administration

by the

School of Nuclear Engineering
Georgia Institute of Technology
Atlanta, Georgia 30332

September 1, 1977

ACKNOWLEDGMENTS

This work was supported by NASA Grant NSG-1288, Supplement No. 1. The authors wish to express their appreciation to the program manager, Dr. Frank Hohl, for helpful suggestions during the performance of the research.

The following graduate students, supported by the grant, made significant contributions to the research project: Bruce Byrne, John Massey, and Pak Tai Wan.

In addition, the NASA research program was also used as a design project for the Nuclear Engineering design course in the academic curriculum. The following graduate students were of great assistance in the research work: Constantine Bratianu, Stanley Chow, Trent Primm, and Scott Revolinski.

TABLE OF CONTENTS

LIST OF TABLES

LIST OF TABLES (Continued)

LIST OF FIGURES

LIST OF FIGURES (Continued)

LIST OF FIGURES (Continued)

ABSTRACT

The work summarized in this report, which was carried out as a part of a NASA sponsored fissioning plasma research program, consisted of design power plant studies for two applications of the plasma core reactor:

(1) As a breeder reactor

(2) As a reactor able to transmute actinides effectively.

In addition to the above applications the reactor produced electrical power with a high efficiency.

A reactor subsystem was designed for each of the two applications. Tables 1 and 2 summarize the reactor design parameters for the breeder and the actinide transmuter, respectively.

For the breeder reactor, neutronics calculations were carried out for a U-233 plasma core with a molten salt breeding blanket. The primary objectives of the overall nuclear design were to design a reactor with a low critical mass (less than a few hundred kilograms U-233) and also a breeding ratio of 1.01. The later objective was a safety precaution to guard against diversion of fissionable material during blanket reprocessing. Since only enough U-233 would be bred in the blanket to replenish the amount depleted in the core, any diversion of U-233 during reprocessing would result in an insufficient amount of fissionable material to replenish the core and the reactor would shut down. Both of the above objectives were met in the final design. It is also possible to design for much higher breeding ratios in the range 1.1-1.2.

The Plasma Core Actinide Transmutation reactor was designed to transmute the nuclear waste from conventional LWR's. Each LWR is loaded with

Table 1. Plasma Core Breeder Reactor Reference Design

Dimensions of Reactor Regions

U^{233} Plasma	- 165 cm O.D.
Helium	- 285 cm O.D.
BeO Moderator	- 325 cm O.D.
Molten Salt*	- 355 cm O.D.
BeO Reflector	- 375 cm O.D.
Fe Pressure Shell	- 415 cm O.D.

Critical Mass	- 26.3 Kg
Breeding Ratio	- 1.0099
Power	- 2000 MWt
Average Thermal Flux in Plasma	- $3.42 \times 10^{15} \frac{\text{neutrons}}{\text{cm}^2 \text{ sec}}$
Reactor Pressure	- 200 atm
Average Temperatures	
U^{233} Plasma	- 25,000°K
Helium	- 3,000°K
Molten Salt	- 1,015°K
Molten Salt Mass Flow Rate	- 542 Kg/sec

*Molten Salt Composition - 71.7% LiF (99.995% Li^7), 16% BeF_2, 12.3% ThF_4

Table 2. Reactor Characteristics of Plasma Core Actinide Transmutation Reactor

Reference Design:

Geometry: Spherical

Dimensions of reactor regions:

U^{233} plasma	200 cm	thickness
He	120 cm	thickness
Be moderator	17 cm	thickness
*Act. Oxide + Zr + He	0.85 cm	thickness
Be reflector	80-90 cm	thickness

Critical mass = 380 Kg

Mass of actinides = 1.27 metric tonne

Power = 2000 MWt

Avg. thermal flux in plasma = 2.06×10^{15} n/cm^2-sec

Avg. thermal flux in actinides = 1.23×10^{14} n/cm^2-sec

Reactor pressure = 200 atm.

Temp:

U^{233} plasma	25000°K
He	3000°K
Be moderator	1000°K
Act. Oxide + Zr + He	800°K
Be Reflector	400-600°K.

*Actinide Composition: 74 atomic% Np^{237}; 7 atomic% Am^{241}; 14 atomic% Am^{243} 4 atomic% Cm^{244}.

88 metric tonne of uranium (3.3% U^{235}) and operated until a burnup of 33,000 MWD/MTU is reached. The fuel is discharged from the reactor and cooled for 160 days. Next, the spent fuel is reprocessed during which 100% of Np, Am, Cm, and higher actinides are separated from the other components. The concentrations of these actinides are calculated by ORIGEN and tabulated. These actinides are then manufactured as oxides into zirconium clad fuel rods and charged as fuel assemblies in the reflector region of the plasma core actinide transmutation reactor. Results of actinide burnup calculations for an equilibrium plasma core transmuter servicing 27 PWR's show that after 13 cycles the actinide inventory has stabilized to about 2.6 times its initial loading. There are two mechanisms for the removal of actinides:

(1) They are fissioned directly in the plasma core actinide transmuter

(2) They are removed as U or Pu.

The U and Pu can be used in other reactors. In the equilibrium cycle, about 7% of the actinides are directly fissioned away, while about 31% is removed by reprocessing.

Fluid mechanics, heat transfer, and mechanical design considerations for both reactors are described in the report.

Since it is desirable to have the Plasma Core Breeder Reactor (PCBR) be a self-contained unit, generating its own new fuel, an on-line reprocessing system for the molten salt blanket is a necessity. Chapter 8 describes protactinium removal and salt purification processes, calculations of expected flow rates, and equilibrium concentrations of various isotopes present in the system.

In order to achieve maximum effectiveness from the high temperature coolants from either of the two plasma core reactors, it was decided that a ternary power cycle would produce the highest efficiency power plant. The ternary cycle consists of a combination of MHD, gas turbine, and Rankine cycle energy conversion units. Two concepts were investigated — systems with and without a high temperature regenerator in the helium loop.

The achieved objectives of the study were as follows:

(1) Model the nuclear MHD power plant cycle.

(2) Analyze the power output from the three energy conversion units and evaluate plant overall efficiency.

(3) Make a parametric study of the effect of changing operating variables on plant overall performance.

All studies used values for input data according to current commercial technology (i.e. efficiencies for steam cycle components, gas turbine, and compressors) or with current use in MHD research.

The modeling of the MHD cycle consisted of defining a pseudo-Brayton cycle and treating the expansion within the MHD generator in a similar manner as in a gas turbine. In order to analyse the two systems it was necessary to write two computer codes:

(1) NMHD-1 — code to analyze the nuclear MHD power plant without regeneration in the helium loop

(2) NMHD-2 — code to analyze the nuclear MHD power plant with regeneration in the helium loop.

Table 3 lists input parameters for each system.

A study was made of the effect on overall efficiency of varying the reactor coolant outlet temperature from 3000°K to 4000°K for the two

systems. Table 4 lists typical results, showing an overall plant efficiency as large as 70%.

For Nuclear MHD Power Plant with regeneration, the major contribution of the electric power is produced in the top of the power cycle by the MHD subsystem (33.97% - 45.49% from 100% heat produced by the reactor). The power production has been shifted toward the top of the ternary cycle with a positive effect on overall efficiency. This system produces overall efficiencies that are 25-35% higher than actual power plants in use and that are 15-20% higher than the expected coal-fired MHD power plants.

For Nuclear MHD Power Plants without regeneration, the major contribution of electric power is due to the steam turbine subsystem (36.03% - 36.36% from 100% heat produced by the reactor). Due to a significant fraction of the electric power being produced by the steam cycle with a low efficiency (40%), it is desirable to shift the power production toward the top of the cycle to improve the overall efficiency. This can be achieved by reducing the mass flow rate of helium within the inner loop and increasing the pressure ratio of the MHD generator. This system produced overall efficiencies that are 15-20% higher than actual power plants in use and that are 5-10% higher than the expected coal-fired MHD power plant. Due to the relatively low temperatures within the helium loop, this type of power plant could be considered as a first step in a national program of implementation of MHD power plants with a nuclear source.

Table 3. Input Data for NMHD-1 and NMHD-2

Index	NMHD-1		NMHD-2	
1	Boiler Temperature ----	1000°F	Boiler Temperature ----	1000.°F
2	Boiler Pressure -------	1600 psia	Boiler Pressure -------	1600 psia
3	Condenser Pressure ----	1.0 psia	Condenser Pressure ----	1.0 psia
4	Steam Turbine Efficiency	81%	Steam Turbine Efficiency	81%
5	Pump Efficiency -------	80%	Number of Feed Heaters	0,1 or 2
6	Number of Feed Heaters	0,1 or 2	Reactor Temp Difference	200°K
7	Compressor Efficiency -	85%	Compressor Efficiency -	85%
8	MHD Inlet Temp --------	3000°K	MHD Inlet Temp --------	3000°K
9	MHD Inlet Press -------	200 bar	MHD Inlet Press -------	200 bar
10	MHD Pressure Ratio ----	5.0	MHD Pressure Ratio ----	3.0
11	Gas Turbine Pressure Ratio	2.0	Gas Turbine Press. ratio	3.0
12	Feed Heater 1 Pressure	12. psia	Feed Heater 1 press. --	12. psia
13	Feed Heater 2 Pressure -	4. psia	Feed Heater 2 press. --	4.0 psia
14	Bottom Temp Difference -	150°K	Bottom Temp Diff. ----	150°K
15	MHD Inlet Mach No. ----	0.5	MHD Inlet Mach No. ----	0.5
16	Sep Outlet Mach No. ----	0.1	Sep Outlet Mach No. ---	0.1
17	Gas Turbine Inlet Temp -	1500°K	Gas Turbine Inlet Temp	1500°K
18	MHD Efficiency ---------	49%	MHD Efficiency --------	49%
19	Gas Turbine Efficiency -	85%	Gas Turbine Efficiency	85%
20	Number of Compress Stages	3.0	Number of Compress Stages	3.0

Table 4. Plant Net Overall Efficiencies For MHD Inlet Temperature Variation

MHD Inlet Temperature	3000°K		3250°K		3500°K		3750°K		4000°K	
Q_R	4973.45	100.0%	5138.94	100.00%	5299.94	100.00%	5458.27	100.0%	5693.55	100.0%
W_{MHD}	1689.52	33.97%	1914.65	37.26%	2139.78	40.37%	2139.78	43.44%	2590.04	45.49%
W_{GT}	319.12	6.42%	319.12	6.21%	319.12	6.02%	319.12	5.85%	319.12	5.60%
W_{ST}	1112.20	22.36%	1112.20	21.64%	1112.20	20.99%	1112.20	20.38%	1112.20	19.53%
η_{PLANT}	62.75%		65.11%		67.38%		69.56%		70.62%	

Q_R = REACTOR HEAT RATE

W_{MHD} = MHD NET ELECTRIC POWER: $W_{MHD} = W_{MHD}$ OUTPUT $- W_{COMPRESSOR}$

W_{GT} = GAS TURBINE ELECTRIC POWER: $W_{GT} = W_{GT}$ OUTPUT $- 2 \times W_{COMPRESSOR}$

W_{ST} = STEAM TURBINE ELECTRIC POWER: $W_{ST} = W_{ST}$ OUTPUT $- W_{PUMP}$

$$\eta_{PLANT} = \left(\frac{W_{MHD}}{Q_R} + \frac{W_{GT}}{G_R} + \frac{W_{ST}}{Q_R}\right) \times 100 = \left(\frac{W_{MHD}}{Q_R}\,100\right) + \left(\frac{W_{GT}}{Q_R}\,100\right) + \left(\frac{W_{ST}}{Q_R}\,100\right) \quad [\%]$$

1. INTRODUCTION

As part of its policy of supporting research and development programs which reside on the frontier of power technology, the National Aeronautics and Space Administration has sponsored work in gaseous fueled reactors and plasma research. The original thrust of the NASA sponsored research, aimed toward development of a space propulsion engine, led to two gas-core reactor concepts - the light bulb and the coaxial flow nuclear reactor concepts.[1-10] Although budgetary and policy factors terminated the development of nuclear powered propulsion engines, the concept of a UF_6 fueled gas core reactor was shown to be very attractive for several other applications.

NASA has continued supporting an ongoing fissioning plasma research program consisting of cavity reactor criticality tests, fluid mechanics tests, investigations of uranium optical emission spectra, radiant heat transfer, power plant studies, and related theoretical work.[10-13] These studies have shown that UF_6 fueled reactors can be quite versatile with respect to power, pressure, operating temperature, and the modes of power extraction. Possible power conversion systems include Brayton cycles, Rankine cycles, MHD generators, and thermionic diodes.[12,13,14,17,18] Recent results of research on the pumping of lasers by fission fragment interactions with a laser gas mixture indicate the possibility of the power extraction in the form of coherent light.[10,12] Another potential application of the gas core reactor is its use for nuclear waste disposal by nuclear transmutation (Gas Core Actinide Transmutation Reactor, GCATR).[10,12,19,20]

Recent work sponsored by NASA at Georgia Tech on the Gas Core Breeder Reactor was reported in References 17 and 18. Further work on

the Gas Core Actinide Transmutation Reactor was reported in Refs. 19 and 20.

This semi-annual report summarizes results of work performed from March 1, 1977 to August 31, 1977 and NASA Research Grant NSG-1288. Work was performed in connection with the UF_6 fuel under near "state-of-the art" temperature conditions, and also on the high temperature fissioning-plasma co-axial flow scheme. This report contains results for the application of the high temperature fissioning-plasma core to transmutation and breeding.

Chapters 2 to 5 apply to the plasma core transmutation reactor and Chapters 6 and 7 relate to the breeder. Chapter 8 applies to both the MHD generator, a component in both systems, and Chapter 10 encompasses the system designs for both applications, showing why the fissioning plasma system is so extraordinarily attractive.

REFERENCES FOR CHAPTER 1

1. RAGSDALE, R. G., "To Mars in 30 Days by Gas Core Nuclear Rocket," Astronautics and Aeronautics, 10, 1 (1971).

2. KUHRT, W. A., "Space Propulsion in the Fiscal Year 2001," Fourth Goddard Memorial Symposium, Space Age in the Fiscal Year 2001, American Astronautical Society, Washington, D. C., (1966).

3. THOM, K., and R. T. SCHNEIDER, editors, "Research on Uranium Plasmas and Their Technological Applications," Proceedings of a Symposium, NASA SP-236 , U. S. Government Printing Office, (1971).

4. RAGSDALE, R. G., "2nd Smyposium on Uranium Plasmas: Research and Applications," AIAA (1971).

5. CLEMENT, J. D., and J. R. WILLIAMS, "Gas Core Reactor Technology," Reactor Technology, 13, 3 (1970).

6. THOM, K., "Review of Fission Engine Concepts," J. Spacecraft and Rockets, 9 (1972).

7. THOM, K., and R. T. SCHNEIDER, "Fissioning Uranium Plasmas," Nuclear Data in Science and Technology, 1, 15-38, International Atomic Energy Agency, Vienna, Austria (1973).

8. ROM, F. E., and RAGSDALE, R. G., "Advanced Concepts for Nuclear Rocket Propulsion," NASA SP-20, U. S. Government Printing Office (1969).

9. SCHWENK, F. C., and FRANKLIN, C. E., "Comparison of Closed-and Open-Cycle Systems," Research on Uranium Plasmas and Their Technological Applications, NASA SP-236, 3-13, U. S. Government Printing Office (1971).

10. THOM, K., R. T., SCHNEIDER, and F. C. SCHWENK, "Physics and Potentials of Fissioning Plasmas for Space Power and Propulsion," International Astronautical Federation 25th Congress, Paper No. 74087, Amsterdam (October 1974).

11. WILLIAMS, J. R., J. D. CLEMENT, and J. H. RUST, "Analysis of UF_6 Breeder Reactor Power Plants," Progress Rept. No. 1, NASA-7067, Georgia Institute of Technology, Atlanta, Ga. (November 1974).

12. SCHWENK, F. C., and K. T. THOM, "Gaseous Fuel Nuclear Reactor Research," Paper presented at the Oklahoma State University Conference on Frontiers of Power Technology (October 1974).

13. WILLIAMS, J. R., and J. D. CLEMENT, "Exploratory Study of Several Advanced Nuclear-MHD Power Plant Systems," Final Status Report, NASA Grant NGR-11-002-145, Georgia Institute of Technology, Atlanta, Georgia (March 1973).

14. CLEMENT, J. D., J. H. RUST, and J. R. WILLIAMS, "Analysis of UF_6 Breeder Reactor Power Plants," Semi-annual Report NASA Grant NSG-1168 (October 1975).

15. PATERNOSTER, R., M. J. OHANIAN, R. T. SCHNEIDER, and K. THOM, "Nuclear Waste Disposal Utilizing a Gaseous Core Reactor," Transactions of the American Nuclear Society, 19, 203 (October 1974).

16. WILLIAMS, J. R., J. D. CLEMENT, and J. R. RUST, "The UF_6 Breeder: A solution to the Problems of Nuclear Powers." Presented at the Inter Society Energy Conversion Conference (August 11-15, 1975).

17. CLEMENT, J. D., and J. H. RUST, "Analysis of UF_6 Breeder Reactor Power Plants, Final Report NASA Grant NSG-1168 (February 1976).

18. CLEMENT, J. D., J. H. RUST, and F. HOHL, "UF_6 Breeder Reactor Power Plants for Electric Power Generation," Invited Paper, presented at Third Symposium on Uranium Plasmas, Princeton University, New Jersey (June 1976).

19. RUST, J. H., J. D. CLEMENT, and F. HOHL, "Georgia Tech Research on the Gas Core Actinide Transmutation Reactor (GCATR)," Invited Paper, presented at Third Symposium on Uranium Plasmas, Princeton University, New Jersey (June 1976).

20. CLEMENT, J. D., J. H. RUST, and F. HOHL, "Analysis of the Gas Core Actinide Transmutation Reactor (GCATR)," Final Report, NASA Grant NSG-1288 (February 1977).

2. NUCLEAR ANALYSIS OF THE PLASMA CORE ACTINIDE TRANSMUTATION REACTOR

The objectives of the nuclear analysis of the plasma core actinide transmutation reactor are:

(1) design a reactor system capable of producing power;

(2) design a reactor able to effectively transmute actinides.

The spent fuel discharged from a LWR consists of structural materials, unfissioned uranium, converted plutonium, other actinides, and fission products. The ratio of these components by weight is as follows:

structural	uranium	plutonium	fission products	other actinides
256	1023	9	36	1

Despite the fact that the other actinides is the smallest component, they are very long lived. After 10^5 years, most of the other components will have decayed to stable isotopes, but these actinides will still be radioactive and may be a significant health hazard in the future. This is the rationale for putting these actinides in a reactor to transmute them to short lived fission products.

The transmutation strategy used for the present calculations is shown in Fig. 2.1. The analysis was performed using the cross section code[2] MC^2, the multi-group diffusion code[3] MACH-I, and the isotope depletion code[1] ORIGEN. The flow diagram for the analysis is shown in Fig. 2.2.

Each LWR is loaded with 88 metric tonne of uranium (3.3% U^{235}) and operated until a burnup of 33,000 MWD/MTU is reached. The fuel is discharged from the reactor and cooled for 160 days. Next, the spent fuel is reprocessed during which 100% of Np, Am, Cm, and higher actinides are separated from the other components. The concentrations of these

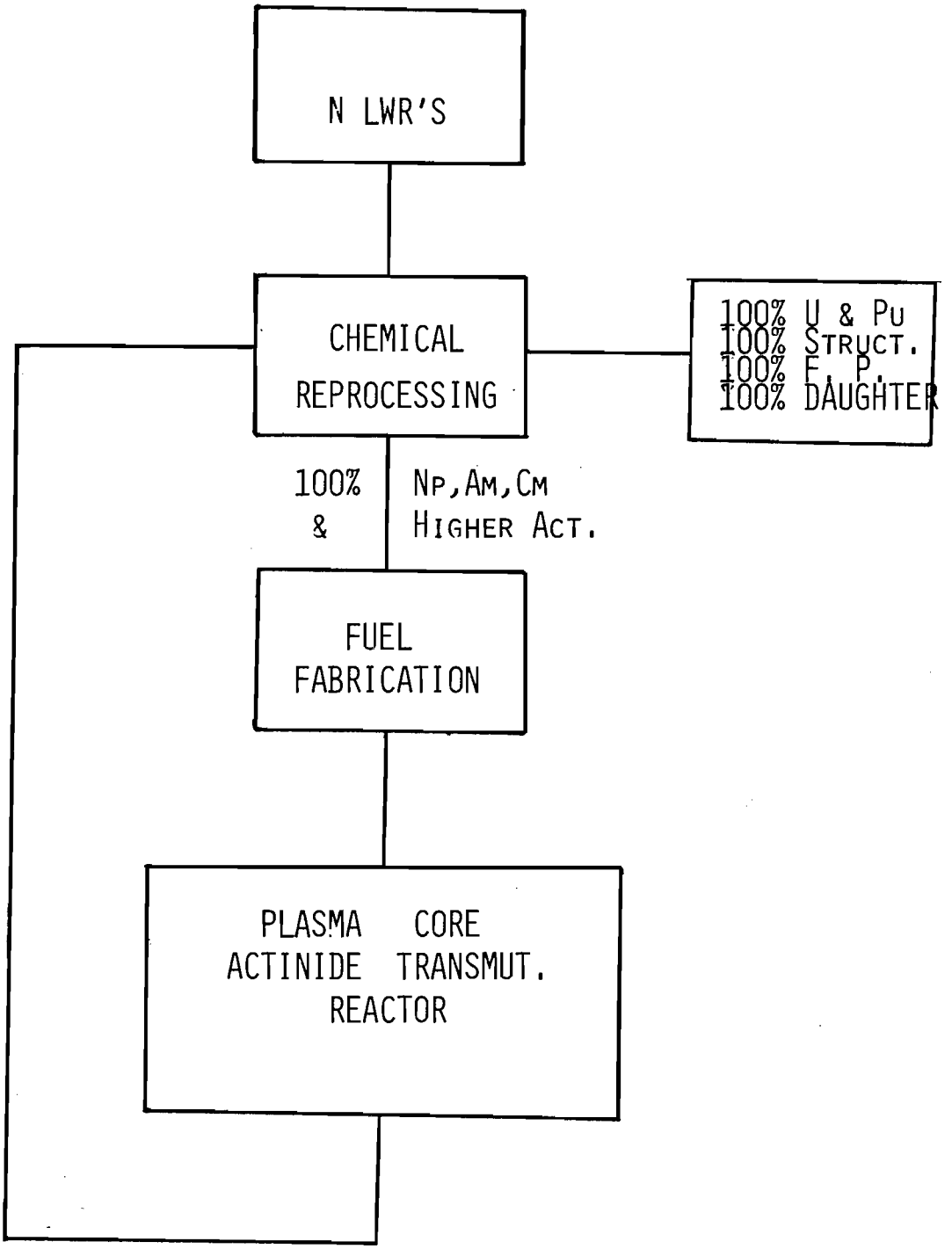

Fig. 2.1 Strategy for actinide transmutation

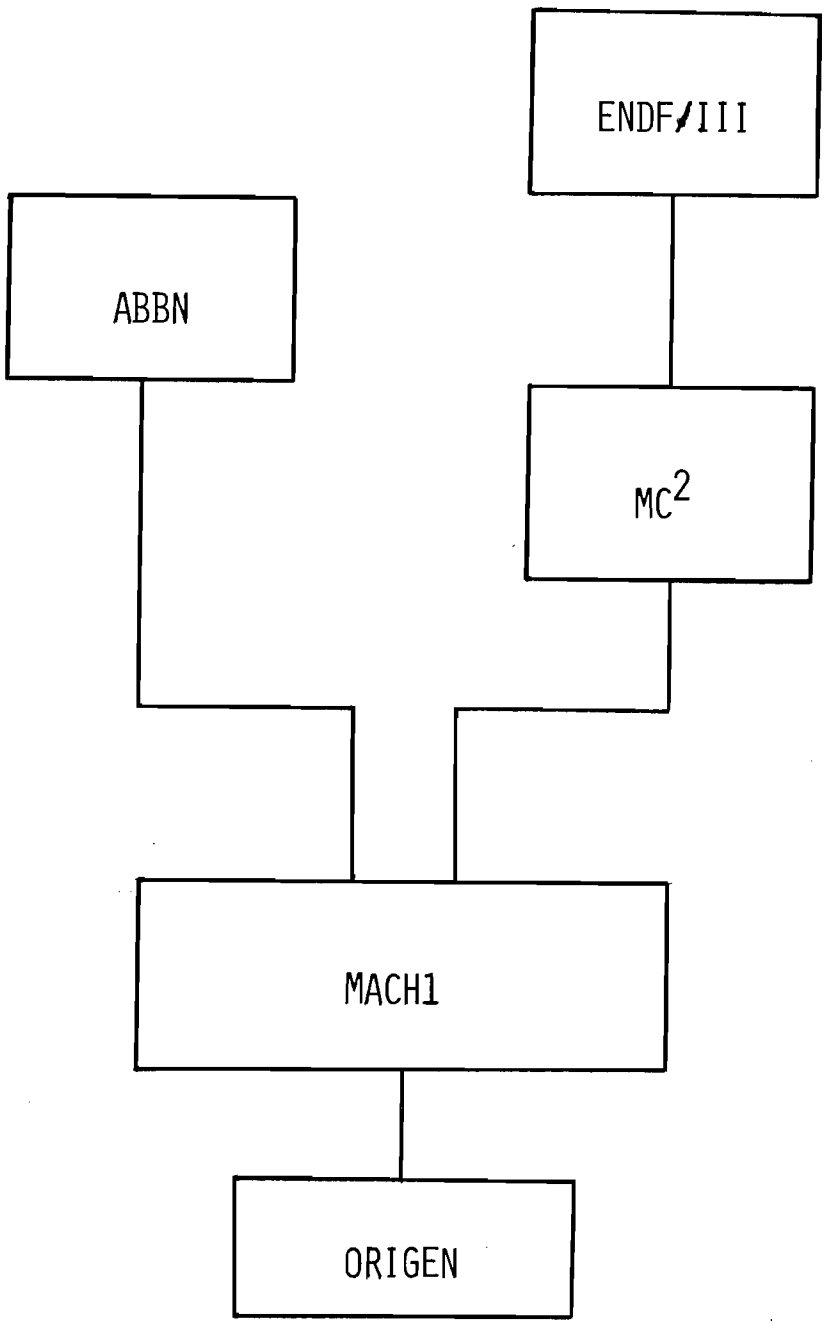

Fig. 2.2 Flowsheet of nuclear analysis computation

actinides are calculated by ORIGEN[1] and are tabulated in Table 2.1. These actinides are then manufactured into fuel rods and charged into the plasma core actinide transmutation reactor.

The basic core configuration is shown in Fig. 2.3.

For simplicity, spherical geometry is used. There are five regions:

(1) Region I consists of the hot fissioning uranium 233 plasma. The bulk temperature is assumed to be around 25,000°K at a pressure of 200 atmospheres. Because of the ionization of the uranium atoms at such temperatures, the U^{233} plasma density is lower than that predicted by the perfect gas law. The equation of state of uranium at such temperatures and pressures is given by Ragsdale.[4]

(2) Region II consists of a helium layer. The bulk temperature is assumed to be at 3,000 K at 200 atm. The perfect gas law is assumed to be valid for helium at these conditions.

(3) Region III consists of a solid liner at 1000 K. For a fast system, stainless steel is chosen as the liner material. For a thermal system, beryllium is used to act as reflector and moderator.

(4) Region IV consists of He cooled, Zr clad actinide fuel rods at 800 K, and 200 atmospheres. The actinides are assumed to be present as oxides. Only the principal actinides, Np-237, Am-241, Am-243 and Cm-244 are included. The other actinides are very small. The concentrations of this region by volume is assumed to be 43% actinide rods, 12% Zr cladding, and 45% He coolant.

(5) Region V consists of a reflector. For a fast system, iron is used; for a thermal system, beryllium is chosen.

Nuclide	Gram-atoms	Kg.
Np237	2.04+4	4.82+3
Np239	3.27-3	7.81-4
Am241	1.93+3	4.65+2
Am242m	3.87+1	9.36+0
Am242	4.65-4	1.12-4
Am243	3.89+3	9.44+2
Cm242	4.50+1	1.09+1
Cm243	3.22+0	7.82-1
Cm244	1.17+3	2.86+2
Cm245	7.89+1	1.93+1
Cm246	9.00+0	2.22+0
Cm247	1.16-1	2.86-2
Cm248	7.78-3	1.93-3
Cm250	4.49-11	1.12-11
Cf249	7.01-5	1.74-5
Cf250	1.28-5	3.20-6
Cf251	6.89-6	1.73-6
Total	2.76+4	6.57+3

Table 2.1

Actinide Concentrations Charged to Plasma Core Actinide Transmutation Reactor

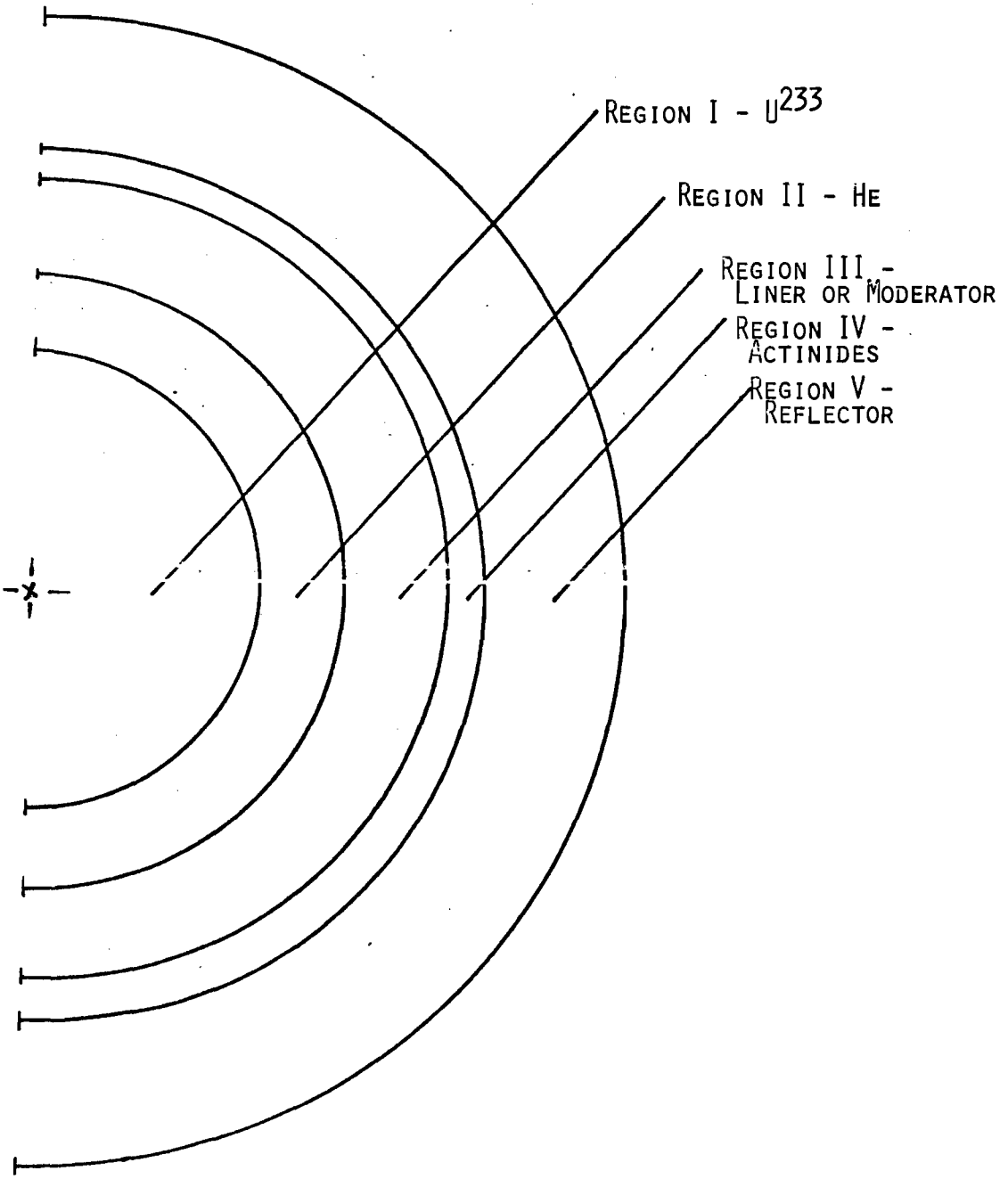

Fig. 2.3 Basic Core Configureation

Both fast and thermal reactors were studied, but the reference design was chosen to be thermal in order to keep the critical mass at a reasonable value. In thermal reactors, beryllium is placed in region III and V.

Table 2.2 summarizes the results obtained for the thermal plasma core reactor.

Table 2.2. Critical Parameters Characterizing Thermal and PCATR

Be thickness	10 cm	13 cm	15 cm	17 cm	20 cm
Critical mass	22000kg	2640kg	562kg	215kg	53kg
Critical radius	778 cm	383 cm	229 cm	166 cm	104 cm
$\bar{E}$ (source)	0.109 kev	2.08 ev	0.37 ev	0.437	0.35 ev
$\langle\sigma_f\rangle$ in act. reg.	0.29 b	0.245 b	0.186 b	0.222	0.152 b

He thickness = 25 cm., Act. region thickness = 0.85 cm., Outside Be reflector = 100 cm.

It is observed that increasing the moderation available to core neutrons reduces the critical mass of the plasma core by a factor of 400. However, as the core becomes more thermal, the average fission cross section in the actinide region also decreases.

The dimensions of the reference plasma core actinide transmutation reactor is shown in Table 2.3.

Table 2.3. Reference Plasma Core Actinide Transmutation Reactor

Region No.	Material	Thickness
I	U^{233} (25000°K, 200 atm)	200 cm (375 kg)
II	He (3000 K, 200 atm)	120 cm
III	Be (1000 K)	17 cm
IV	Act. Oxide + Zr + He (800 K, 200 atm)	0.85 cm
V	Be (400 - 600 K)	80-90 cm

Results of actinide burnup calculations for an equilibrium plasma core transmuter are shown in Table 2.4. It is observed that after 13 cycles, the actinide inventory has stabilized to about 2.6 times its initial loading. There are two mechanisms for the removal of actinides: (1) they are fissioned directly in the plasma core actinide transmuter and (2) they are removed as U or Pu. The U and Pu can be used in other reactors. In the equilibrium cycle, about 7% of the actinides are directly fissioned away, while about 31% is removed by reprocessing. This situation is illustrated in Table 2.5.

Table 2.4

Actinide Burnup in Plasma Core Actinide Transmutation Reactor
1100 days of irradiation, 265 days of cooling, 365 days of reprocessing (100% removal of U and Pu, F.P., and Daughters) and fuel fabrication, 27 PWR's serviced (1.27 metric tonnes of actinides charged per cycle).
THERM = 0.53648, RES = 1.035, FAST = 4.450, Avg. Thermal Flux = 7.04+12

Batch No.	Cycle No.												
	1	2	3	4	5	6	7	8	9	10	11	12	13
1	1.27	.752	.447	.267	.160	.099	.065	.045	.033	.026	.022	.020	.018
2		1.27	.752	.447	.267	.160	.099	.065	.045	.033	.026	.022	.020
3			1.27	.752	.447	.267	.160	.099	.065	.045	.033	.026	.022
4				1.27	.752	.447	.267	.160	.099	.065	.045	.033	.026
5					1.27	.752	.447	.267	.160	.099	.065	.033	.026
6						1.27	.752	.447	.267	.160	.099	.065	.033
7							1.27	.752	.447	.267	.160	.099	.065
8								1.27	.752	.447	.267	.160	.099
9									1.27	.752	.447	.267	.160
10										1.27	.752	.447	.267
11											1.27	.752	.447
12												1.27	.752
13													1.27
⋮													
Total	1.27	2.02	2.47	2.74	2.90	3.00	3.06	3.11	3.14	3.16	3.19	3.20	3.22

Table 2.5 Actinide Inventory During Equilibrium PCATR Cycle

Beginning of Cycle	3.3MT
Fissioned	- 0.23MT (7%)
Reproc.	- 1.02MT (31%)
End of Cycle	2.05MT
Charge	1.27MT
Beginning of Next Cycle	3.32MT

REFERENCES FOR CHAPTER 2

1. BELL, M. J., "ORIGEN - The ORNL Isotope Generation and Depletion Code," ORNL-4628 (May 1973).

2. TOPPEL, B. J., A. L. RAGO, and D. M. O'SHEA, MC^2 - A Code to Calculate Multigroup Cross Sections," ANL - 7318 (1967).

3. MENELEY, D. A., L. C. KVITEK, and D. M. O'SHEA, "MACH1 - A One-Dimensional Diffusion-Theory Package," ANL - 7223 (June 1966).

4. RAGSDALE, R. G., "Relationship between Engine Parameters and the Fuel Mass Contained in An Open-Cycle Gas Core Reactor," Proceedings of the Symposium on Research on Uranium Plasma and Their Technological Applications, Univ. of Florida (January 1970).

3. FLUID MECHANICS OF PLASMA CAVITY REACTORS

In plasma core reactors (PCR) the gaseous uranium is confined in a somewhat spherical geometry by the hydrodynamic forces exerted by the coolant. The coolant enters radially towards the central uranium plasma, providing both containment and cooling. Due to the nature of processes inherent to PCRs, there are some very interesting fluid dynamic problems. The gaseous uranium metal is not completely confined by the coolant and, therefore, moves slowly through the cavity and is exhausted with the coolant. As the plasma moves through the core it radiates its energy to the coolant, which leaves the reactor in the neighborhood of $3000^{o}K$.

Figure 3.1 shows a schematic of the flow expected to be encountered in a PCR. The advantages and the disadvantages of the PCR all stem from the gaseous state of uranium fuel. By being in the gaseous form the maximum operating temperature is increased by 10 fold over conventional power sources. Also, very small critical masses are possible. One of the main disadvantages is that the fuel moves through the reactor as shown in Fig. 3.1. The amount of fuel that goes through the system is very important. Small core loadings are of no value if the mass flow rate of uranium is excessively high, and if a large piping system is required to be full of expensive fully enriched uranium. Therefore, one of the first goals of any PCR fluid dynamic analysis and design would be a small fuel to coolant flow ratio.

In the late 1960's and early 1970's a considerable amount of work was done with hydrodynamic containment schemes. These consisted of

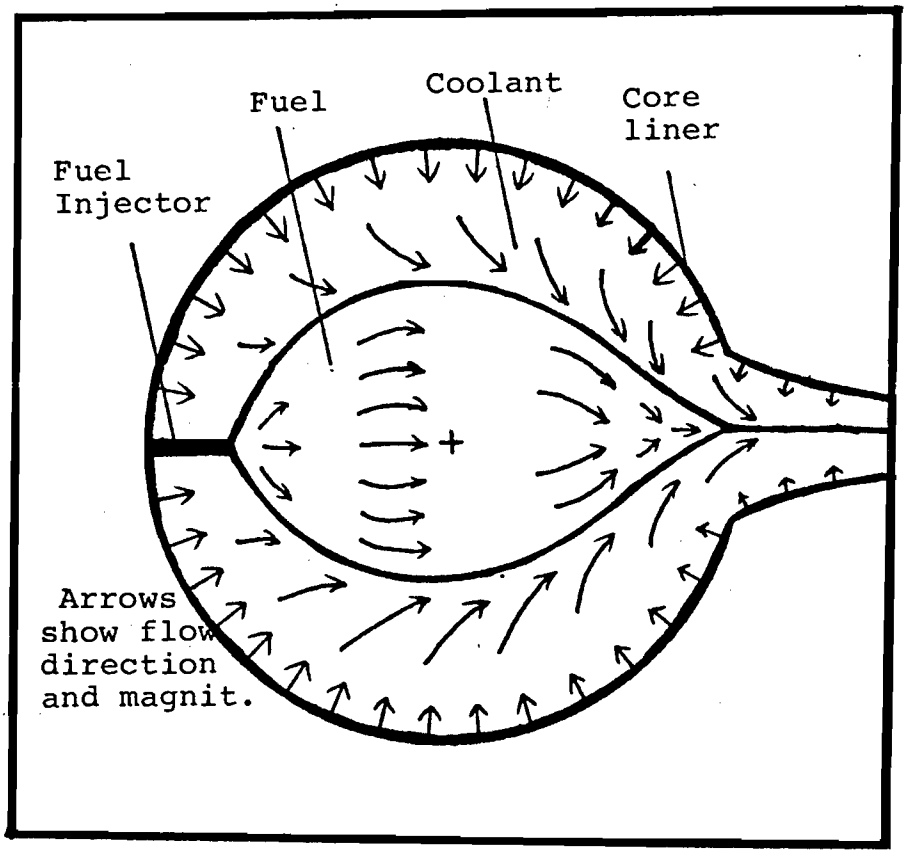

Fig. 3.1 Flow Field of PCR.

rotating cylindrical flows, vortex flows, coaxial flows, and spherical-radial flows. Experiments and analysis were done on all flow arrangements to identify trends and establish parameters important to good confinement and heat transfer. The results of two of these efforts are shown in Fig. 3.2. The data shown are for both cylindrical and spherical coaxial flows. The mass flow ratio ($\dot{m}_{coolant}/\dot{m}_{fuel}$) is shown as a function of the ratio fuel volume/cavity volume. Both graphs show that for a spherical geometry a high mass flow ratio (above 100/1) is obtained only when the volume ratio is less than 0.25. This implies a radius ratio r_{fuel}/r_{total} of less than 0.63. For the reactor core sizes studied in this report the above finding leads to the following conclusions for cavity size:

	CORE I	CORE 20
Fuel Radius	~50 cm	~200 cm
Fuel + coolant radius for $\dot{m}_s/\dot{m}_e = \frac{1}{100}$	~95 cm	~320 cm
for $\frac{\dot{m}_c}{\dot{m}_c} = \frac{1}{1000}$	~109 cm	~430 cm

Reactors of the size listed above would be of about 2000 MW(th) and range from about $\frac{1}{2}$ to 2 times the size of present day PWR pressure vessels.

The exact nature of the flow pattern in the core is unknown at this time. Knowledge of this would require extensive experimentation and analytical work to solve the coupled energy and momentum equations. For this project it is felt that identification of the main design goal

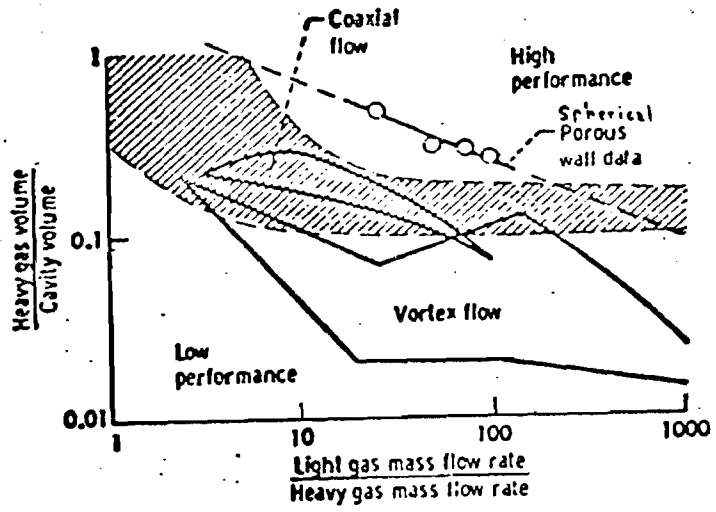

Fig. 3.2(a) Porous Wall Data on Gas Core Performance Map (4)

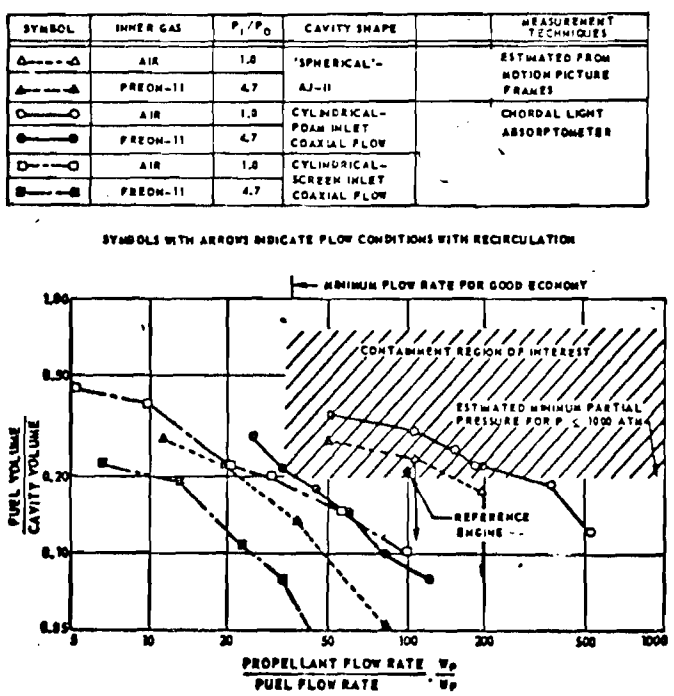

Fig. 3.2(b) Comparison of Coaxial-Flow and Spherical Cavity Containment Results (5)

(low fuel flow rate) and the parameters which control the attainment of this goal is sufficient. The problems of core temperature profiles and wall cooling needs will be discussed in later sections.

For the plasma core reactor the coolant will have to absorb the thermal radiation emitted by the uranium plasma and transfer this energy to a MHD generator, gas turbine, and various heat exchangers. Due to the high operating temperature of the uranium plasma (~25,000°K) and the MHD cycle, the coolant used in the PCR will have to have some additional characteristics above and beyond those of conventional coolants. Table 3.1 shows some of the properties which the PCR working fluid must have. Items 6-7-8 are the "extra" characteristics required by the PCR.

When the PCR was being considered by NASA as a propulsion device, hydrogen was used as the coolant because of its high specific impulse.[1,6,7,8] However, for central station power (on earth, other planets, or a space station) the dangers and chemical reactivity of hydrogen seem to make other choices more attractive. Also, hydrogen is optically transparent to radiation below 1216Å until a temperature of 5000 to 6000 °K is reached. As Fig. 3.3. shows, the emission spectra of uranium plasmas is in the range of 3000 to 8000Å , and hence, hydrogen requires an added submicron sized seed to increase its absorption. Unfortunately, most gases suffer from low absorption in the range of interest and will also require a seed.

Other coolants for central station power plants are listed in Table 3.2. Hydrogen and nitrogen can be discarded immediately because of their high chemical reactivity. Carbon dioxide is good from a thermodynamic and heat transfer point of view, but chemical reactivity and decomposition at high temperatures could cause numerous problems. Helium and other rare gases are good because of their chemical, nuclear, and temperature stability.

Table 3.1 Coolant Properties for the PCR

A. Physical and Nuclear Characteristics

1) Low neutron absorption cross section
2) Low induced radioactivity
3) Good radiation stability
4) Good thermal stability
5) Compatibility with structural and component materials at high temperature
6) Large thermal radiation absorption cross section
7) High electrical conductivity @ $3000^{\circ}K$
8) Molecular or atomic weight much lower than uranium (to enhance separation)

B. Economic Characteristics

1) Resumable cost
2) Good availability
3) Low pumping or compressing power requirements
4) High thermal conductivity and small viscosities

Table 3.2 Possible Coolants for the PCR

1) Hydrogen
2) Helium
3) Carbon Dioxide
4) Nitrogen

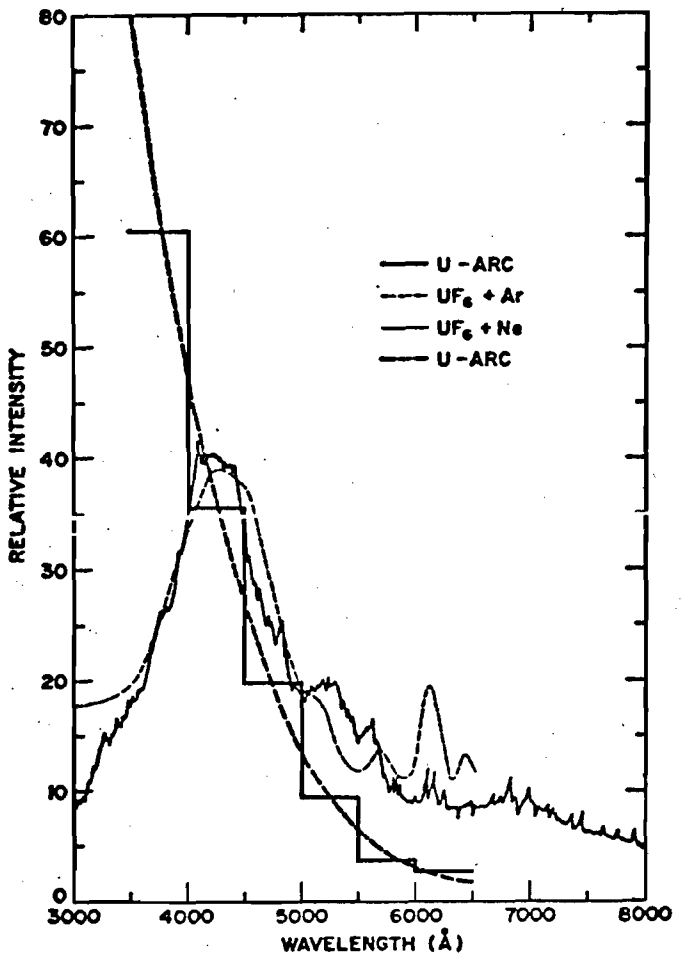

Fig. 3.3 Spectral Distribution of Radiation from Various Uranium Light Sources(10)

These gases also have acceptable thermodynamic and heat transfer properties. Helium, due to its extensive operational experience, low atomic weight and availability is the final choice.

Helium has been shown to readily meet the requirements set forth in Table 3.1 , except for items 6 and 7.[1,9,11] Helium, like other gases, has line absorption being the predominate absorption mechanism; thereby only absorbing a substantial amount of radiation at certain wavelengths. Since the width of these lines is small, the integrated absorption over a range of photon energies would be negligible.[1,6] Exact data for helium absorption in the range emitted by the PCR has not been found. A literature search revealed data only down to 10eV (~124Å). Figure 4 shows data in which helium absorption is compared to that of hydrogen (for which data in the PCR range of interests is available). The data shows that the helium absorption is a little higher than hydrogen in the low energy ranges. Evidence of seeded helium radiation absorption experiments were found, but energy content of the seeded aerosols was reported instead of absorption cross sections.[13] Figure 3.5 shows typical results of these experiments. Here the helium seeded aerosols tend to show a somewhat smaller absorption than hydrogen.

Since no data were found for helium absorption, a few assumptions were made which enabled the study to continue.

1) Since the Lyman Series for helium ranges from 230 to 300Å, it was assumed that discrete absorption would take place in radiation fields of longer wavelength, therefore, necessitating seeding no matter what the absorption coefficient.

2) Since all data found indicated helium absorption

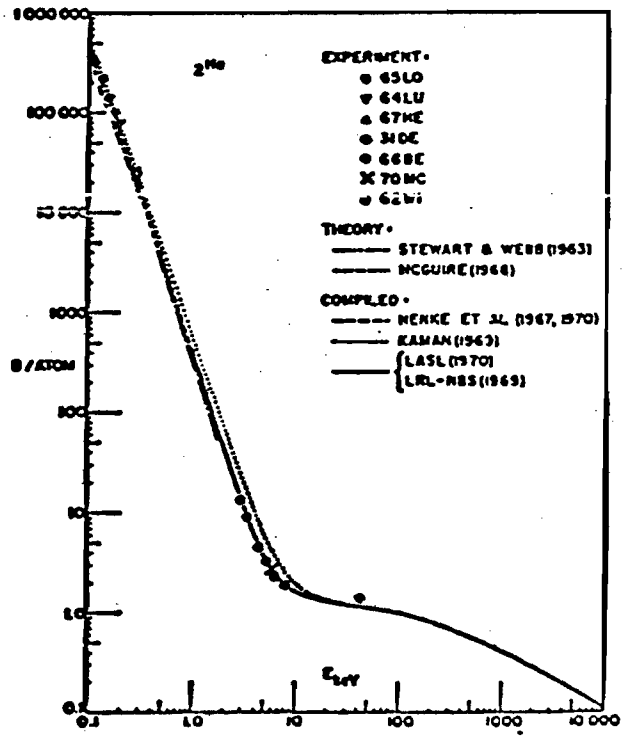

Fig. 3.4 Photon Cross Sections for He and Hydrogen(12)

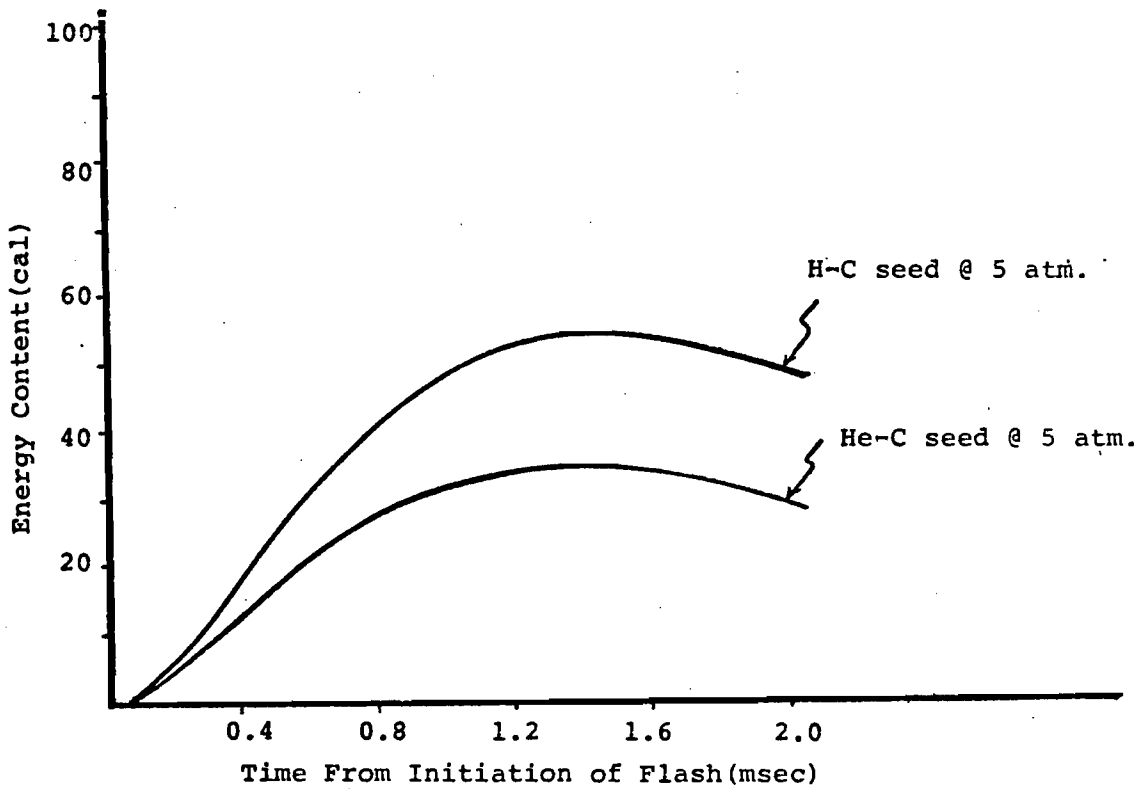

Fig. 3.5 Comparison of H and He Cloud Absorption(13)

of low energy radiation to be "close" to that of hydrogen, and since the absorption in a seeded gas is governed by the seed more so than the gas, data for absorption coefficients in hot seeded hydrogen will be used for this report.

The purpose of seeding the helium is twofold: to increase its absorption coefficient and to make this coefficient as independent of wavelength as possible. Therefore, the first requirement for a seed material is a high, wavelength independent absorption cross section. Secondly, the seed material cannot readily react with the coolant, uranium, or any structural material. Also, the seed should not agglomerate as this causes a decrease in uniformity and decreases the absorption efficiency. These requirements are listed in Table 3.3.

A large amount of work, both theoretical and experimental, has been carried out with seeds of carbon, tungsten, iron, and silicon. Carbon was originally dismissed because of its reactivity with hydrogen, but with helium as the carrier gas this should not be a problem. Figure 3.6 shows a comparison of theoretical absorption coefficients for tungsten, silicon, and carbon at 2000Å as a function of particle size. Figure 3.7 shows the attenuation coefficient of a hydrogen-carbon aerosol at 3450°F.

Table 3.3: Seed Material Requirements

1. Good absorption; independent of wavelength
2. Chemically non-reactive with PCR materials
3. Does not agglomerate easily
4. Compatible with MHD power generation
5. Easily introduced into the helium gas.

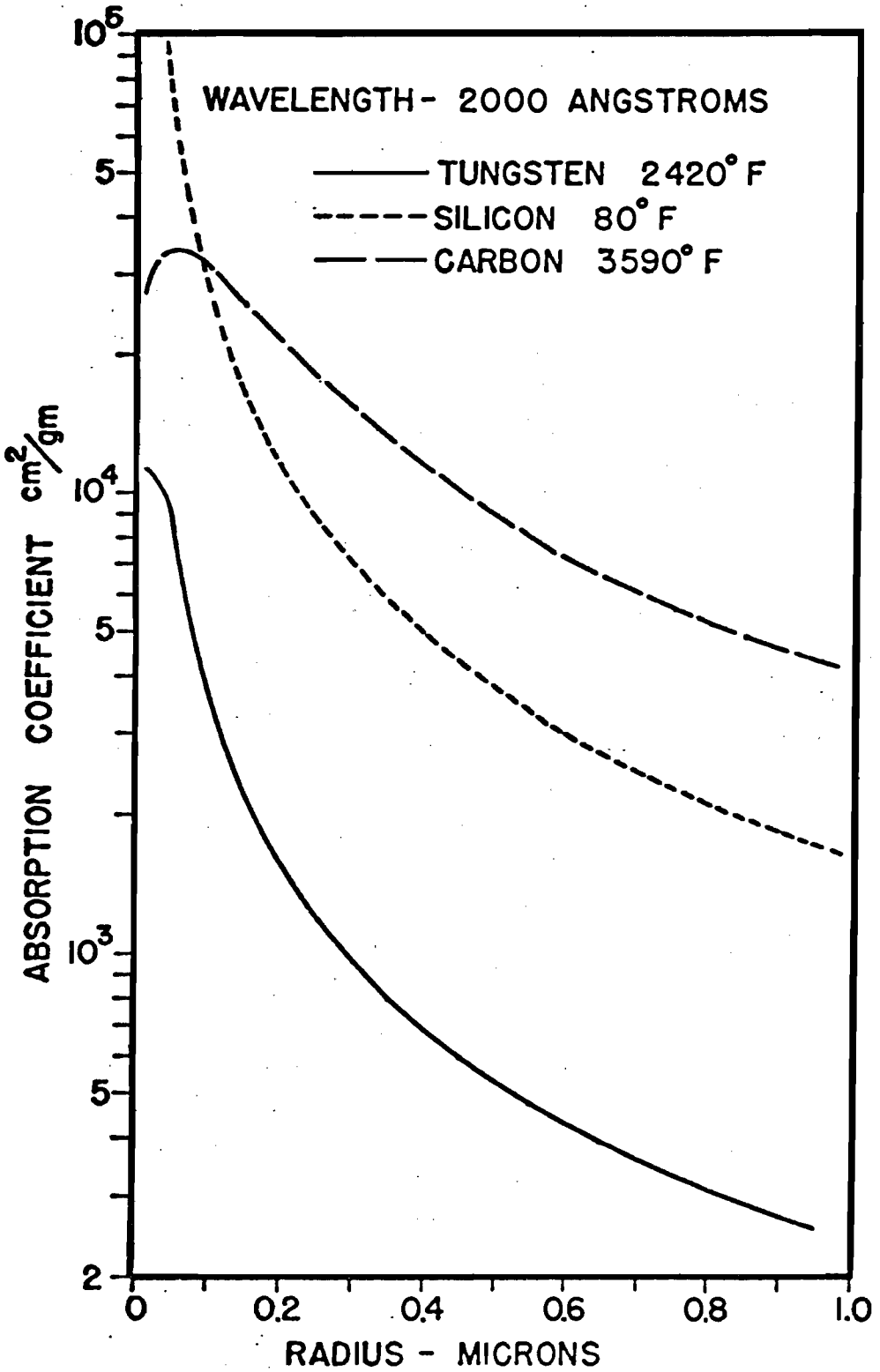

Fig. 3.6 Theoretical Absorption Coefficient of Tungsten, Silicon and Carbon as a Function of Particle Radius

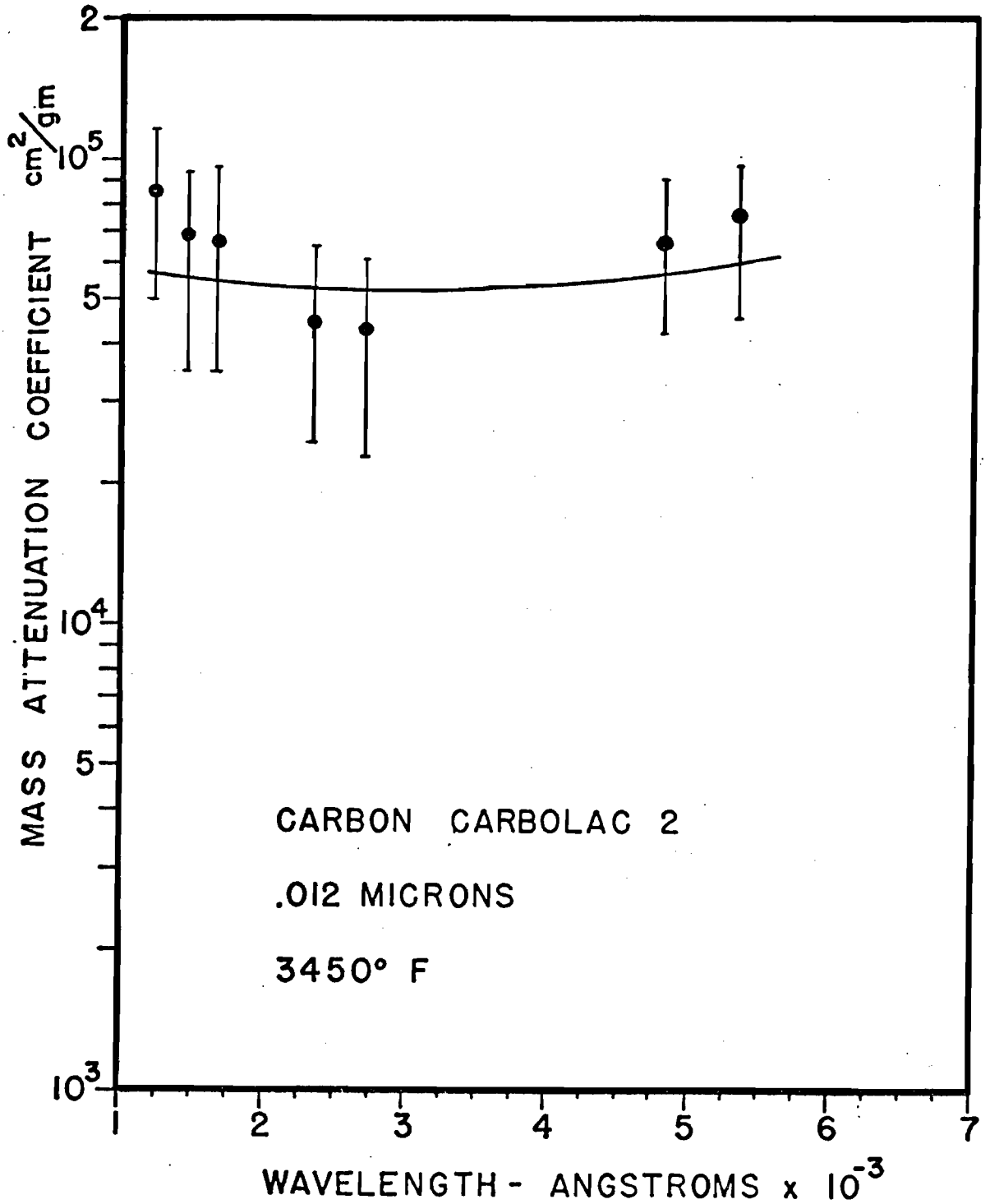

Fig. 3.7 Attenuation Coefficient of Carbon-Hydrogen Aerosol at 3450°F

Comparing this with Fig. 3.8 , which shows the attenuation coefficient for tungsten aerosols at $3000^{\circ}F$, one can see that carbon aerosols have a clear advantage. Also, Fig. 3.7 shows that the carbon seeds produce the required independence with wavelength and have a high overall absorption coefficient, being around $5 \cdot 10^4$ cm^2/gm. For these reasons carbon was chosen as the seed material for use in the PCR.

The overall ability of the gas-seed mixture to attenuate thermal radiation is a function of not only the absorption coefficient of the seed, but also the density of the seed. The density of the seed is in turn limited by the aerosol generator capabilities, the degree of agglomeration, and the particle size.

Aerosol particle densities from 4×10^{-7} to 8×10^{-5} gm/cc have been successfully produced. From this range of particle densities the attenuation parameter $R(cm^{-1})$* can be calculated for various seed-to-coolant density ratios. The results of these calculations are presented in Table 3.4.

The amount of seed needed in the PCR will be determined by the heat loading on the liner wall. Since the core liner will be composed of moderator and structural material, the temperature and heat flux limitations on this component will have to be compatible with the material properties. Beryllium is proposed as the moderating material and stainless steel is for the structural material. Use of these materials will limit the temperature and heat flux to values somewhat close to those of present LMFBR designs ($600^{\circ}K$ and 2.5 MW/M^2). Figure 3.9 shows the fraction of one core power deposited in the liner. For the two core configurations

---

*R is the parameter for exponential attenuation of radiation in the formula

$$I/I_o = e^{-Rt}$$ where I is the intensity,

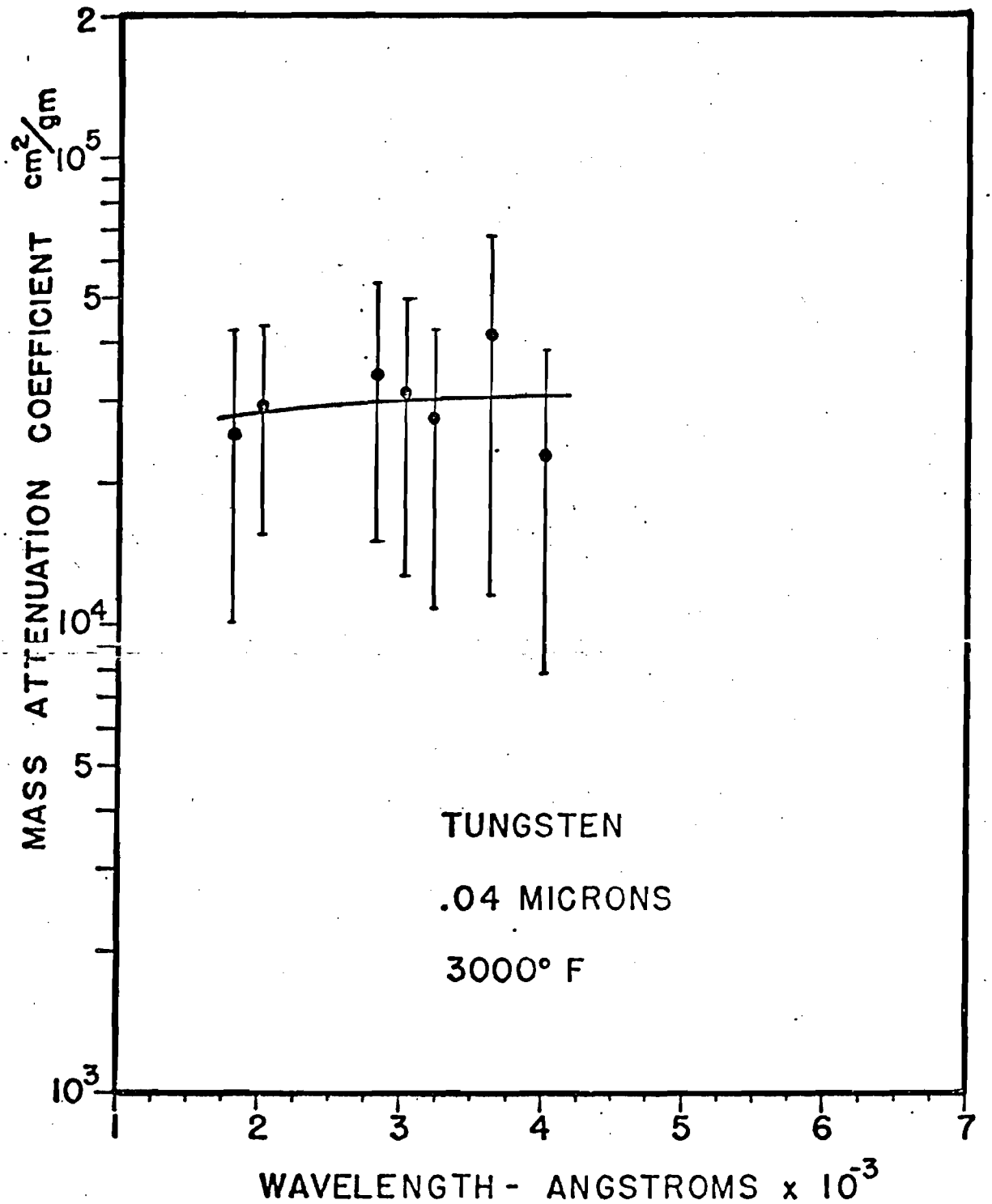

Fig. 3.8 Attenuation Coefficient of Tungsten-Hydrogen Aerosol at 3000°F

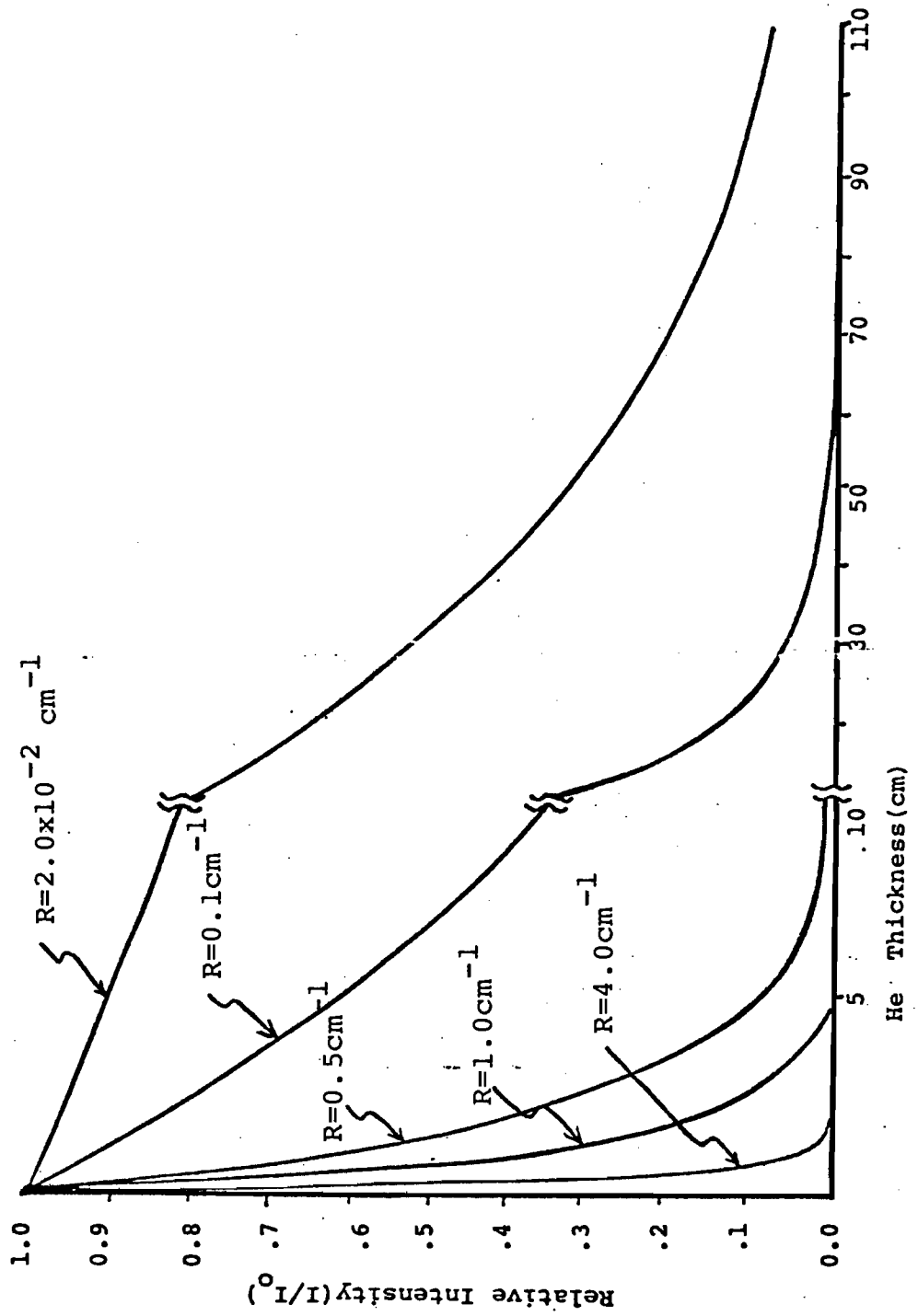

Fig. 3.9 Fraction of Power Deposited in the Core Liner

studied, a value of R from 0.1 to $0.5 cm^{-1}$ would result in a very small heat load on the liner. Table 3.5 summarizes the thermal radiation absorption results for the two cores studied. The fraction of the heat deposited in the liner ranges from negligible to 13.5 MW with a maximum heat flux of 1.07 MW/m^2. This value, although high, is completely within today's technology (the average heat flux in the CRBRP is ~1.27 MW/m^2).[15] To obtain the attenuation shown in Table 3.5 would require particle densities in the range of $2 \cdot 10^{-6}$gm/cc to $1 \cdot 10^{-5}$gm/cc. These are well within current technological capabilities and the resulting particle to carrier densities are low-enough to keep agglomeration to a minimum. Operation in the geometrical and property ranges of Fig. 3.9 should solve the problem of wall heating in the core. The core exhaust nozzle and the MHD duct and its associated piping will still require extensive calculations to determine the cooling required.

Upon absorbing the radiant energy from the uranium plasma, the particle seeds will transfer this energy to the helium coolant. Unlike convential power sources which are limited in the possible ΔT which can be tolerated, the PCR, since it has no structure in the core region proper, can produce any ΔT desired. The desired ΔT can be established by adjusting the mass flow rate of helium. The core inlet temperature is really the only fixed temperature in the entire reactor-power plant system. Since the core liner must be made of a material such as stainless steel and the actinide fuel rods must be clad in zircoloy, the core inlet temperature must be limited to somewhere around $600^{o}K$. The outlet temperature may now be adjusted to any desired level for efficient and reliable MHD

Table 3.4 Seed Density Ranges

P particles gm/cc	$\frac{P\ particles}{P\ H_e} \times 100\%$ @1273°K	@3773°K	R cm^{-1}
$4 \cdot 10^{-7}$	0.005%	0.015%	$2 \cdot 10^{-2}$
10^{-6}	0.013%	0.039%	$5 \cdot 10^{-2}$
10^{-5}	0.14%	0.39%	$5 \cdot 10^{-1}$
$5 \cdot 10^{5}$	0.65%	1.94%	2.5
10^{-4}	1.31%	3.87%	5.0

Table 3.5 Seed Absorption Summary

	core radius(cm)	the thickness(cm)	seed period	$R_{cm^{-1}}$	fraction of power in liner	required heat flux to remove liner heat
CORE I	~50 ~50	~50 ~50	0.059% 0.14%	0.1 0.5	13.5 MW $2.8 \cdot 10^{-8}$MW	1.07 MW/m^2 $2.2 \cdot 10^{-9} MW/m^2$
CORE II	~200 ~200	~120 ~220	1.015% 0.015%	0.1 0.1	$1.23 \cdot 10^{-2}$MW $5.6 \cdot 10^{-7}$MW	$1.0 \cdot 10^{-3} MW/m^2$ $4.4 \cdot 10^{-8} MW/m^2$

operation. Figure 3.10 shows the required mass flow rates for a given temperature rise. For efficient MHD operation the reactor exit temperature needs to be in the range of $2500^{o}K$ to $3500^{o}K$, which implies a ΔT of $\sim 1900^{o}K$ to $2900^{o}K$. For this ΔT a mass flow rate of 190 to 130 kg/sec would be required. For the sizes of the reactor cavity studied here this would result in incore velocities of 190 to 1600 cm/sec for a 50 cm radius core and 10 to 100 cm/sec for a 200 cm radius core. For efficient MHD operation an entrance Mach number of 0.5 is also required. For the MHD unit used in this design study, the entrance area is $0.0387m^2$. This implies an area ratio of (A/A^*; where A^* is the critical area size) of 1.524. Working backwards from A_2 to A_1 (see Fig. 3.11) we can find that for a core exit Mach number of 0.1 (low Mach number is needed here to reduce friction and aerodynamic heating of the walls) we need an exit area of $0.175m^2$ (or pipe diameter of 0.472m). This will in turn give us a reactor exit velocity of $4.20 \cdot 10^4$cm/sec. to $2.65 \cdot 10^4$cm/sec.

No attempt has been made to tackle the problem of the details of the flow stability and confinement of the plasma-coolant system. These would be out of the scope of this design project. Attempts have been made to ascertain an "order of magnitude" of the effects and parameters specically associated with the PCR. Geometry, mass flow and coolant property ranges which would be characteristic of a 2000 MW(th) central power station have been examined. A summary of the fluid mechanical aspects of the PCR design is given in Table 3.6.

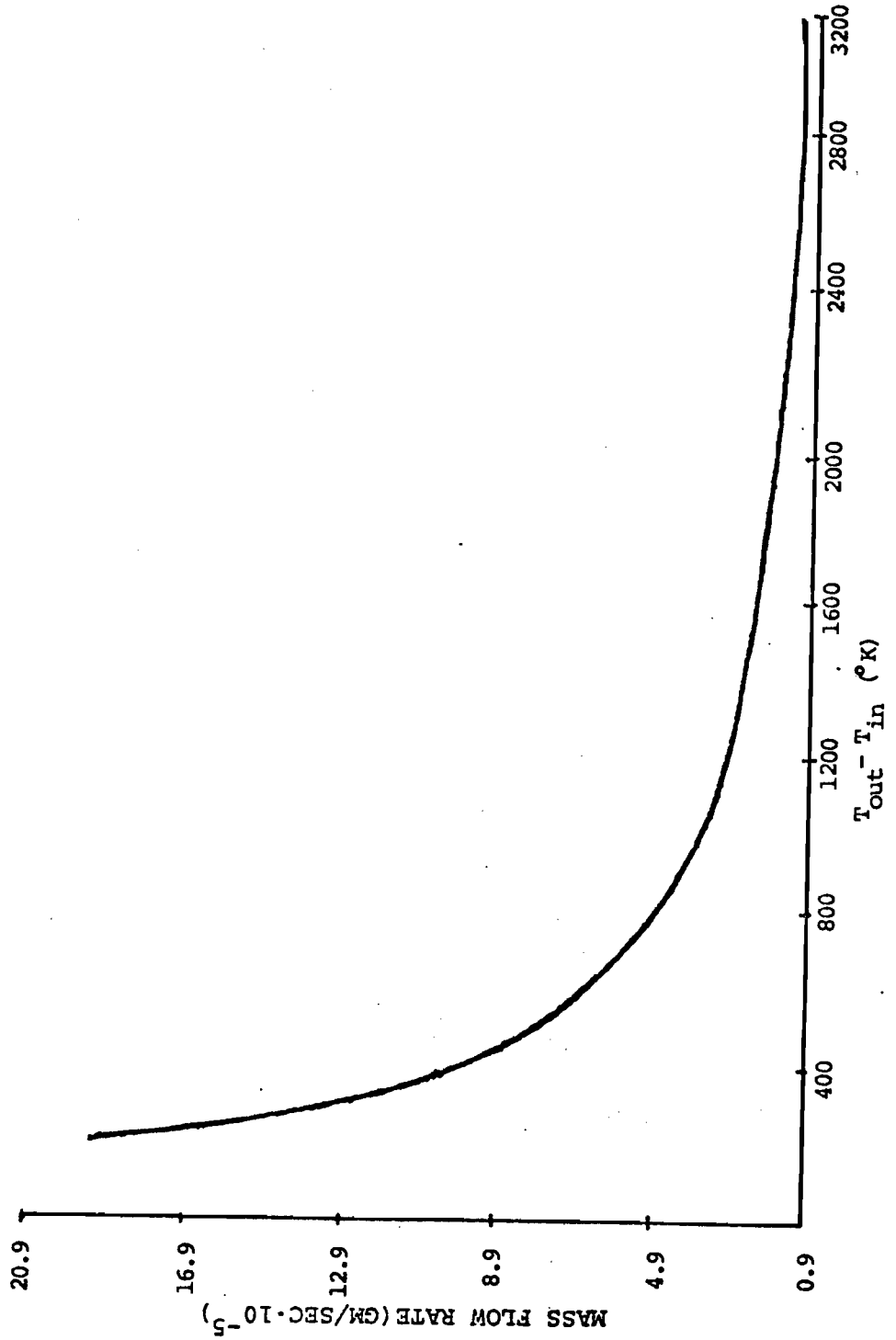

Fig. 3.10 Mass Flow Rate vs Reactor Core Temperature Difference

Table 3.6 Fluid Mechanical Summary

(Item) Coolant	(Value) or name Helium
Exit Temp Range	3000 to 3500°K
Fuel to coolant mass flow core	1/100 to 1/1000
Coolant thickness	45 to 220 cm
Plasma radius	50 to 200 cm
Coolant mass flow	120 to 190 kg/sec
Seed material	carbon
Seed size	0.012 microns
Seed density	10^{-6} to 10^{-5} gm/cc
Coolant exit pipe diameter	$2.65 \cdot 10^{4}$ to $4.2 \cdot 10^{4}$

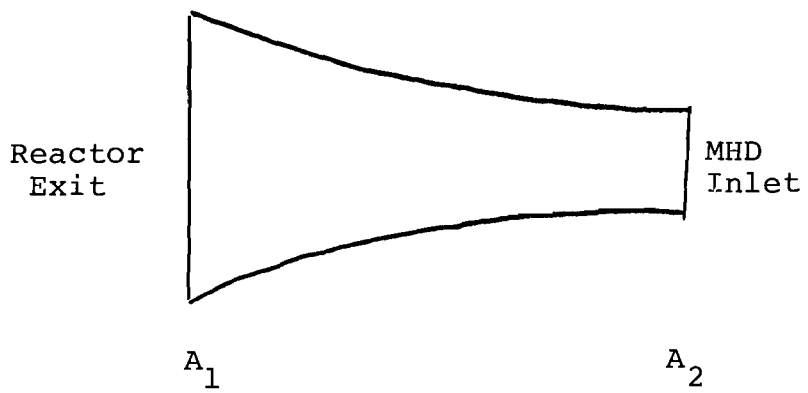

@ A_1 known:

$m_1 = 0.1$

$T_1 = 3000$ K

calculated:

$A_1 = 0.175\ m^2$

@ A_2 known:

$A_2 = 0.0387\ m^2$

$m_2 = 0.5$

calculated:

$A^* = 0.0254\ m^2$

Equation:

$$A/A^* = 1/m[2/(\gamma+1)(1 + (\gamma-1)m^2/2)]^{[(\gamma+1)/2(\gamma-1)]}$$

Fig. 3.11 Area Calculation Technique

REFERENCE FOR CHAPTER 3

1. Moore, F. K. and S. Leibouich, "Self-Confined Rotating Flows for Containment," Research on Uranium Plasmas and their Technological Applications, NASA SP-236, 95, (1966).

2. Mensing, A. E. and J. F. Jaminet, "Experiments on the Containment of Simulated Fuel in Unheated and Heated Vortices," Research on Uranium Plasmas and their Technological Applications, NASA SP-236, 65, (1971)

3. Poutre, H. A., "Estimates of Fuel Containment in a Coaxial Flow Gas Core Nuclear Rocket," Nuclear Technology, 12, 209, (Oct. 1971).

4. Lanzo, C. P., "A Flow Experiment on Curved-Porous Wall Gas-Core Reactor Geometry," Nuclear Applications and Technology, 8, 6 (Jan. 1970).

5. Johnson, B. V. and J. C. Bennett, "Experimental Study of the Effects of Injection Conditions on the Flow in Cylindrical and Spherical Chambers," 2nd Symposium on Uranium Plasma: Research and Applications, Am. Institute of Aeronautic and Astronautics, 204 (Nov. 1971).

6. Meghreblian, R. V., "Gaseous Fission Reactors for Booster Propulsion," American Rocket Society J, 32, 13 (1962).

7. Duke, E. E. and W. J. Houghton, "Gas-Core Nuclear Rocket Engine," Journal of Spacecraft, 4, 12 (1967).

8. Karlheinz, Thom, "Fission Engine Concepts," 2nd Symposium on Uranium Plasmas, Atlanta, Ga. (Nov. 1971).

9. Trauger, D. B., "Operating Experience and Design Trends for Helium Cooled Nuclear Power Reactors," The Helium Soc. Symposium Proceedings, Washington, D. C., 20, (March 1970).

10. Miller, M. H., "Measured Emissivities of Uranium and Tungsten Plasmas," 2nd Symposium on Uranium Plasma: Research and Applications, Atlanta, Ga., 120, (Nov. 1971).

11. Trauger, D. B., Helium Cooled Reactors, USAEC Report TM-2297, Oak Ridge National Lab (1968).

12. Hubbell, J. H., "Photon Cross-section Compilation Activity in the U. S. in the Range 1 KeV to 100 GeV," Journal De Physique C4, C4-14 (Oct. 1971).

13. Birkig, V. C., "Theoretical Absorption in Seeded Gases," Douglas Report DAC 59985, Nasw 1310 (Jan. 1967).

14. Shenoy, A. S., The Attenuation of Radiant Energy in Hot Seeded Hydrogen, Ph.D. Thesis, Georgia Inst. of Tech. School of Nuclear Engineering, (May 1969).

15. Clinch River Preliminary Safety Analysis Report, Project Management Corp., June 1975.

16. Zucrow, M. J. and J. D. Hoffman, Gas Dynamics, 1, 160-241, John Wiley and Sons, Inc., New York (1976).

4. HEAT TRANSFER IN THE PLASMA CORE REACTOR

Plasma core reactors are capable of producing heat at extremely high temperatures for use in rocket propulson, MHD power generation, or process heat applications. Most of the work dealing with heat transfer in a gaseous core reactor has been concerned with reactors used in rockets. Here the uranium plasma heated a hydrogen coolant that was used for propulsion. For central station power production the difference is that helium is used as a coolant and is exhausted through a MHD nozzle. Therefore, previous work on heat transfer of gaseous core reactors can be readily applied to this design study.

The simplest case to analyze is when there is no mixing of the fuel and coolant in the uranium-helium core region.[1] In reality there will be some mixing and some convection effects at the outside surface of the uranium plasma. Therefore, the case analyzed would be a "first estimate" of the temperature distribution in the core.

In this study the steady state temperature profile as a function of radius in a spherical geometry is analyzed. Figure 4.1 shows the geometry and pertinent data. The helium and uranium gases are assumed to be grey gases, which means the radiation absorption coefficient is independent of wavelength. The containment wall is also assumed to be grey so that wall emissivity and reflectivity are independent of wavelength. The approach used is that proposed by Ragsdale and Kascak.[2] In this method the volume heat generation term (q''') is assumed radially dependent and the absorption parameters temperature dependent.

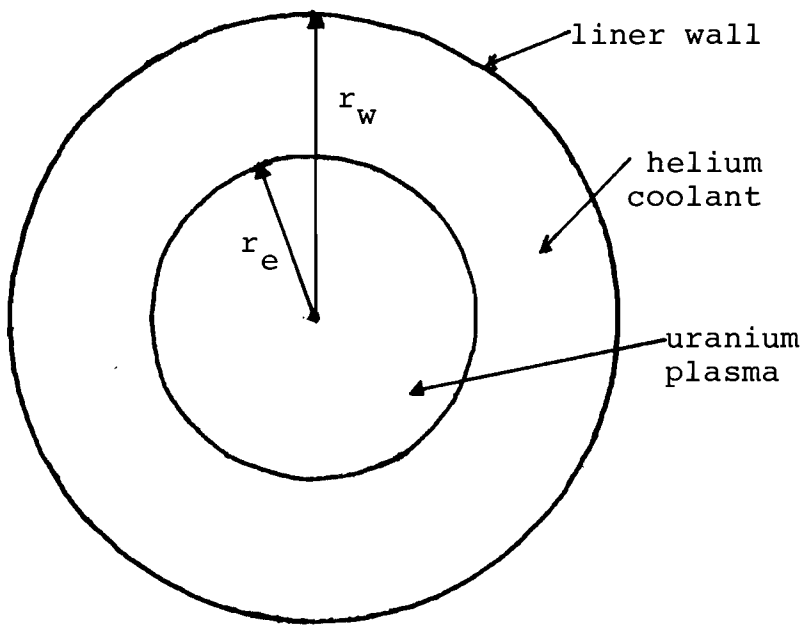

item	value	
r_e	200cm	radius
r_w	320cm	radius
power	2×10^9 watts	reactor power
q''_{edge}	3.98×10^3 watts/cm^2	core edge heat flux
e_w	0.7-0.8	wall emissivity
T_w	800 K	wall temperature
σ	5.7×10^{-12} w/cm°K^4	Stefan-Boltzmann constant

Fig. 4.1 Geometry and Data

If one assumes that the heat flow is basically a diffusion process the heat flux in the core may be expressed by[2]

$$q''(r) = \frac{-4}{3k(T)} \frac{d(\sigma T^4)}{dr} \tag{4.1}$$

where q'' = heat flux

σ = Stefan-Boltzmann constant

T = temperature

r = radius

k = absorption coefficient.

At steady state the heat flux can be related to the volumetric heat generation $q'''(r)$ by

$$q''(r) = \int_o^r q'''(r)\, 4\pi r^2 dr / 4\pi r^2 \ . \tag{4.2}$$

Figure 4.2 shows calculated fission densities for these different PCR radii. If the fission density, and hence the heat generation rate is fitted by a polynominal such as:

$$q'''(r) = \sum_{i=o}^{n} q_i r^i \tag{4.3}$$

then integration of Eq. 4.2 yields

$$q''(r) = \sum_{i=0}^{n} \frac{q_i r^{i+1}}{i+3} \ . \tag{4.4}$$

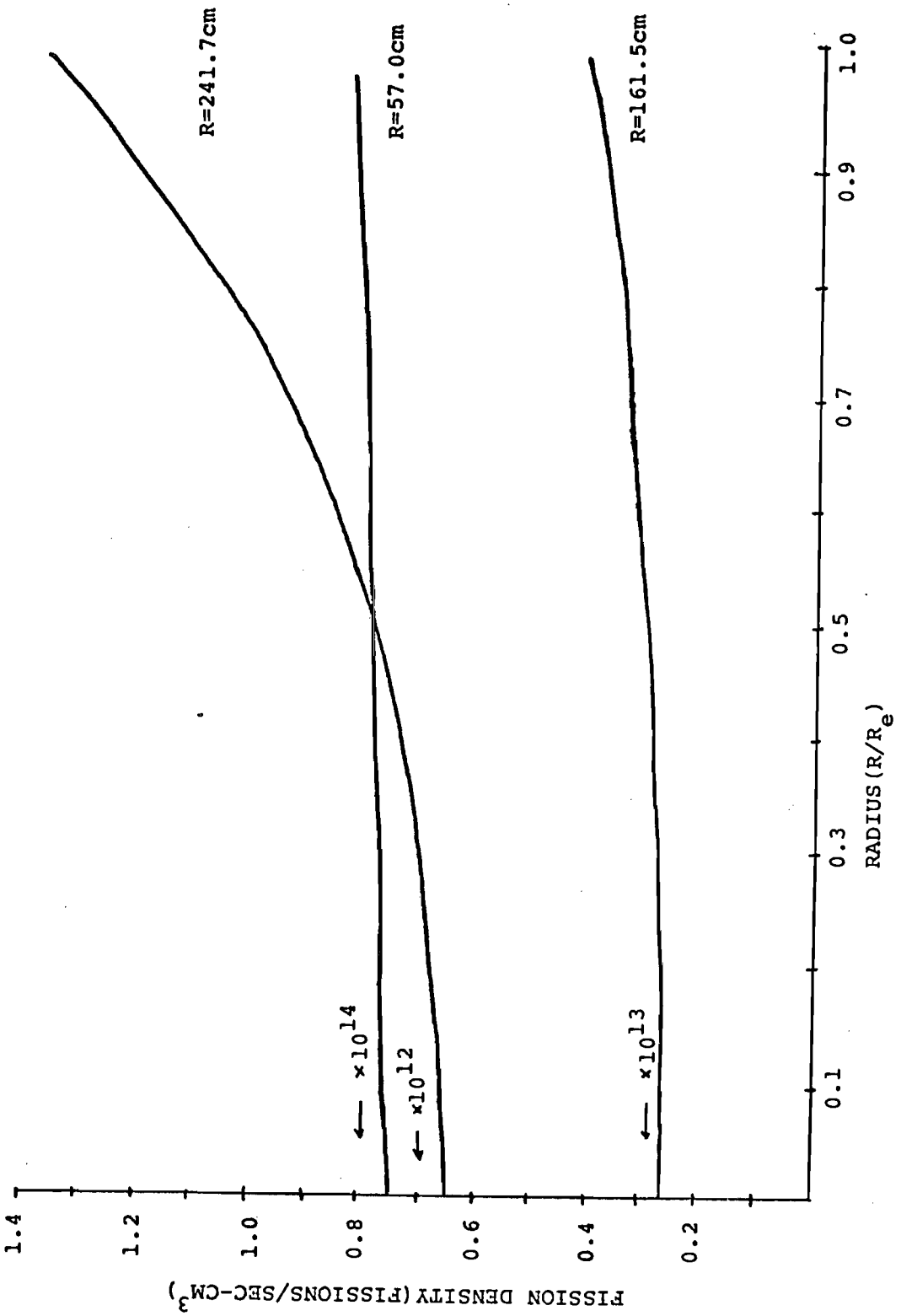

Fig. 4.2 Fission Density vs Radius

Substituting into Eq. 4.1 and rearranging yields

$$\frac{\partial T}{\partial r} = \frac{-3k(T)}{16\sigma T^3} \sum_{i=o}^{n} \frac{q_i \quad r^{i+1}}{i+3} \tag{4.5}$$

Equation 4.5 can be solved by numerical techniques with k(T) being supplied via experiment results.

To solve Eq. 4.5 one must also have the boundary conditions for the edge temperature of the reactor (T_e). Unfortunately, this temperature is not known, but because of wall stress and creep limitations the wall temperature (T_w) is known. This temperature will in turn affect the core edge temperature. To get a relationship between T_w and T_e let us first consider a brightness temperature T_b. T_b is defined so that σT_b^4 gives the radiated heat flux at the core edge. T_b is defined by the expression:

$$q_e'' = \sigma F(T_b^4 - T_w^4) \tag{4.6}$$

where

$$F = \left[1 + \left(\frac{r_e}{r_o}\right)^2 \left(\frac{1 - \varepsilon_w}{\varepsilon_w}\right)\right]$$

ε_w = emissivity of the wall.

Thus the brightness temperature is found to be:

$$T_b = \left\{\frac{q_e''}{\sigma}\left[1 + \left(\frac{r_e}{r_o}\right)^2 \left(\frac{1 - \varepsilon_w}{\varepsilon_w}\right)\right] + T_w^4\right\}^{1/4} \tag{4.7}$$

where $q''_e = \sum_{i=o}^{n} \frac{q_i \, r_e^{i+1}}{i+3}$ = edge heat flux

To determine the edge temperature from T_b, Ragsdale and Kascak proposed the following relationship:[2]

$$T_e = T_b \left[\frac{1}{2} \left(1 + \frac{3}{2 r_e k(T)} \right) \right]^{1/4} \tag{4.8}$$

Since k(T) is a function of T and, therefore, must be evaluated at T_e, Eq. 4.8 must be solved iteratively. The use of the secant method provides quick convergence.

Once T_e is known T(r) can be solved by any appropriate numerical method. A fourth-order Runga-Kutta program was written and implemented for this purpose. The data for k(T) was input into the program as a polynomial fit to the data shown in Fig. 4.3. The program was checked for accuracy against previous work[1,2] and showed good agreement.

Temperature distributions for the design basis core of 200 to 20 cm in radius were calculated and are shown in Fig. 4.4. The combination of lower temperature (and hence higher absorption coefficient) and a higher fissioning rate at the core edge cause the very rapid temperature increase in the first few centimeters inside the core. This rapid rise could also mean that the core edge temperature has been underestimated; however, the calculations were checked and the values used for T_b and T_e were consistent. These calculations showed that maximum

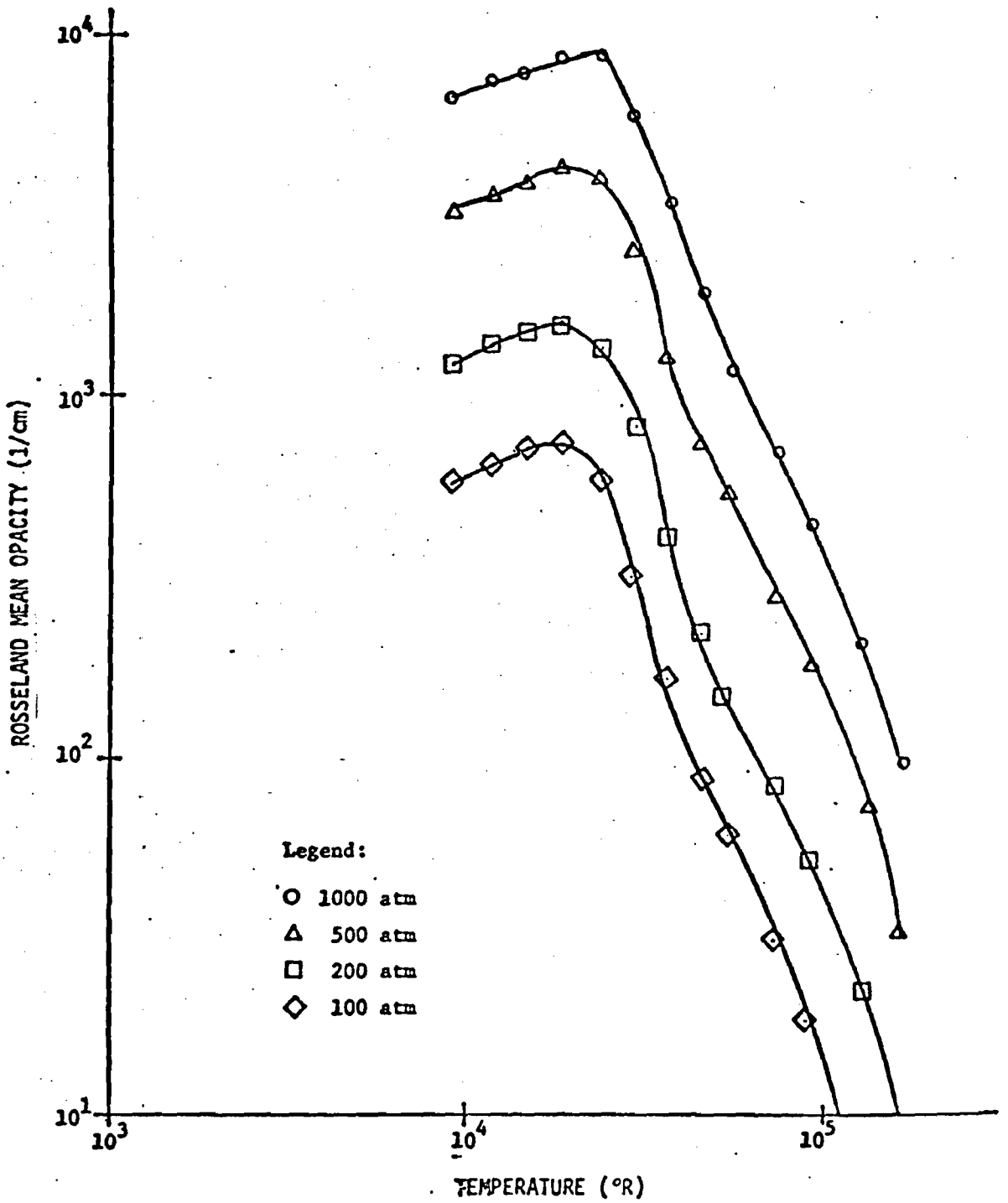

Fig. 4.3 Rosseland Mean Opacity versus Temperature for Uranium.[3]

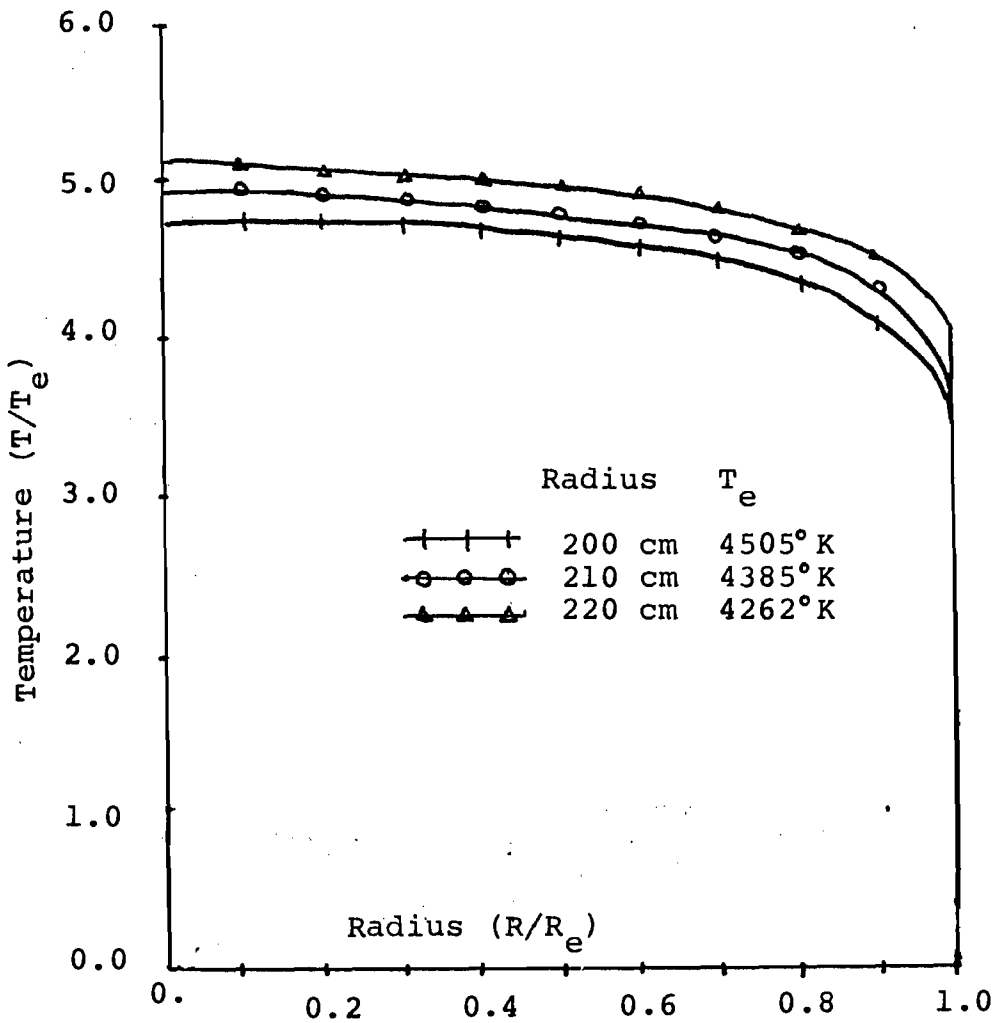

Fig. 4.4 Core Temperature vs Radius

core temperatures ranged from 21,400 to 21,800^{o}K with an average temperature in the neighborhood of 18,500^{o}K.

The transuranium actinides (neptunium, plutonium, americium, curium, etc.) will be introduced into the PCR in the form of zirconium alloy clad rods located just outside the beryllium reflector. The actinides will be in the form of oxides and will be cooled by the helium coolant used in the core. The design constraints for the actinide rods will have to be the same as those used for present day power reactors for safety reasons. These are:

Linear heat rate. . . 500 watts/cm. . . to control amount of stored energy in the fuel.

Maximum clad temperature. . . 500°C. . . to maintain clad strength.

There is a scarcity of thermal-physical property data on the oxides of transplutonium actinides and there is no data on the behavior of mixtures. Their known melting points, are high (~2400°C) and actinide oxide densities are all about the same being ~11 gm/cc.[4] Consequently, since little is known about the actinide oxides, and a sizable fraction of the actinide rods will be uranium oxide, it is assumed that their physical properties are the same as UO_2.[5]

A high burnup rate in the actinide fuel rods is desirable so as to shorten the time required for transforming the actinides by fission. The burnup rate is directly proportional to the volumetric heat generation rate, which is:

$$q'''(r) = \sum_{i=1}^{n} R_i \; \rho_{fission}(r) \tag{4.9}$$

where

q''' = heat generation rate, watts/cm^3

R_i = energy released per fission (Joules) of ith isotope

$\rho_{fission}$ = fission density of ith isotope, fissions/cm^3-sec.

The value of R_i for the actinides is not known, but it should be close to that of uranium or plutonium (~200MeV/fission). Consequently, the volumetric heat generation for the actinide rods is:

$$q''' = \left(200 \frac{\text{MeV}}{\text{fission}}\right) \cdot \left(\frac{1 \text{ Joule}}{6.242\times10^{12} \text{ MeV}}\right) \cdot \left(\bar{\rho}_{fission} \frac{\text{fissions}}{\text{cm}^3 \text{ sec}}\right). \tag{4.10}$$

For the initial actinide fuel loading into the PCR

$$\bar{\rho}_{fission} = 4.34\times10^{11} \text{ fissions/cm}^3\text{-sec}$$

which gives

$$q''' = 13.90 \text{ watts/cm}^3.$$

This value is considerably lower than the heat rate in present LWRs so the probability of exceeding one of the design limits is very small.

The geometry for the actinide fuel rods was chosen to give a minimum actinide region thickness, as this helped give low critical masses. This also helped keep the flux flat in the actinide region (for even

burn-up), and helped to limit the volume of actinides required to fill the region (at an inner radius of 3.4 meters even a small thickness has quite a large volume). The radius for the fuel rods was set at 0.268 cm with a 0.035 cm thick clad and a gap thickness of 0.015 cm. This gave an overall radius of 0.318 cm (0.25 in. diameter). The rods will be spaced with a 0.142 cm diameter wire wrap with a pitch of 25 cm.

The actinide fuel rods are one meter long and positioned just outside the beryllium liner as shown in Fig. 4.5. Calculations showed, that for the dimensions shown in Fig. 4.5, the neutron flux variation in going from the center of the actinide rods to either end is only 1.0%. Hence, it is a good assumption to assume that the flux and, thus, the power does not change over the rod length. Therefore,

$$q''' \neq f(r,z); \quad q''' = \text{const} = 13.90 \text{ watts/cm}^3.$$

With this value we can now calculate the helium temperature at the exit to the actinide fuel rods. Unfortunately, this is an iterative procedure because the design point temperatures are the core outlet and the actinide inlet. Thus the mass flow rate will have to be varied until the design core outlet temperature is met. The procedure will be:

1) Assume mass flow rate $\dot{m}_1$

2) Calculate $T_{out\ actinides} = T_{o_a} = T_{in_a} + \dfrac{\pi r_f^2 \, Hq''' \cdot n}{C_p \dot{m}}$

3) Calculate $T_{out\ core} = T_{o_c} = T_{o_a} + \dfrac{P}{C_p \dot{m}}$

4) Check if $T_{o_c} = 3500^{o}K$ if not,

redo calculation with new mass flow $\dot{m}_2$.

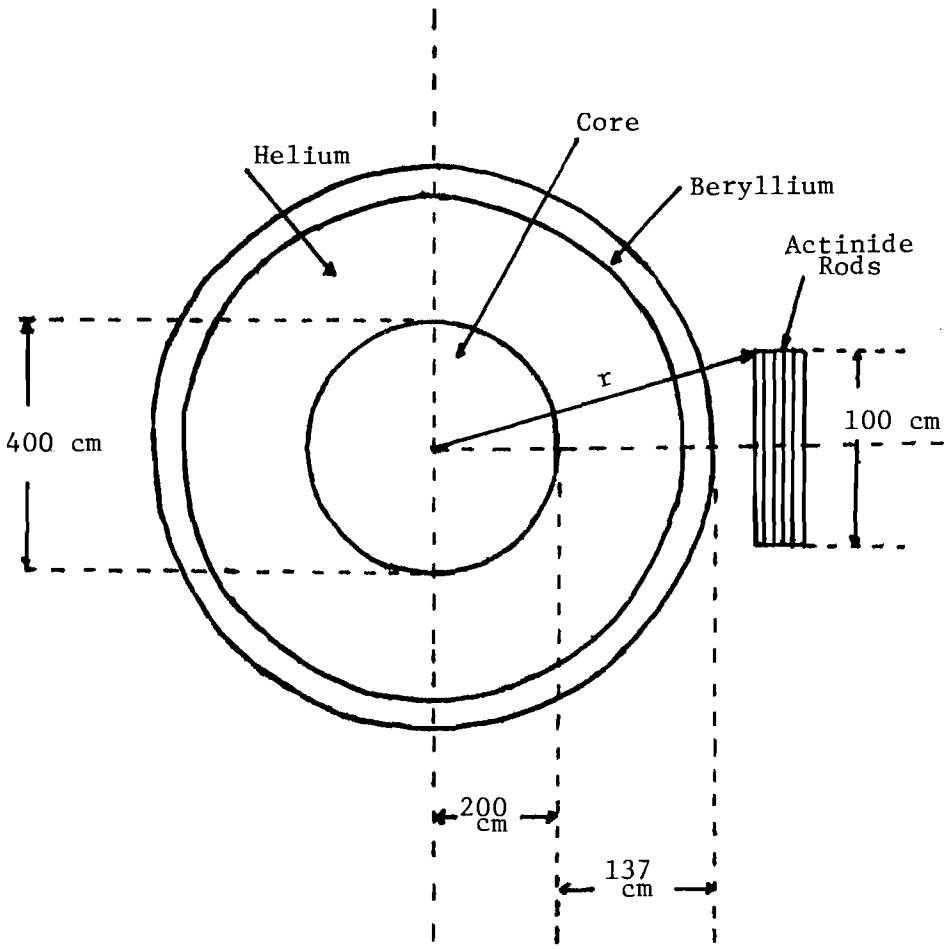

Fig. 4.5 Actinide Location

The above procedure must be done within the design limits set forth and with the following data:

$P = 2000$ MW

$r_f = 0.269$ cm

$H = 100$ cm

n = number of actinide fuel rods:

= 2725 for first fuel loading

$T_{in_a} = 642^{\circ}K$

$C_{P_{helium}} = 5.20 \frac{J}{gm^{\circ}K}$

$q''' = 13.9$ watts/cm^3

$r_w = 0.318$ cm

The calculation must also be done taking into account the effects of the uncertainties due to manufacturing tolerances, physical property variations and flow maldistributions. The effects these uncertainities have on the temperature can best be accounted for by applying hot channel/hot spot factors to the computation. Because of the similarity of the actinide rods and the fuel rods of the Clinch River Breeder Reactor the same hot channel/hot spot factors used in its design will be used here.[6] The nuclear hot spot factor for axial variation in the flux will be ignored here due to the arguments given earlier for assuming a flat heat generation rate in the actinide fuel rods. The factors used are:

Coolant	Film	Heat Flux
$F_{\Delta h}$	$F_{\Delta T}$	F_q
1.232	1.168	1.081

Using these factors the actinide fuel rod heat transfer calculations yielded the results shown in Table 4.1. As can be seen the maximum clad temperature turns out to be 647°C (374°C) and is still well within the design limit of 500°C. These calculations are for startup of actinide transmutation. The calculated temperatures at later cycles will probably be higher.

Table 4.1 Actinide Region Thermal Parameters

Maximum CLAD Temperature	646°K
Inlet Helium Temperature	642°K
Outlet Helium Temperature	643.7°K
Mass Flow Rate	134.65 kg/sec
Helium Velocity	5.9×10^4 cm/sec (M = 0.4)

These calculations represent scoping type work and are intended to give "order of magnitude" values for temperatures in each region. A more exact temperature profile for the core region would require detailed information about the flow field inside the uranium plasma and in the helium coolant. Items that were not considered, such as fuel-coolant mixing and the energy of the uranium swept out of the core, need to be analyzed. Also, detailed pressure loss calculations need to be performed for the actinide and core regions. This work, however, is enough to permit a fairly accurate description of the operating conditions inside a PCR. Table 4.2 summarizes design points relevent to the heat transfer analysis of the PCR.

Table 4.2 Heat Transfer Summary

ITEM	VALUE
Actinide Region:	
Helium Inlet Temperature	$642^{\circ}K$
Maximum Actinide Temperature	$652^{\circ}K$
Maximum Clad Temperature	$646^{\circ}K$
Helium Exit Temperature	$643.7^{\circ}K$
Core Region:	
Mass Flow Rate	134.65 kg/sec
Helium Exit Temperature	$3500^{\circ}K$
Maximum Fuel Temperature	$\sim 21,400^{\circ}K$
Exit Helium Velocity	2.85×10^{4} cm/sec

REFERENCES FOR CHAPTER 4

1. Rust, J. H. and R. Farr, "Heat Transfer in Gas Core Power Reactors," Exploratory Study of Several Advanced Nuclear MHD Power Plant Systems, Final Status Report, NASA Grant NGR-11-002-145, J. R. Williams and J. D. Clement project directors, 139 (March 1973).

2. Ragsdale, R. G. and A. F. Kascak, "Simple Equations for Calculating Temperature Distribution in Radiating Grey Gases," NASA TN D-5226 (May 1969).

3. Parks, D. E., G. Lane, J. C. Stewart and S. Peyton, "Optical Constants of Uranium Plasma," NASA-CR-72348, GA-8244 (Feb. 1968).

4. Kirk and Othner, Encyclopedia of Chemical Technology, 1, 2nd ed., John Wiley and Sons (1963).

5. Rust, J. H. and J. D. Clement, Analysis of the Gas Core Actinide Transmutation Reactor (GCATR), Annual Report for NASA grant NSG-1288, (Feb. 28, 1977).

6. Cavelli, M. D. and R. A. Markley, "Preliminary Thermal Hydraulic Design and Predicted Performance of the CRBRP Core," 75-HT-71, presented at AIChE-ASME Heat Transfer Conference, San Francisco (Aug. 1975).

5. DESIGN CONSIDERATIONS OF PLASMA CAVITY REACTORS

Figure 5.1 is a schematic of the design base reactor. The relevant dimensions, obtained from the fluid mechanical, nuclear analyses, and thermal-hydraulic analysis are also shown. The reactor is almost 3.40 meters in radius and 7.20 meters in length. Table 5.1 gives the region volumes and components weight.

The beryllium liner, besides serving as the reactor moderator, is also the porous wall and flow director for the helium coolant entrance into the reactor cavity. Beryllium was chosen for the liner because of its exceptional moderating capabilities. The helium temperature in the beryllium liner ranges from 370°C to 400°C which is approximately one-fourth its melting point, so the metal should be able to withstand such a thermal load. There will also be very little pressure difference between the liner inside and outside so the overall stress on the liner should be small. The beryllium metal is encased in a jacket of zirconium alloy and bolted under a small compressive load. Since the thermal expansion of beryllium is greater than zircaloy, at operating temperatures the beryllium should be in even more of a compressive load that should equalize any pressure load on the beryllium. Figure 5.2 shows a detail drawing of the liner.

The actinide fuel rods presented the first real problem in the overall system layout. Since spherical geometry is best from a neutronic and hydrodynamic standpoint for the core, the cylindrical actinide fuel rod did not really "fit" anywhere. It was decided to place the rods just outside the beryllium reflector in a cylindrical annulus region. Each

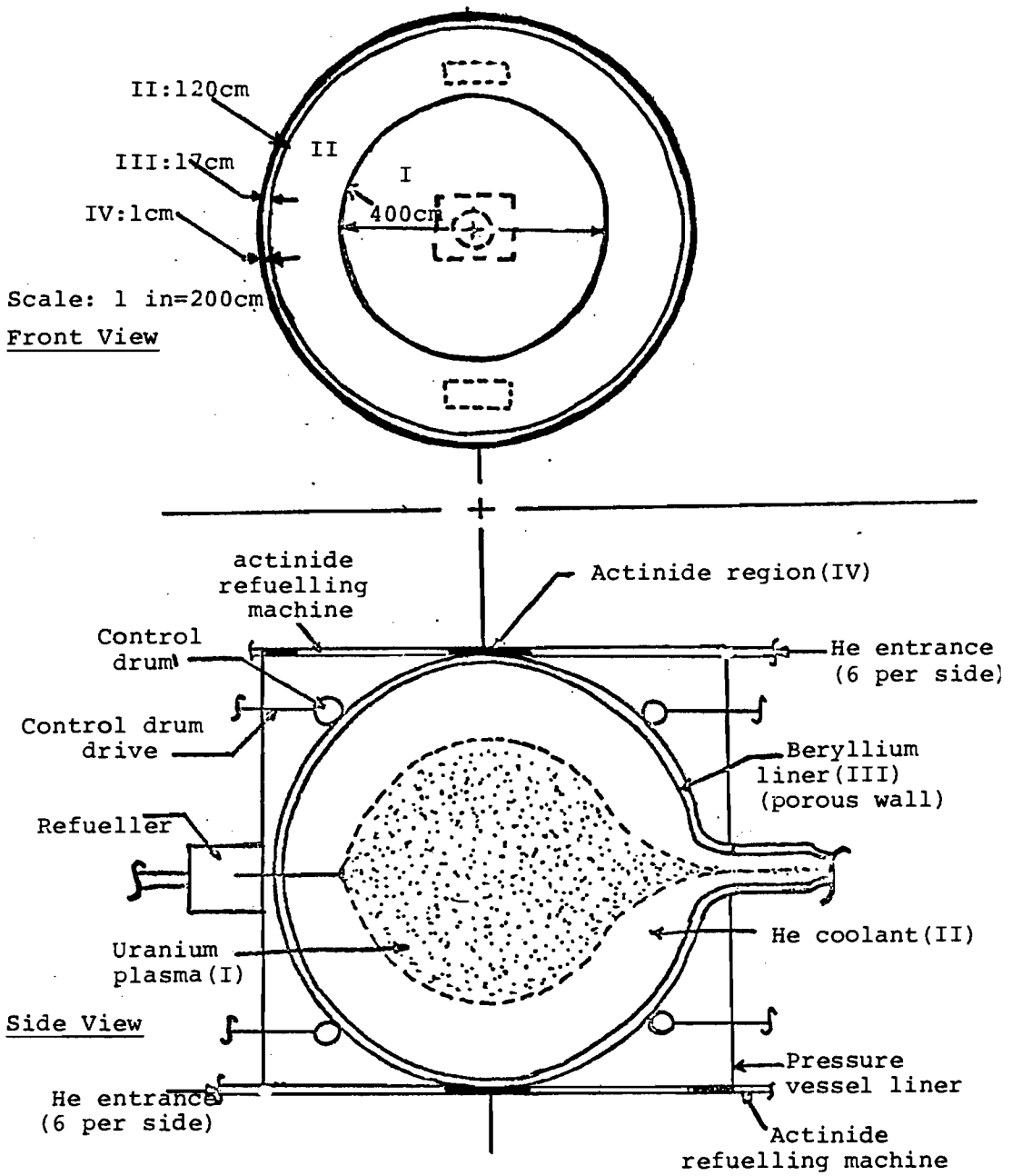

Fig. 5.1 Reactor Schematic

Table 5.1 Volume and Weight of Reactor Components

	Region	Volume	Material Weights
(I)	Uranium plasma	33.51 m^3	~374.0 Kg
(II)	Helium coolant	103.75 m^3	487.0 Kg
(III)	Beryllium liner:	16.0 m^3	29440 Kg
	Zirconium Alloy:	1.29 m^3	8452 Kg
	Helium coolant:	5.73 m^3	26.9 Kg
IV)	Actinide rods:	.0405 m^3	445.43 Kg*
	Zirconium Alloy:	.04126 m^3	270.3 Kg*
	Helium coolant and bond:	.1095 m^3	0.838 Kg*
(V)	Control drums:		
	Cd:	0.000057 m^3	0.493 Kg
	Beryllium Shield:	0.5027 m^3	923.7 Kg
	Zirconium Alloy:	0.1335 m^3	874.6 Kg
(VI)	Helium coolant outside of Beryllium liner and Actinide Region:	101.16 m^3	474.86 Kg

*These are loadings for each year; equilibrium, total region size and weights would be 3 to 4 times these numbers.

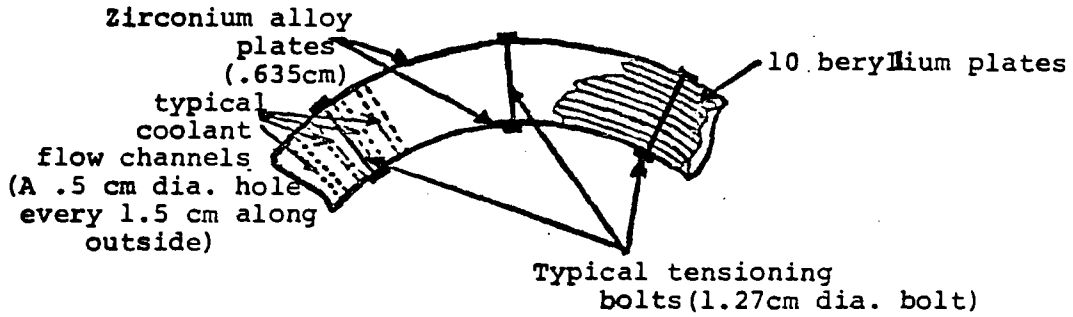

Fig. 5.2 Liner Details

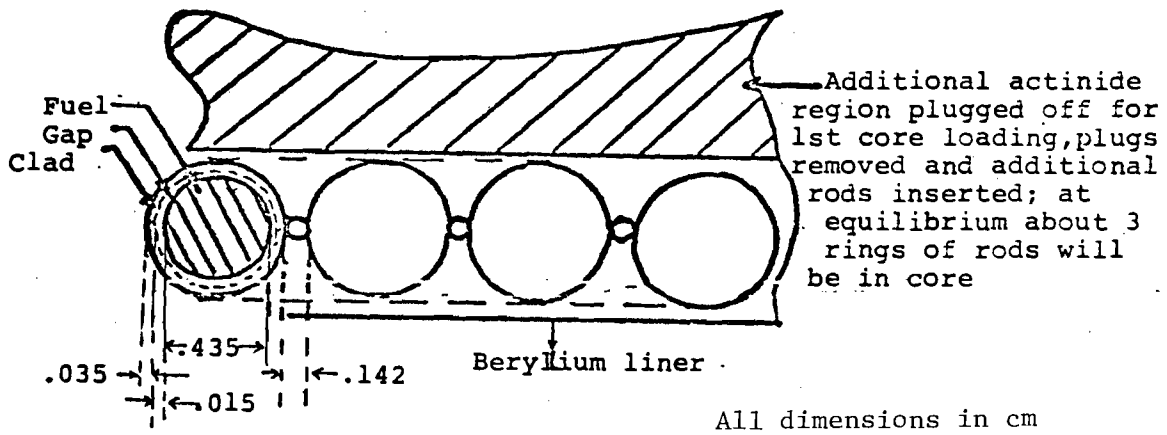

Fig. 5.3 Actinide Fuel Rods

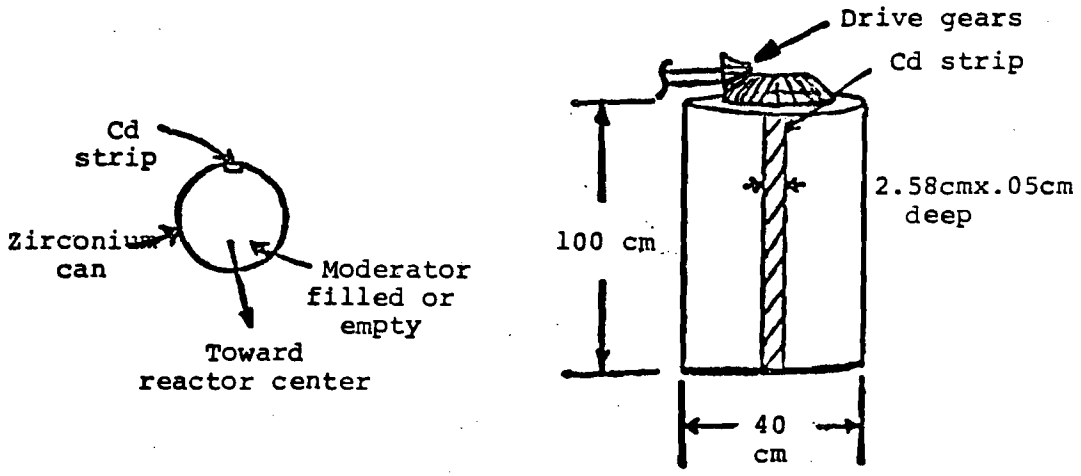

Fig. 5.4 Control Drum Details

rod with its associated clad and wire wrap will require 0.9194 cm width. The rods will be loaded in overlapping annulus regions as more actinides are introduced into the core. The initial charge of actinides should be about 445 Kg of actinide-oxides. This represents the yearly discharge from about 20 PWRs and requires one ring of actinide rods around the core. The equilibrium actinide loading would be about three rings of actinide rods or about 1500 Kg of actinide-oxides. Figure 5.3 shows the detail of the actinide region.

The control drums will be zirconium alloy cylindrical cans filled with beryllium or beryllium oxide with a strip of cadmium on one side. Figure 5.4 shows a typical control drum. These drums will provide the reactivity control needed to assure adequate dynamic control during operation.

A possible reactor layout is shown in Fig. 5.5.

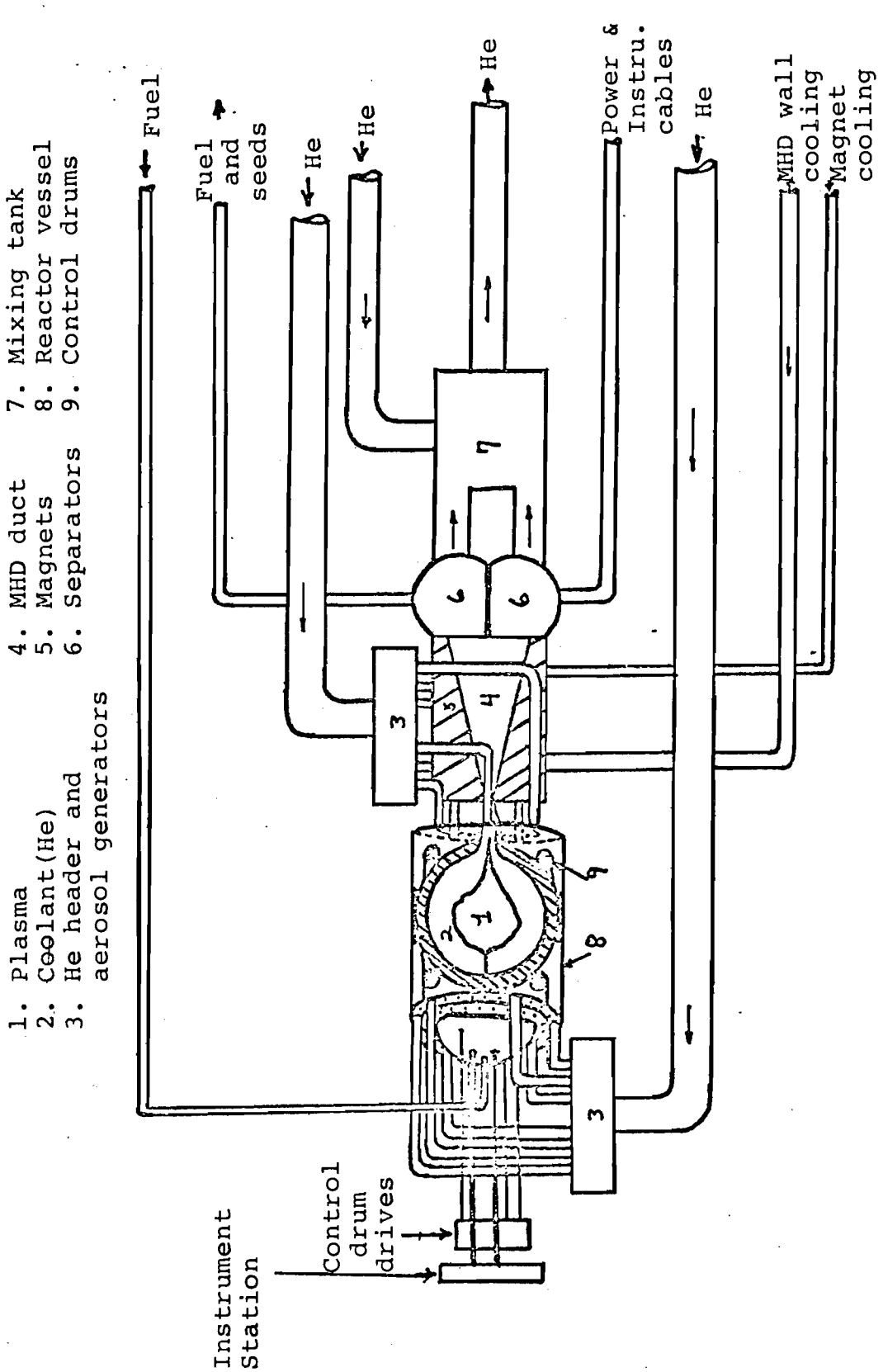

Fig. 5.5 Reactor Layout

REFERENCES FOR CHAPTER 5

1. SESONSKE, Alex, and Samuel GLASSTONE, "Nuclear Reactor Engineering," Van Nostrand Reinhold Company, New York, New York (1967).

2. WHITE, D. W., and J. E. BURKE (Eds.), "The Metal Beryllium," American Society of Metals, (1955).

3. KUNZE, J. F., and J. H. LOFTHOUSE, "Flow and Criticality in the Open Cycle Gas Core," 2nd Symposium on Uranium Plasmas: Research and Applications, 197, Atlanta, Georgia, November (1971).

6. NUCLEAR ANALYSIS-PLASMA CORE BREEDER REACTOR

Neutronics calculations were carried out for a U-233 plasma core with a molten salt breeding blanket. The primary objectives of the overall nuclear design were to design a reactor with a low critical mass (less than a few hundred kilograms U-233) and also a breeding ratio of 1.01. The later objectives was a safety precaution to guard against diversion of fissionable material during blanket reprocessing. Since only enough U-233 would be bred in the blanket to replenish the amount depleted in the core, any diversion of U-233 during reprocessing would result in an insufficient amount of fissionable material to replenish the core and the reactor would shut down. Both of the above objectives were met in the final design.

The Mach-I code[1] was used as the primary computational tool in the nuclear analysis. Mach-I is a one-dimensional diffusion theory code which uses the 26-group ABBN cross section set of Bondarenko, et al.[2] All neutronic calculations were performed by varying the plasma core radius to obtain $K_{eff} = 1.000$ with other dimensions held constant.

Initially, four moderators were analyzed to determine the one most suitable for the final reactor design. The moderators selected were graphite, beryllium, beryllium-oxide, and heavy water. Properties of each of these are listed in Table 6.1.

The geometry used for comparing the moderators is shown in Fig. 6.1. Region I is the core region (U-233 plasma). The pressure is maintained at 200 atmospheres and the average core temperature is 25,000°K.

Table 6.1 Selected Properties of Moderators

Moderator	$\rho(gm/cm^3)$	Atoms or Molecules $/cm^3$	$\Sigma a(cm^{-1})$	$\Sigma s(cm^{-1})$
Graphite	1.60	0.08023×10^{24}	2.728×10^{-4}	0.3851
Be	1.85	0.1236×10^{24}	1.174×10^{-3}	0.8652
BeO	2.96	0.07127×10^{24}	6.771×10^{-4}	0.4846
D_2O	1.105	0.03323×10^{24}	3.323×10^{-5}	0.4519

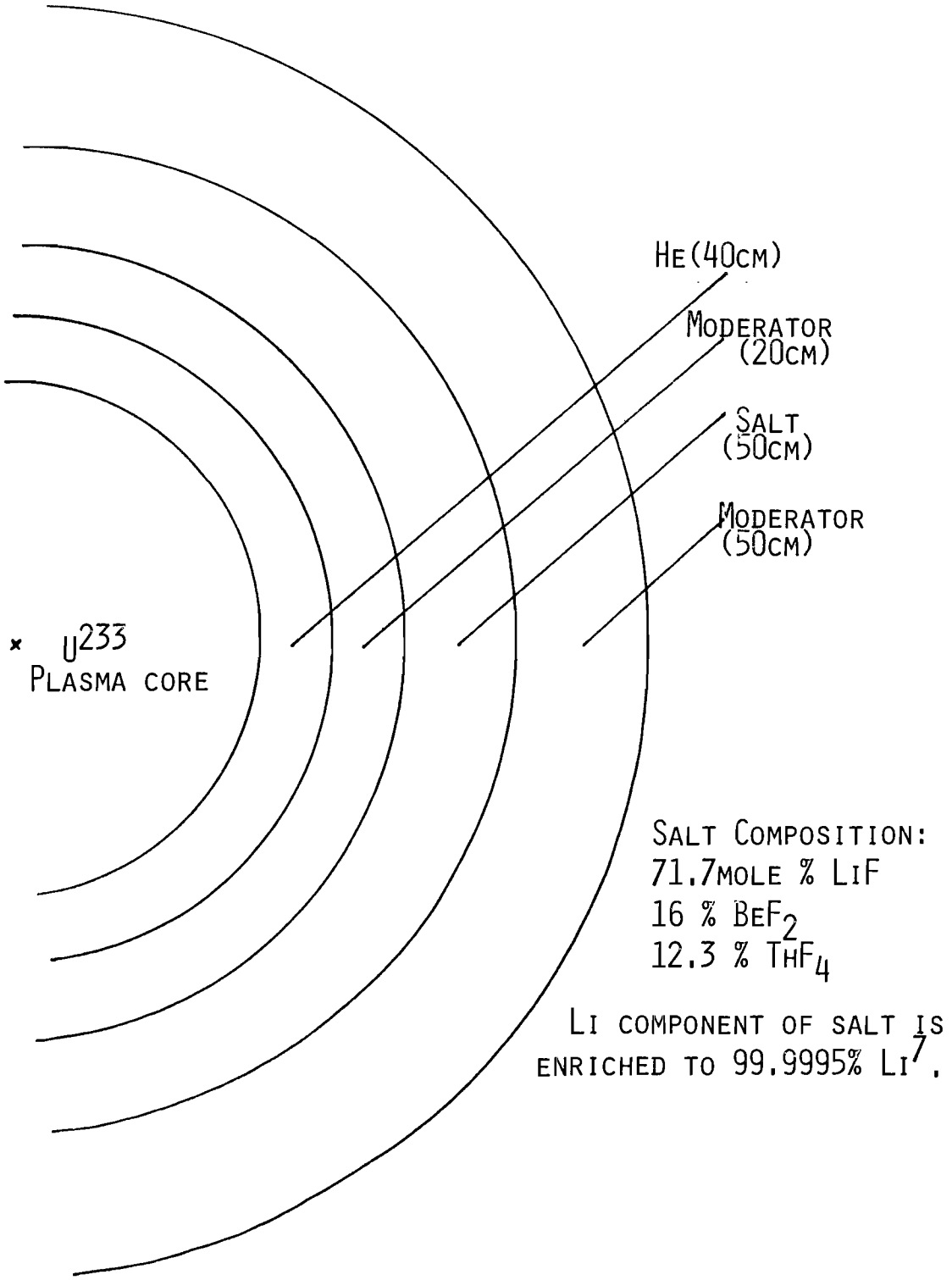

Fig. 6.1 Geometry Used For Moderator Comparison

Region II is the helium region with a pressure of 200 atmospheres and average temperature of $3000^{\circ}K$. This region serves to contain the plasma core as well as remove heat from the plasma core. This region was maintained at a thickness of 40 cm. in these initial calculations. Region III is the moderator region of 20 cm. thickness. This region is necessary to moderate the plasma core sufficiently to attain a small critical mass. Region IV is the molten salt region (50 cm.). The molten salt composition is 71.7 mole % Li F, 16 mole % BeF_2, and 12.3 mole % ThF_4. The Li is enriched to 99.99% in the Li^7 isotope in order to optimize neutron economy. The average temperature in this region is assumed to be $650^{\circ}C$. Region V was another moderator region (50 cm.). This region is necessary to maintain a breeding ratio greater than 1.0.

Results for the moderator comparison are shown in Table 6.2. It is evident from these calculations that either beryllium or beryllium-oxide could be used to meet the two primary objectives of the nuclear design. Beryllium-oxide was selected mainly due to its good thermal properties (m.p. of 2550°C) and also its good moderating and nuclear properties. Metallic beryllium could have been used if sufficient cooling were provided to ensure no melting would occur. All subsequent calculations were performed using BeO as the moderator.

Following the initial calculations to determine the most suitable moderating medium, calculations were performed to determine the effect of salt thickness, inner BeO liner thickness, and outer BeO thickness on critical mass and breeding ratio. These results are presented in Tables 6.3, 6.4 and 6.5. All dimensions except the one being studied remain as shown in Figure 6.1

Table 6.2 Breeding Ratios and Control Masses for Various Moderators

Moderator	Breeding Ratio	Critical Mass (Kg)
Graphite	1.06	2900
Be	1.12	14
BeO	1.14	17
D_2O	1.13	80

Table 6.3 Effect of Salt Thickness (BeO Moderation)

Salt Thickness	B. R.	Mass (KG)
50 cm.	1.14	17
40 cm.	1.139	16.53
30 cm.	1.130	16.49
20 cm.	1.105	16.33
10 cm.	1.026	14.94

Table 6.4 Effect of Inner Moderator Thickness

Thickness	B. R.	Mass (KG.)
10 cm.	1.143	1250
15 cm.	1.181	50.5
20 cm.	1.140	17
25 cm.	1.086	9.5
30 cm.	1.024	6.7

Table 6.5 Effect of Outer BeO Thickness

Thickness	Critical Mass (KG)	B. R.
50 cm.	17	1.14
40 cm.	17	1.1423
30 cm.	17	1.1420
20 cm.	17	1.1414
10 cm.	17	1.1397
5 cm.	17	1.1376
1 cm.	17	1.1334

The final reactor configuration is shown in Figure 6.2. For this configuration the critical core radius was 82.5 cm. The critical U-233 mass is 26.3 Kg. and the reactor breeding ratio is 1.0099. The helium region is 60 cm. in thickness which gives a $\frac{\text{r-helium}}{\text{r-core}} = 0.727$. This is sufficient for stable plasma confinement.

The final configuration is the only one not feasible. The overall critical mass could be decreased but the molten salt volume would need to be increased to maintain a constant breeding ratio. Table 6.6 summarizes the operating parameters for the plasma core breeder reactor.

Table 6.6 Operating Parameters for Plasma Core Breeding Reactor

1.	Power	2000 MW(th)
2.	Power Density ($^{kw}/\ell$) in Plasma	848.8
3.	Core Volume (cm^3)	2.35×10^6
4.	Core Radius (cm)	82.5
5.	Average Thermal Flux in Plasma ($^n/cm^2$-sec)	3.42×10^{15}
6.	Average Fission Density in Plasma ($^{fissions}/cm^3$-sec)	2.63×10^{13}
7.	Critical Mass U-233 (KGS.)	26.36
8.	Reactor Breeding Ratio	1.0099
9.	Peak/Average Fission Density in Plasma	1.126
10.	Fuel Absorption/Fissions in Plasma	1.113

REFERENCES FOR CHAPTER 6

1. MENELEY, D. A., et al., "Mach-I, A One-Dimensional Diffusion Theory Package," ANL-7223, (1966).

2. BONDARENKO, I. I., Ed., Group Constants for Nuclear Reactor Calculations, Consultants Bureau, New York (1964).

7. DESIGN CONSIDERATIONS OF THE BREEDER REACTOR

The material chosen for the pressure vessel was type 347 stainless steel. The pressure vessel is spherical and calculated minimum pressure vessel thicknesses are indicated on Figure 7.1. The designed operating temperature of the pressure vessel is $422^{\circ}K$. The inside radius is 193 cm. with an operating pressure of 200 atm. The minimum wall thickness is then 15.3 cm. and the designed wall thickness is 20 cm.

Figure 7.2 illustrates the helium and molten salt flow paths for the breeder reactor. Approximately 7% of the fission energy appears as energy of the neutrons and gamma rays. This energy, 140 MW, will ultimately be deposited in the reactor moderator, molten salt, and other structural materials. Also, 0.1% of the radiated energy from the plasma core; or 1.86 MW, will be deposited at the BeO wall of the cavity. This heat will be absorbed by the helium passing through the porous wall. The helium cooling the molten salt enters the heat exchanger at $422^{\circ}K$ and exits at $649^{\circ}K$.

The molten salt enters the reactor at $920^{\circ}K$ (nearly the minimum temperature possible) and is directed by Zircaloy baffles radially inward. The molten salt cools the inner BeO moderator layer and then leaves the reactor at $1110^{\circ}K$. Assuming that the salt absorbs all 140 MW of the heat from the inner layer, the flow rate of the salt will be 542 kg/sec and assuming a 10% pressure loss in the molten salt system, the needed pumping work is 330 KW. Part of the molten salt from the hot leg, 0.332 gm/sec, is diverted to the reprocessing systems. The amount of salt in the reactor is 1.75×10^{4} kg and the time spent by the salt in the reactor is 32 sec. There is a 2 cm. gap filled with helium between the molten salt

and the outer BeO moderator layer. This is to insulate the outer moderator and the pressure vessel from the high temperature molten salt.

Zircaloy is used for internal structural materials because of its low neutron absorption. There is a thin Zircaloy layer between the various regions of the reactor. The inner porous liner is a Zircaloy shell filled with BeO, 25% of the volume is passages for the helium coolant.

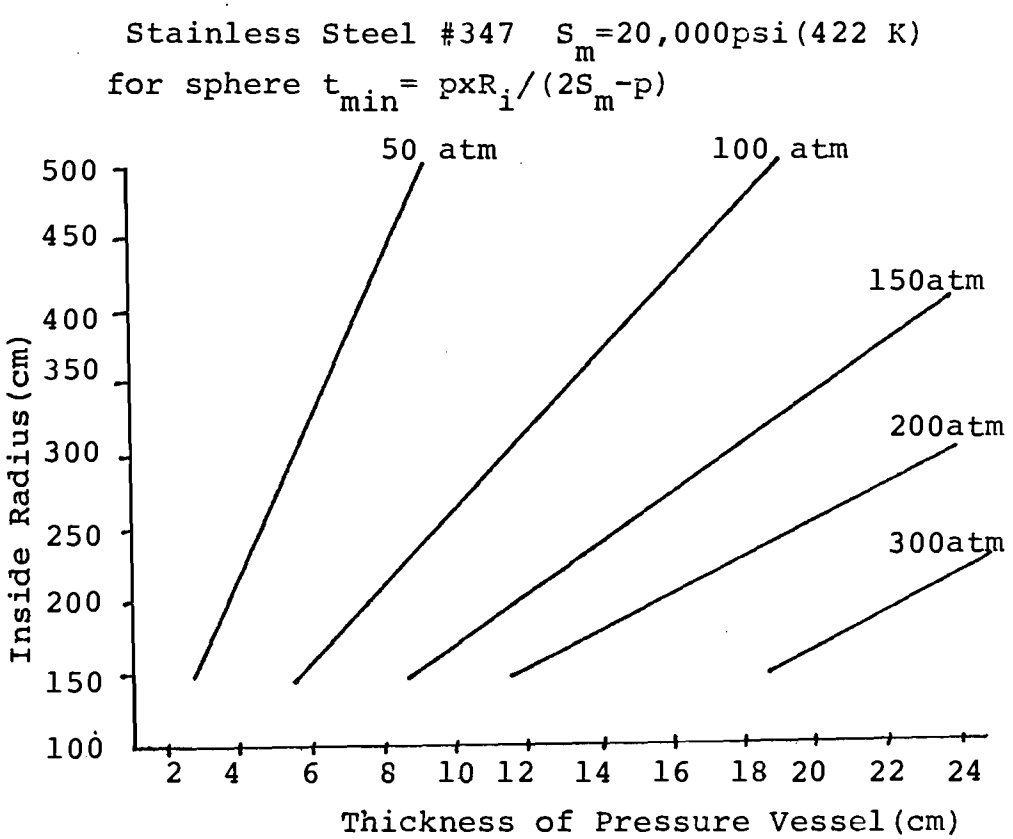

Fig. 7.1 Stainless Steel Pressure Vessel Wall Thickness as a Function of Inside Radius for Various Operating Pressures.

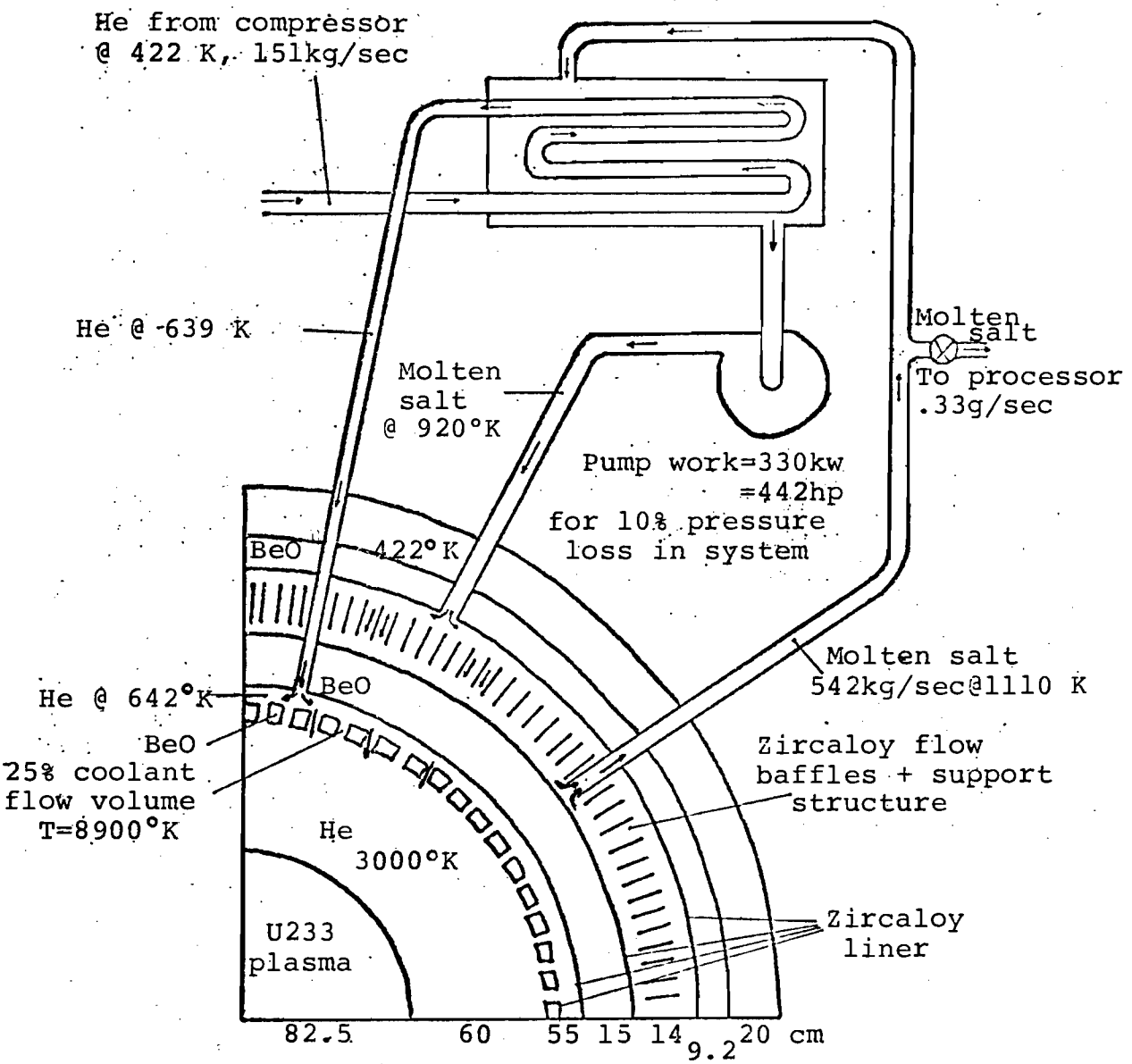

Fig. 7.2 Breeder Reactor Molten Salt Flow Schematic

8. REPROCESSING SYSTEM FOR PLASMA CORE BREEDER REACTOR

Since it is desirable to have the Plasma Core Breeder Reactor (PCBR) be a self-contained unit, generating its own new fuel, an on-line reprocessing system for the molten salt blanket is a necessity. This chapter describes protactinium removal and salt purification processes, calculations of expected flow rates, and equilibrium concentrations of various isotopes present in the system.

The salt used in the blanket is an eutectic mixture composed of LiF, BeF_2, and ThF_4 in the ratios of 72:16:12 mole percent. This particular combination was developed at Oak Ridge National Lab in conjunction with the Molten Salt Breeder Reactor program.

When thorium atoms contained in the salt enter the neutron field around the core, some of the atoms absorb a neutron and transmute to protactinium as shown in Figure 8.1. The protactinium eventually decays to uranium which can then be fed to the core as new fuel. However, as seen in Figure 8.1, Pa^{233} has a substantial cross section (22 barns) and since its half life is 27 days, Pa acts as a poison, siphoning off neutrons which could otherwise irradiate Th atoms. For this reason, it is desirable to remove Pa from the molten salt loop and allow it to decay outside the core.

However, since it is impossible to have a zero protactinium concentration in the molten salt blanket, there will be some uranium present in the core. Some of these atoms will fission and, consequently, there will be some uranium fission products in the molten salt loop. Some of

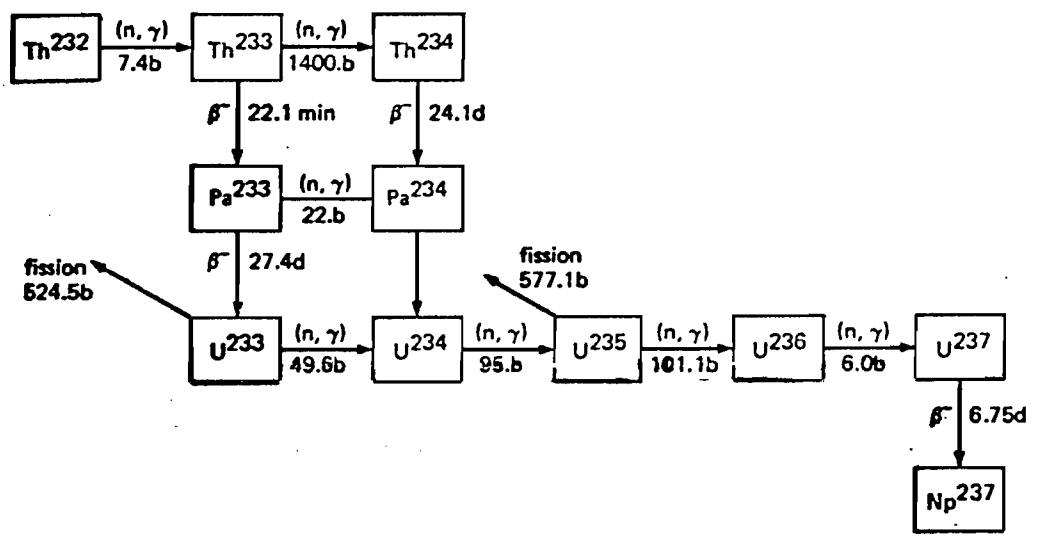

Fig. 8.1 The chain of isotopes created by neutron irradiation of Th232.

these fission products have large cross sections as shown in Table 8.1. Note that Xe and other gaseous fission product poisons are not listed because it is assumed that the blanket can be vented and these gaseous products easily removed. As will be shown later, the necessity of keeping the concentration of fission products at a low level determines the amount of time which the salt can stay in the irradiated blanket region.

In order to achieve the above neutronics goals, a fluorination-reductive extraction system was developed at Oak Ridge National Lab. A description of this process is as follows:[2]

> The fluorination-reductive extraction system for isolating protactinium is shown in its simplest form in Figure 8.2. The salt stream from the reactor first passes through a fluorinator, where most of the uranium is removed by fluorination. Approximately 90% of the salt leaving the fluorinator is fed to an extraction column, where it is countercurrently contacted with a bismuth stream containing lithium and thorium. The uranium is preferentially removed from the salt in the lower extractor, and the protactinium is removed by the upper contactor. A tank through which the bismuth flows is provided for retaining most of the protactinium in the system.
>
> The bismuth stream leaving the lower contactor contains some protactinium as well as the uranium that was not removed in the fluorinator and the uranium that was produced by the decay of protactinium. This stream is contacted with a H_2-HF

Table 8.1 Rare Earth Fission Product Absorption Cross Section

Nd-143	330 barns
La-139	8.9 barns
Eu-153	320 barns

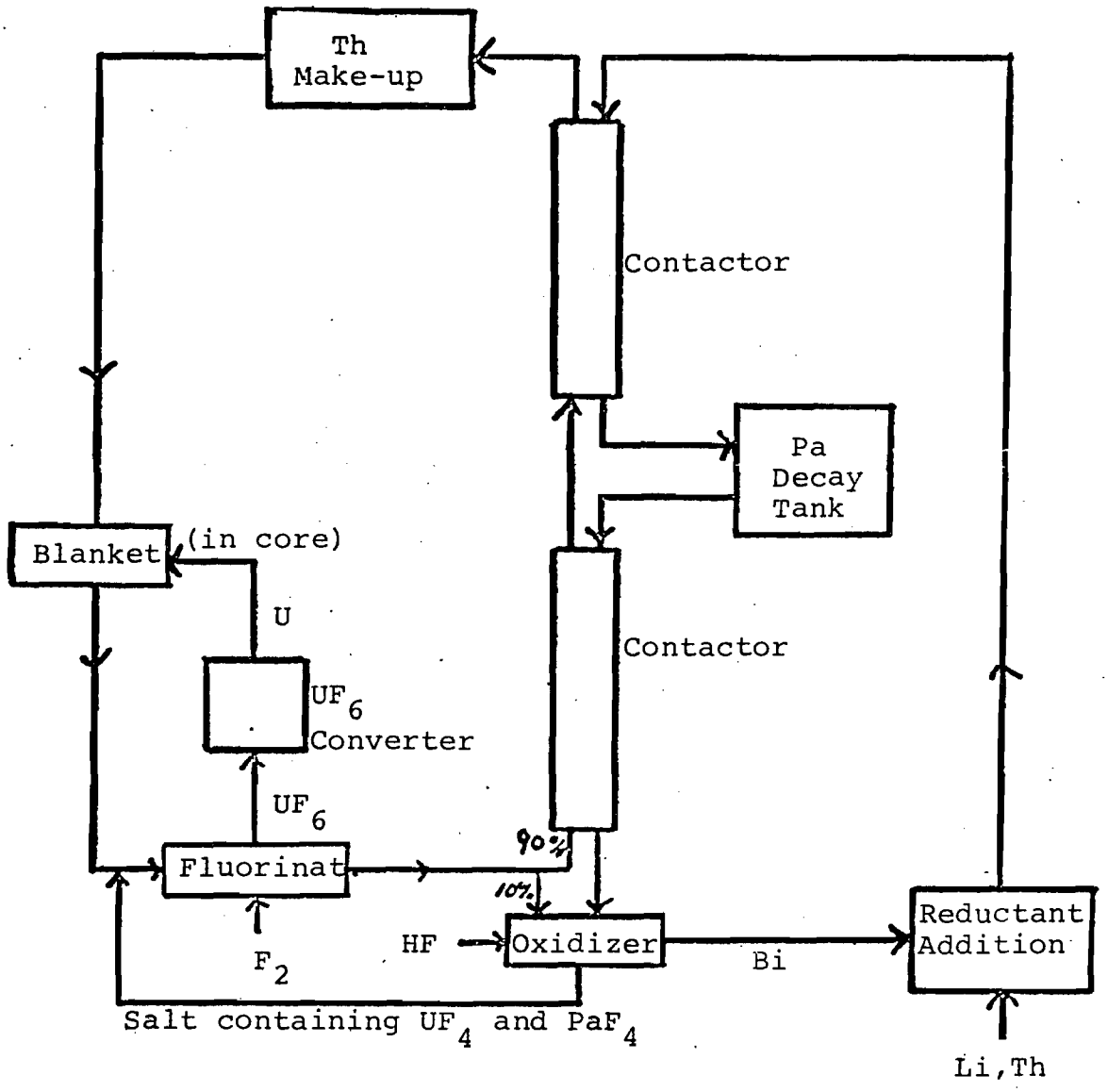

Fig. 8.2 Plasma Core Reactor Reprocessing System

mixture in the presence of approximately 10% of the salt leaving the flourinator in order to transfer the uranium and the protactinium to the salt. The salt stream, containing UF_4 and PaF_4, is then returned to a point upstream of the fluorinator, where most of the uranium is removed. The protactinium passes through the fluorinator and is subsequently extracted into the bismuth. Reductant (Li and Th) is added to the Bi stream leaving the oxidizer, and the resulting stream is returned to the upper contractor. The salt stream leaving the upper contactor is essentially free of uranium and protactinium and would be processed (for removal of any fission product gases and additional thorium added to compensate for that which had been consumed.)

Figure 8.3 describes the UF_6 to U metal conversion process. Unfortunately this is a batch process instead of a continuous flow system as is present in the remainder of the reprocessing set-up. However, there should be no problem providing temporary storage tanks for UF_6.

The UF_6 initially enters a reaction chamber where it is mixed with hydrogen. A reaction is triggered and UF_4 powder and HF gas is produced. The UF_4 is then loaded into a steel "bomb" which has been coated with fused dolomitic lime--lime is one of the few oxides that does not react with molten uranium. The "bomb" is then heated to 565°C where an exothermic reaction takes place and uranium metal solidifies on the bottom of the "bomb". The MgF_2 is removed and U metal of high purity can then be taken from the bottom of the "bomb" and sent to the reactor.[4]

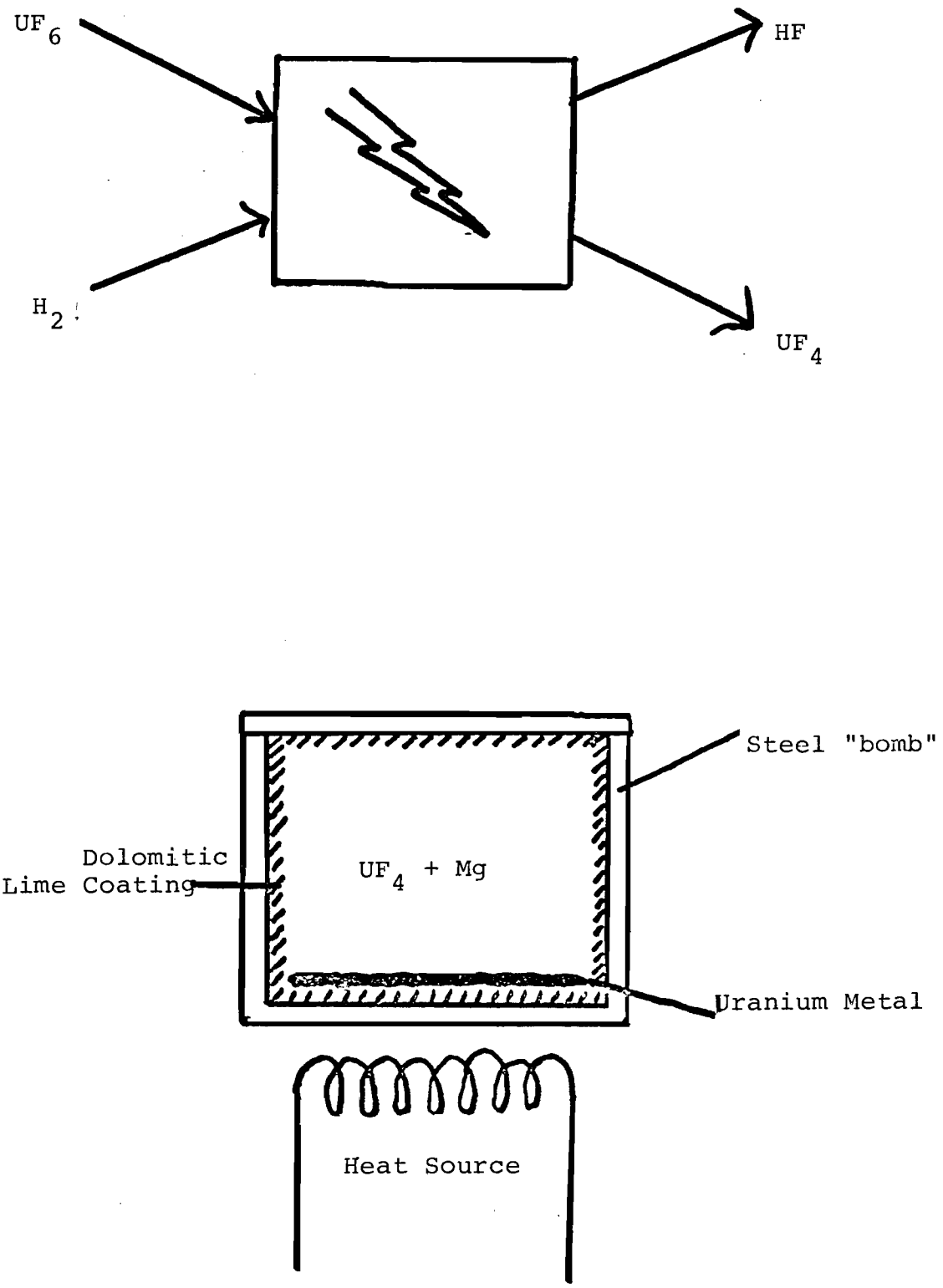

Fig. 8.3 UF_6 to U Metal Batch Process

Given certain constraints on the reprocessing system it is possible to calculate the flow rates which would exist in both the molten salt and bismuth loops. It is also possible to calculate protactinium concentrations throughout the reprocessing system and therefore determine uranium concentrations throughout the system. The constraints which are placed on the reprocessing system are as follows:

1) The protactinium concentration in the molten salt blanket is allowed to reach 95% of the equilibrium value obtained if the salt remained in the active region of the reactor for an infinite amount of time, provided that the concentration of protactinium does not cause parasitic absorption of neutrons by fission products greater than 1% of the absorptions which are due to thorium captures.

2) The volume of the blanket and the flux in the blanket shall be determined by breeding ratio constraints as explained elsewhere in this report.

3) The uranium removal efficiency of the fluorinator and oxidizer is 98%.[4]

4) The operating temperature of the system shall be 640°C (necessary because the salt is a eutectic mixture).[4]

5) The Li concentration in the Bi loop shall be 1%. The Th concentration in the Bi loop shall be held at less than 50% of the solubility of Th in Bi.[5]

6) The Pa distribution coefficient for the contactors, defined as (mole fraction of Pa in Bi at equilibrium)/(mole fraction of Pa in salt at equilibrium), is taken to be 100.[5]

7) The following physics data is assumed:

Neutron Flux	1.0E+14 n/cc-sec.
Volume of Blanket	5.29E+06 cc.
Molar Volume of Salt	0.0598 moles/cc.
Molar Volume of Bi	0.0469 moles/cc.
Pa Absorption Cross section	22 barns
Th Absorption Cross section	7.4 barns
U Absorption Cross section	571.3 barns
U Fission Cross section	524.5 barns
Pa Decay Constant	2.97E-07 sec^{-1}
Concentration of Th in salt	4.32E+21

8) Due to its very short half-life Th^{232} is assumed to transmute directly to Pa^{233} upon being struck with a neutron.

To satisfy assumption 1, we must examine if the Pa concentration in the salt from the output of the blanket will be governed by the rate of fission product captures. To determine the number of fission product captures we must first solve for the Pa and U concentrations. This is done as follows:

$$\frac{d\ Pa}{dt} + \lambda Pa = \sigma_a^{Th}\ \phi\ Th \tag{8.1}$$

where ϕ is the flux, Th is the thorium concentration, and λ the Pa decay constant.

Solving Eq. 8.1 gives

$$Pa = \frac{\sigma_a^{Th}\phi\ Th}{\lambda} - e^{-\lambda t}\left[\frac{\sigma_a^{Th}\phi\ Th}{\lambda} - Pa_o\right] \tag{8.2}$$

The equation for the uranium concentration as a function of time is

$$\frac{dU}{dt} = - \phi \sigma_a^u U + \lambda Pa \tag{8.3}$$

where U is the U-233 concentration.

Solving this equation we have

$$U = U_o e^{-\sigma_a^u \phi t} + \frac{\sigma_a^{Th}\ Th}{\sigma_a^u} \left(1 - e^{-\sigma^u \phi t}\right)$$

$$- \lambda \left[\frac{\sigma_a^{Th} \phi\ Th}{\lambda} - Pa_o\right]\left[\frac{e^{-\lambda t} - e^{-\sigma^u \phi t}}{\sigma^u \phi - \lambda}\right] \tag{8.4}$$

If a given atom of material is assumed to spend time T in the blanket, then the number of fissions which occurs during this time is

$$\text{No. of fissions} = \int_o^T \sigma_f^U \phi\ U(t)dt \tag{8.5}$$

Evaluating this integral we have

$$\text{No. of fissions} = \sigma_f^u \phi \left[\frac{\sigma_a^{Th}\ Th}{\sigma_a^u} \left(T - \frac{e^{-\sigma_a^u \phi T} - 1}{\sigma_a^u \phi}\right) - \right.$$

$$\left. \frac{\lambda}{(\sigma_a^u \phi - \lambda)} \left[\frac{\sigma_a^{Th} \phi Th}{\lambda} - P_{ao}\right]\left[\frac{1 - e^{-\lambda T}}{\lambda} + \frac{e^{-\sigma_a^u \phi T} - 1}{\sigma_a^u \phi}\right]\right] \tag{8.6}$$

and the fission product concentration at the end of a cycle of length T is given by

$$[F.P.] = \left[\int_o^T \sigma\phi\ U(t)\ e^{\sigma_f^u \phi t} dt\right] e^{-\sigma_f^u \phi T} << \gamma\ (\text{No. of fissions}) \tag{8.7}$$

where γ is the probability per fission of getting a particular fission product. Since the fluorinater removes 98% of the uranium in the molten salt on each pass through the system, the entering concentration to the blanket region can be taken as effectively zero.

Solving Eq. 8.7 for a variety of times T, the results, given as $\frac{\Sigma_{Eu}}{\Sigma_{Th}}$ where Σ_{Eu} is the absorption cross section of one of the most troublesome rare earth fission products, Eu^{153}, are shown in Table 8.2. It should be stated that this estimate of the Eu^{153} concentration is high due to the approximation in Eq. 8.7. However, even with this high estimate it can be seen that no fission product removal system is necessary.

To determine the flow rates and concentrations in the system, one must make use of the following mass balance equations.[6] If one refers to the hypothetical exchange column shown in Figure 8.4

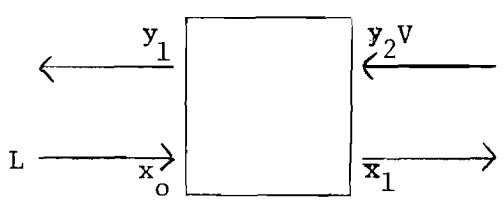

Figure 8.4: Exchange Column Flows

then a material balance yields the following equation:

$$Lx_o + Vy_2 = Lx_1 + Vy_1 \tag{8.8}$$

or

$$L\ (x_o - x_1) = V\ (y_1 - y_2) \tag{8.9}$$

Table 8.2 Protactinium and Europium Concentrations in Blanket

Time in Blanket (days)	Pa Concentration (% of equilibrium)	$\frac{\Sigma_a^{Eu}}{\Sigma_a^{Th}}$ (%)
114	.95	6
45.5	.70	.75
26.1	.50	.165
19.1	.40	.072
10.7	.25	.0135
3.91	.10	$6.9(10^{-4})$

where L and V are flow rates in moles/sec and x and y are concentrations of the transferring material expressed in mole fractions. Now at equilibrium

$$y_1 = K \cdot x_1 \tag{8.10}$$

where K is a constant known as the distribution coefficient. Substituting for x_1 in Equation 8.9 and solving for y_1 we have

$$y_1 = \frac{y_2 + \frac{L}{V} x_o}{\frac{L}{KV} + 1} \tag{8.11}$$

So if we knew the two inlet concentrations and if we can find the flow rates then the outlet concentrations can be calculated.

The value of the flow rates in the Bi and blanket loops must be solved for iteratively. A flow chart of the solution process is shown in Fig. 8.5 and a FORTRAN program written to solve this problem. A value for the Bi flow rate is assumed and for given Pa core concentration, neutron flux, and core volume, the flow rate in the blanket, residence time in the core, and input concentration of Pa to the core can be solved for iteratively.

Now, as referenced above, ORNL report number 4344 gives the distribution coefficient of Pa as a function of time of contact and relative volumes of salt and Bi. Picking a specific distribution coefficient determines the time of contact and the relative volume of the two components. A new value for the Bi flow rate can then be calculated by using the value of the blanket flow rate calculated above. The entire iterative procedure is then repeated with the new Bi flow rate.

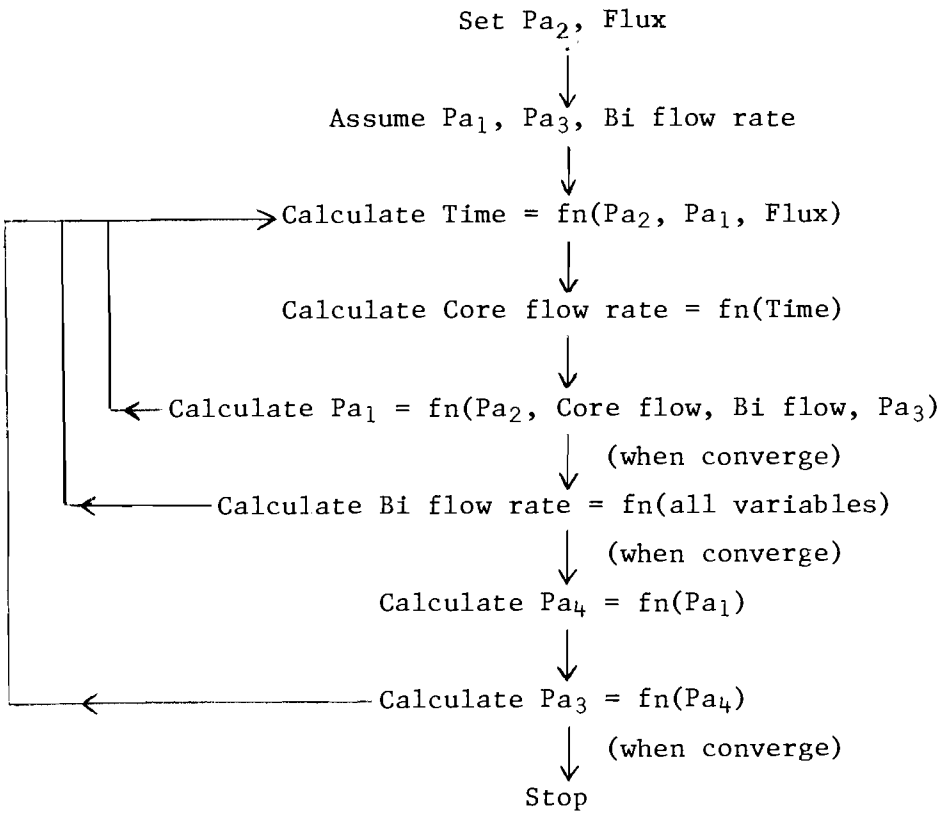

Pa_1 = Core input Pa concentration

Pa_2 = Core output Pa concentration

Pa_3 = Bi loop contactor input Pa concentration

Pa_4 = Bi loop contactor output Pa concentration

Figure 8.5 Flowchart for Calculation of Reprocessing System Flow Rates and Pa Concentration

Once the flow rates have been calculated, the output Pa concentration in the Bi loop from the contactor can then be found from Eq. 8.11 and the input concentration from Eq. 8.9.

It should be noted at this point that if a contactor is composed of several stages with K being the distribution coefficient in each stage, then the procedure described above can be applied to the whole system with the number of stages, N, given by the expression[6]

$$N = \frac{\log \left[\frac{A-1}{A} \left(\frac{y_{n+1} - Kx_o}{y_1 - Kx_o} \right) + \frac{1}{A} \right]}{\log A} \tag{8.12}$$

where A is the absorption factor and is defined by A = L/(KV). However, for simplicity, this report assumes the contactor to have only one stage.

Performing the calculations described above, the reprocessing system parameters shown in Table 8.3 were calculated.

In conclusion, an on-line, on-site reprocessing system for the Plasma Core Reactor is quite feasible. The technology is available today and the chemical processes involved in uranium separation have been proven in various laboratory experiments at Oak Ridge National Lab as a part of the Molten Salt Breeder program. Only a Pa isolation system is required, no fission product removal system is necessary.

Table 8.3

Summary of Reprocessing Systems Parameters for PCBR

The fission concentration in the blanket per cycle is .333E+18 fissions per cc.

The effective time spent in the core is .655E+01 days.

The flow rate through the core is .691E+00 G-moles/sec.

Input protactinium concentration to the core is .549E+18 atoms per cc.

Output protactinium concentration from the core is .145E+20 atoms per cc.

The flow rate in the Bi loop is .180E+00 G-mole/sec.

The Pa concentration in the Bi loop entering the contactor is .848E+18 atoms per cc.

Output Pa concentration from the contactor is .430E+20 atoms per cc.

The number of stages in the contactor is .100E+01.

REFERENCES FOR CHAPTER 8

1. HENRY, A. F., Nuclear Reactor Analysis, M.I.T. Press, 763, (1975).

2. McNEESE, L. E., "Engineering Development Studies for Molten-Salt Breeder Reactor Processing No. 5," ORNL TM-3140, 15-16, (October 1971).

3. BENEDICT, M., and T. H. PIGFORD, Nuclear Chemical Engineering, McGraw-Hill, 156-158, (1957).

4. McNEESE, L. E., Op. Cit., 18.

5. "Molten Salt Reactor Program Semiannual Progress Report for Period Ending August 31, 1968," ORNL-4344, 292-298, (1969).

6. FOUST, A. S., Principal of Unit Operations, Wiley, 45, 77, (1964).

9. MHD GENERATOR AND SEPARATOR

The plasma core reactor-MHD system was first explored by Colgate and Aamodt in 1957.[1] In 1973, Williams and Clement presented calculations for plasma core reactor-MHD power plants which had efficiencies of 70 percent or more.[2]

The problems associated with the plasma core reactor-MHD system are likely to be severe, but the potential of this system is large enough to warrant serious investigation. The growing program in MHD power generation and the ongoing UF_6 reactor tests at Los Alamos[3] will provide information related to some critical components. However, studies are needed to define the problems unique to plasma core reactor-MHD systems, to offer possible solutions, and to formulate an experimental program if such a program is desired. In view of the growing interests in MHD and plasma core reactor technologies and long lead times in research and development of both space and terrestrial applications, it is both timely and beneficial to initiate such studies.

The analysis of the MHD generator follows that of Ref. 2. The generator is a segmented electrode Faraday generator with cesium seeded helium as the working fluid. Since He does not ionize significantly until 8000°K, even at 1.013 pascals (10^{-4} atmospheres), it may be treated as a perfect gas.[4,5] The relevant gas properties are listed in Table 9.1.

Table 9.1 Gas Properties of Helium

Ratio of Specific Heats, γ	1.6667
Specific Heat at Constant Pressure, Cp	5192 $\frac{J}{Kg\,^{o}K}$
Gas Constant	2077 $\frac{J}{Kg\,^{o}K}$

The electrical conductivity of the seeded gas is a function of temperature, pressure, and seed mass fraction. Only thermal ionization was considered in this study, although the actual generator includes several non-equilibrium processes due to slow recombination during expansion through the duct (frozen flow), current caused by a motional emf or an electric field, fission fragment, and electromagnetic radiation. The design parameter that is affected directly by the electrical conductivity is the length of the generator. This in turn will influence other parameters as will be subsequently seen.

The generator is a constant velocity generator which is divided into 15 segments to eliminate the Hall current. The state points which are used in the analysis are shown on Fig. 9.1. Note that for a unit mass of helium, a fraction x is diverted to cool the nozzle, a fraction y is diverted to cool the electrodes, and the remaining fraction 1-x-y cools the blanket before entering the reactor cavity.

Given the cavity power, Q_c, and the cavity inlet and exit stagnation temperatures, T_{t_1} and T_{t_2}, respectively, the mass flow rate at the cavity exit is

$$\dot{m}_2 = \frac{Q_c}{H_{t_2} - H_{t_1}} = \frac{Q_c}{Cp(T_{t_2} - T_{t_1})} \tag{9.1}$$

where H_{t_2} and H_{t_1} are stagnation enthalpies at the reactor entrance and exit, respectively.

The static temperature and pressure at the nozzle exit (MHD duct entrance) for an isentropic process are

$$T_3 = \frac{T_{t_2}}{1 + \frac{\gamma-1}{2} M_3^2} \tag{9.2}$$

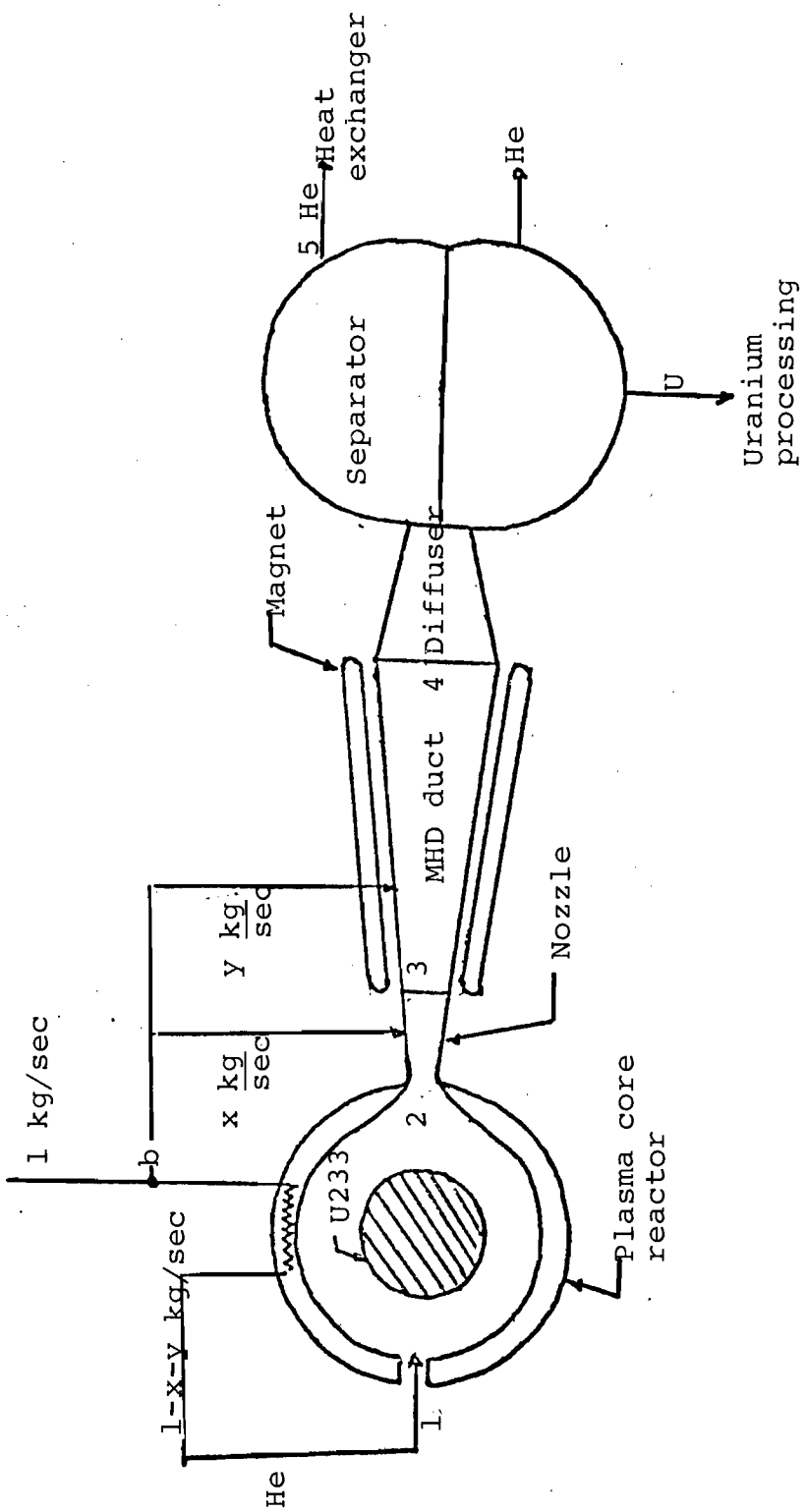

Fig. 9.1 MHD-Separator System

$$p_3' = \frac{p_{t_2}}{\left[1 + \frac{\gamma-1}{2} M_3^2\right]^{\frac{\gamma}{\gamma-1}}} \tag{9.3}$$

where M_3, the Mach number at the MHD entrance and p_{t_2}, the stagnation pressure at the cavity exit are input quantities.

The helium velocity at the MHD inlet is

$$U_3 = \sqrt{\gamma R\, T_3'}\, M_3 \quad . \tag{9.4}$$

This velocity is constant across the generator. The kinetic energy of the gas is

$$K.E. = \frac{U_3^2}{2} \quad . \tag{9.5}$$

The total enthalpy at the nozzle exit has a component from the cavity and a component due to nozzle cooling

$$H_{t_3} = \frac{(1-x-y)H_{t_2} + x\, H_{t_b}}{1-y} \tag{9.6}$$

The static enthalpy at the MHD inlet is

$$H_3 = H_{t_3} - K.E. \tag{9.7}$$

The corresponding static pressure and temperature at the MHD inlet are

$$p_3 = p_3' \tag{9.8}$$

$$T_3 = \frac{H_3}{Cp} \tag{9.9}$$

The inlet density of the gas at the MHD inlet is

$$\rho_3 = \frac{p_3}{R\ T_3} \tag{9.10}$$

while the mass flow rate is

$$\dot{m} = \dot{m}_2 \frac{1-y}{1-x-y} \tag{9.11}$$

The MHD inlet area is then

$$A_3 = \frac{\dot{m}_3}{\rho_3\ U_3} \tag{9.12}$$

The pressure ratio for each segment is

$$p_m = \left(\frac{p_3}{p_4}\right)^{\frac{1}{n}} \tag{9.13}$$

where n is the number of segments and $\frac{p_3}{p_4}$, the pressure ratio across the generator are given.

The exit pressure at each segment is

$$p_{m_{i+1}} = \frac{p_{m_i}}{p_m} \quad i = 1, \ldots, n \tag{9.14}$$

with $p_{m_1} = p_3$. The pressure drop for each segment is

$$\Delta p_i = p_{m_{i+1}} - p_{m_i} \qquad i = 1, \ldots, n \tag{9.15}$$

The exit temperature of the ith segment neglecting electrode cooling is

$$T_{m_{i+1}}' = \frac{T_{m_i}'}{p_m^{\frac{K(\gamma-1)}{\gamma}}} \qquad i = 1,\ldots,n \tag{9.16}$$

where K is the MHD loading factor and $T_{m_1}' = T_3$.

The exit enthalpy of each segment with transpirational cooling of the electrode is

$$H_{m_{i+1}} = \frac{H_{m_{i+1}}'\left[1 - y + (i-1)\frac{y}{n}\right] + H_{t_b}\frac{y}{n}}{\left(1 - y + i\frac{y}{n}\right)} \qquad i = 1,\ldots,n \tag{9.17}$$

with $H_{m_1} = H_{m_1}' = H_3$. The exit temperature at each segment is then

$$T_{m_{i+1}} = \frac{H_{m_{i+1}}}{Cp} \qquad i = 1,\ldots,n \tag{9.18}$$

with $T_{m_1} = T_3$. To find the average conductivity in each segment, σ_i, requires the average temperature and pressure in each segment given by

$$\bar{T}_{m_i} = \frac{T_{m_{i+1}} + T_{m_i}}{2} \tag{9.19}$$

$$\bar{p}_{m_i} = \frac{p_{m_{i+1}} + p_{m_i}}{2} \tag{9.20}$$

The length of each segment is given by

$$\Delta L_i = \frac{\left|\Delta p_i\right|}{B^2 U_3 \sigma_i (1-K)} \tag{9.21}$$

where B is the magnetic flux density and is an input quantity.

The density corresponding to T_{m_i} and p_{m_i} is

$$\rho_{m_i} = \frac{p_{m_i}}{RT_{m_i}} \qquad i = 1,\ldots,n \tag{9.22}$$

which is used to determine the inlet area of each segment

$$A_{I_i} = \frac{\dot{m}_3 + \frac{y}{n}\frac{\dot{m}_3\,(i-1)}{1-y}}{U_3\,\rho_{m_i}} \qquad i = 1,\ldots,n \tag{9.23}$$

The exit area of each segment is

$$A_{E_i} = \frac{A_{I_i}}{p_m\,K\,\frac{(\gamma-1)}{\gamma}\;-1} \qquad i = 1,\ldots,n \tag{9.24}$$

The generator length is

$$L = \sum_{i=1}^{n} \Delta L_i \tag{9.25}$$

$P_4 = P_{m_{n+1}}$ and $T_4 = T_{m_{n+1}}$ so that the MHD exit enthalpy is

$$H_4 = Cp\ T_4 \tag{9.26}$$

The stagnation enthalpy at the MHD exit is

$$H_{t_4} = H_4 + \frac{U_3^2}{2} \tag{9.27}$$

The MHD exit Mach number is

$$M_4 = \frac{U_3}{\sqrt{\gamma R T_4}} \tag{9.28}$$

After leaving the MHD duct, the Mach number of helium is reduced to 0.1 by a diffuser before entering the separators. The temperature and pressure at the separator exit are

$$T_5 = T_4 \frac{(1 + \frac{\gamma-1}{2} M_4^2)}{(1 + \frac{\gamma-1}{2} M_5^2)} \tag{9.29}$$

$$p_5 = p_4 \left[\frac{(1 + \frac{\gamma-1}{2} M_4^2)}{(1 + \frac{\gamma-1}{2} M_5^2)} \right]^{\frac{\gamma}{\gamma-1}} \tag{9.30}$$

Assuming no losses, the thermal energy in the MHD generator is equal to the electric power produced.

$$Q_{MHD} = \dot{m}_2 (H_{t_2} + \frac{x}{1-x-y} H_{t_b} + \frac{y}{1-x-y} H_{t_b} - \frac{1}{1-x-y} H_4) \tag{9.31}$$

Since two separators are used, the flow rate into each separator is

$$\dot{m}_{s_{in}} = \frac{1}{1-y} \frac{\dot{m}_3}{2} \tag{9.32}$$

The gas velocity at the separator exit is

$$U_5 = \sqrt{\gamma R\ T_5}\ M_5 \tag{9.33}$$

The helium density at the inlet or exit of each separator is

$$\rho_5 = \frac{P_5}{R\ T_5} \tag{9.34}$$

The inlet area of each separator is

$$A_{in} = \frac{\dot{m}_{in}}{\rho_5\ U_5} \tag{9.35}$$

The separator has two exits connected with two turbine-compressor units. The exit area is

$$A_{ex} = \frac{\dot{m}_{ex}}{\rho_5 U_5} \tag{9.36}$$

where

$$\dot{m}_{ex} = \frac{\dot{m}_{in}}{2} \tag{9.37}$$

A computer program was developed for the MHD generator and separator. A baseline case was established and is summarized in Table 9.2. The assumed magnetic flux density of 18.0 Teslas is very high compared to fields of normal MHD generators but is within superconducting magnet technology. This large value was due to four constraints on

Table 9.2 MHD Reference Design

Core Power = 2000 MWt

MHD Electric Power = 1022 MWe

Reactor Exit Temperature = 3500°K

Cavity Pressure = 2.027×10^7 Pascals (200 ATM.)

MHD Pressure Ratio = 3.0

MHD Exit Temperature = 2273°K

MHD Inlet Mach Number = 0.500

MHD Exit Mach Number = 0.596

Helium Gas Velocity in MHD Duct = 1672 M/sec.

Load Factor = 0.8

Magnetic Flux Density = 18.0 Teslas

MHD Length = 3.47 M

Length/Diameter = 10.75

MHD Inlet Diameter = 0.222 M

MHD Exit Diameter = 0.323 M

CS Seed Fraction = 0.015

Number of Electrode Segments = 15

Conductivity in First Segment = 206 MHOS/M

Conductivity in Last Segment = 7.1 MHOS/M

the generator. First, a reasonable length had to be found. A large pressure ratio would result in excessive lengths (greater than 10 meters). The length of the generator was a strong function of the pressure ratio (Fig. 9.2). This effect was due to the strong variation of electrical conductivity with temperature. At low exit temperatures (less than $2000^{\circ}K$), corresponding to a large pressure ratio, the conductivity decreases by several orders of magnitude from its value at the MHD inlet resulting in a very long generator.

Even more important was the length to diameter ratio of the generator as a function of the MHD pressure ratio (Fig. 9.2). For inert gas generators, L/D is about 10 to insure a well behaved boundary layer. This value may be conservative but was taken as a constraint on the system. Figure 9.3 shows that the magnetic flux density is also a strong function of the MHD pressure ratio for a L/D of 10.

However, the MHD pressure ratio cannot be taken to be too low; otherwise, very little power is extracted. It is desirable to convert as much of the thermal energy in the fluid in the MHD duct as this leads to a higher plant efficiency. It was desired to extract 1000 MWe or more from the plant at high plant efficiencies. This factor plus the constraints on length and L/D led to the values in Table 9.2.

The magnetic field may be considered too high. In this case, the MHD pressure ratio can be dropped which lowers the magnetic field requirements (Fig. 9.3), but decreases the electrical power output (Fig. 9.4). Another alternative is to keep the electric output constant, but increase the core power and decrease the pressure ratio. Again the magnetic field requirement is lower, but the efficiency of the plant

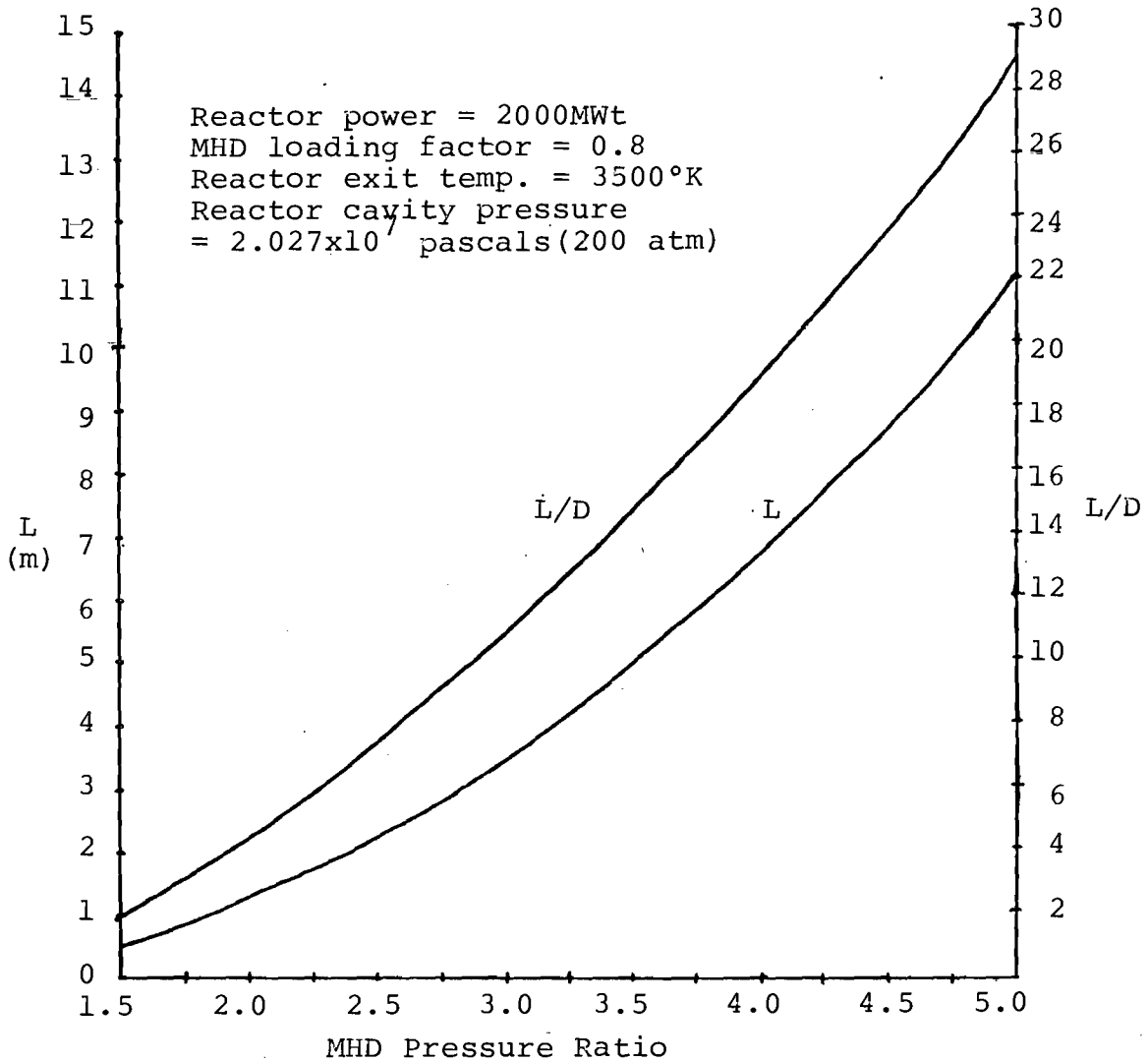

Fig. 9.2 Length and Length-to-Diameter Ratio Versus MHD Pressure Ratio

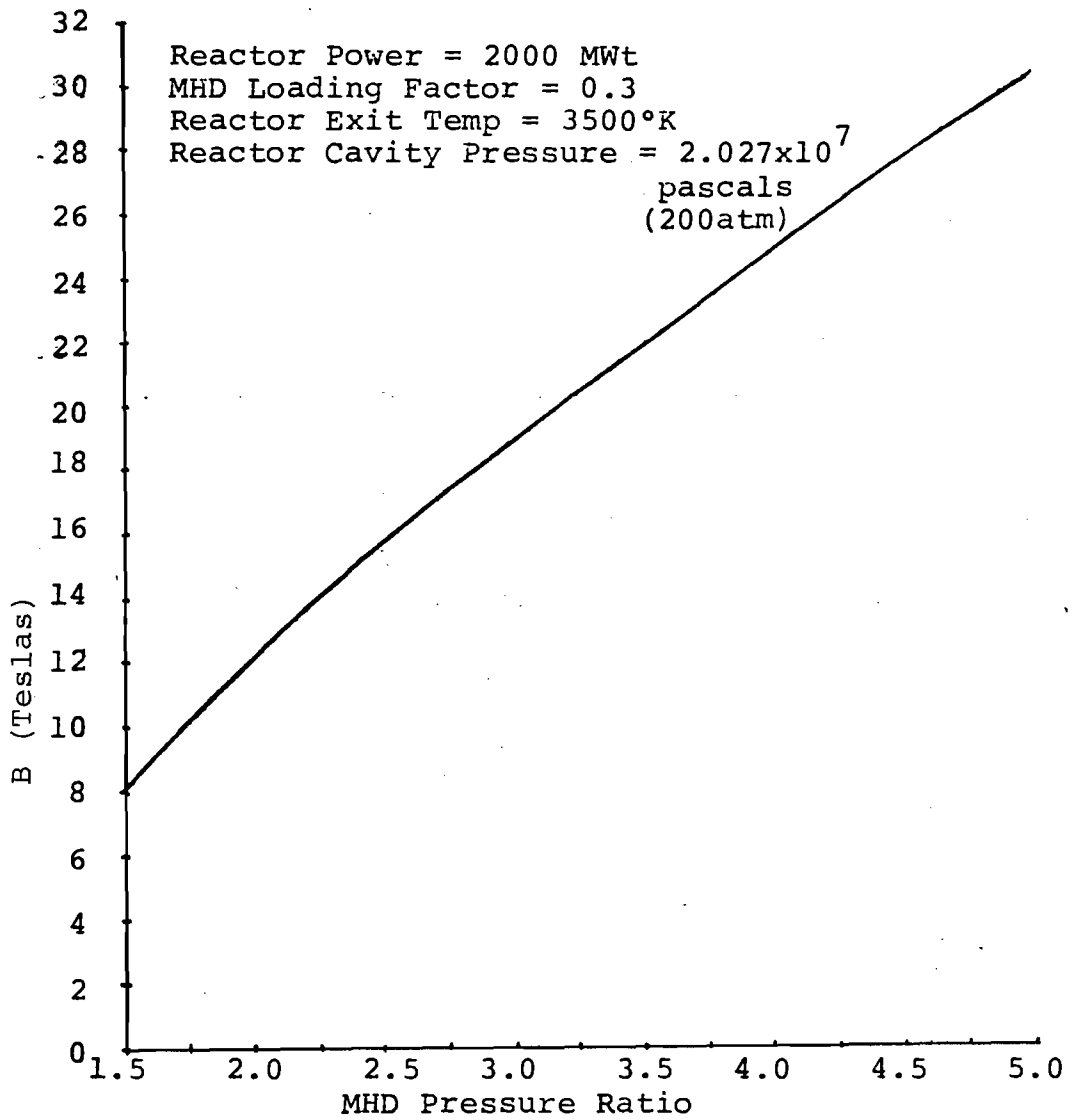

Fig. 9.3 Magnetic Flux Density Versus MHD Pressure Ratio for L/D = 10

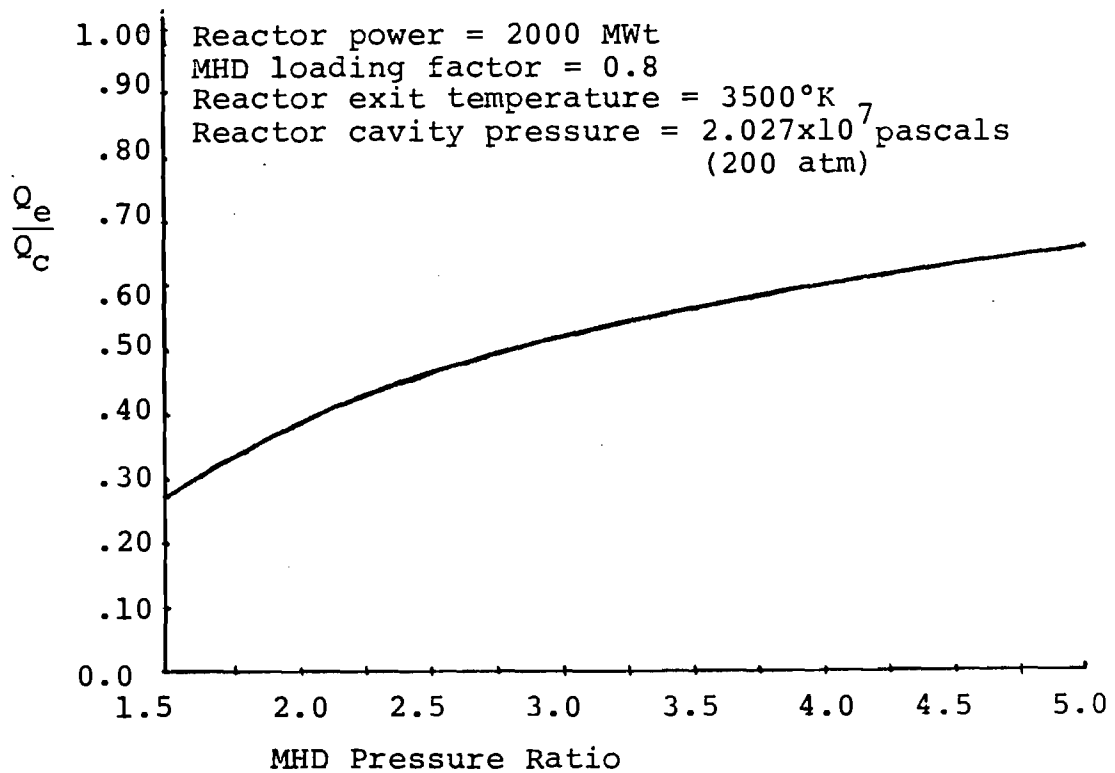

Fig. 9.4 MHD Electric Output Normalized to Cavity Power Versus MHD Pressure Ratio

decreases. The selection of a proper power level depends on economic factors such as capital and fuel costs which is beyond the scope of this study.

In addition, operating at lower cavity pressures would result in an increase in electrical conductivity as large pressures inhibits ionization. However, 200 atmospheres was chosen as the cavity pressure to insure low critical masses for the breeder and actinide transmutation reactor concepts. No optimization of pressure was performed for the combined reactor-MHD system.

The constraints of electric power output, length, length-to-diameter ratio, and cavity pressure lead to a MHD generator with a large magnetic field but is within the technology of superconducting magnets.

An optimization study is needed on cavity power and cavity pressure to obtain a better MHD generator. Also, a two temperature model is needed for the calculation of the electrical conductivity to account for non-equilibrium processes.

The main question of the MHD generator that will have to be answered or solved concerns the flow of uranium through the duct. The fission fragments may enhance ionization in the channel but may also cause serious problems. Some of the problems are:

a) Shielding the superconducting magnet from neutrons and gammas. This should not be too much of a technical problem but may be an economic one. Research on fusion reactors should provide some information in this area,

b) Radiation damage to the electrodes over a prolong period of time. Not much is known in this area and it should be given attention,

c) Condensation of uranium droplets may short out the electrodes. This is probably the most important concern of this type of system and it deserves considerable research.

REFERENCES FOR CHAPTER 9

1. COLGATE, S. A. and A. L. AAMODT, "Plasma Reactor Promises Direct Electric Power," Nucleonics (August 1957).

2. WILLIAMS, J. R. and J. D. CLEMENT, "Exploratory Study of Several Advanced Nuclear - MHD Power Plant Systems," Final Status Report, NASA Grant NGR-11-002-145, Georgia Institute of Technology, (March, 1973).

3. THOM, K., R. J. SCHNEIDER, and F. C. SCHWENK, "Physics and Potentials of Fissioning Plasmas for Space Power and Propulsion," International Astronautical Federation XXVth Congress, Amsterdam, September 30 - October 5, 1974.

4. LICK, W. J. and H. W. EMMONS, Thermodynamic Properties of Helium to 50,000°K, Harvard University Press, (1962).

5. LICK, W. J. and H. W. EMMONS, Transport Properties of Helium from 200 to 50,000°K, Harvard University Press, (1965).

10. POWER PLANT SYSTEMS

In order to achieve maximum effectiveness from the high temperature coolants from plasma core reactors, it was decided that a ternary power cycle would produce the highest efficiency power plant. The ternary cycle consists of a combination of MHD, gas turbine, and Rankine cycle energy conversion units. Two concepts were considered — systems with and without a high temperature regenerator in the helium loop.

The objectives of the study were as follows:

1. Model the nuclear MHD power plant cycle.
2. Analyze the power output from the three energy conversion units and evaluate plant overall efficiency.
3. Make a parametric study of the effect of changing operating variables on plant overall performance.

The components of the propsed systems are shown in Figs. 10.1 and 10.2. For both systems the heat source is a high temperature reactor with a uranium plasma core (UPC). Helium is used to cool the core and is the working fluid for the MHD generator and gas turbine. Helium enters the MHD generator and expands from state 1 to state 2. After the MHD channel it passes through a diffuser and enters the separator where the uranium is separated from the helium. Because of its high temperature at the exit of the separator, the helium needs to be cooled. This process takes place in a mixing tank (MT) where high temperature helium is mixed with helium coming from compressor (C1) in Fig. 10.1. At point 4 the cooled helium enters the gas turbine. After expansion, helium passes through heat exchangers (HE1) and (HE2) where heat is transferred to the steam cycle. Helium is then compressed in the first stage (C1) and

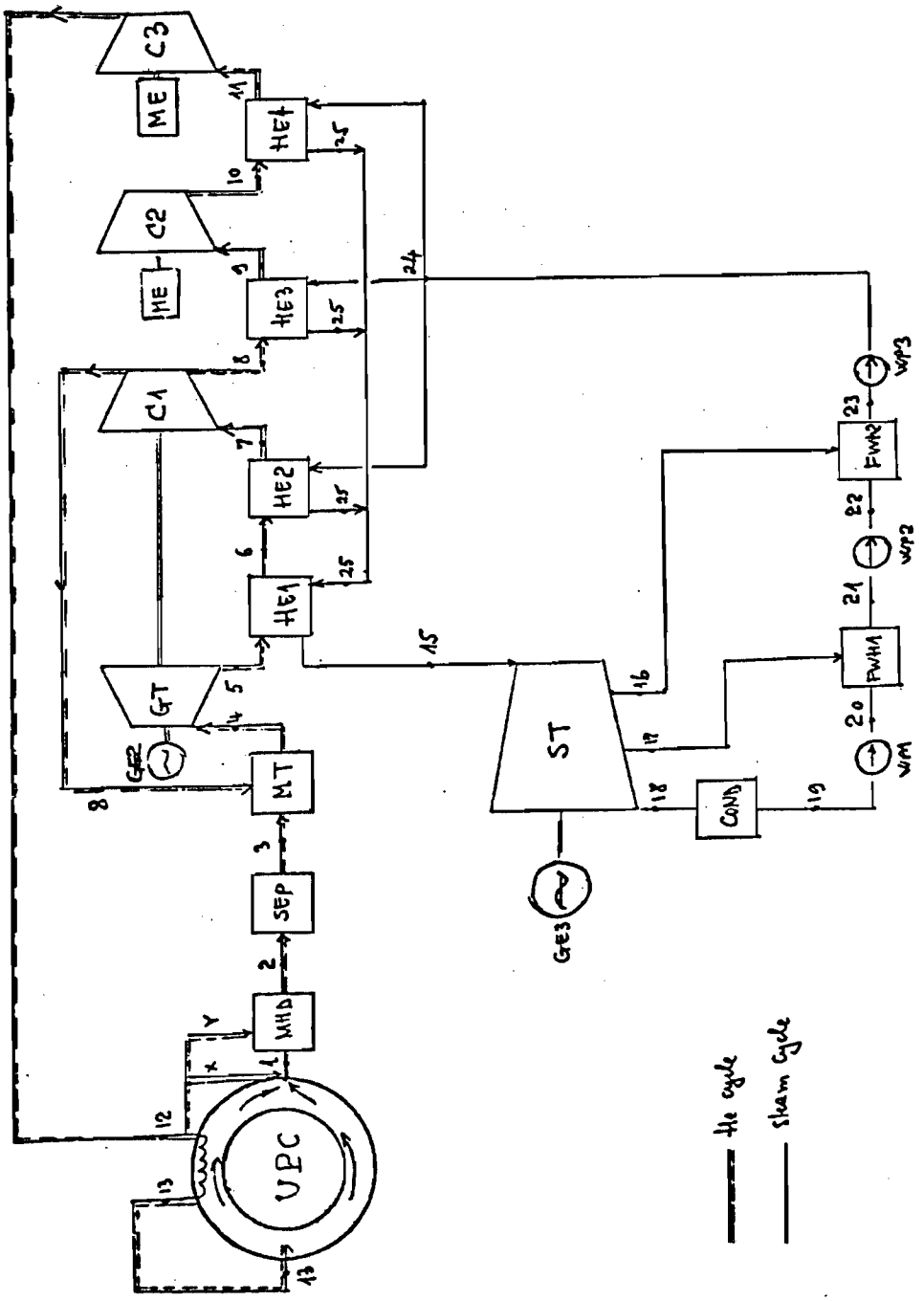

UPC - Uranium Plasma Core; MHD - MHD generator; SEP - Diffuser and Separator; MT - Mixing Tank; GE - Electric Generator; GT - Gas Turbine; C - Compressor; HE - Heat Exchanger; ME - Electric Motor; ST - Steam Turbine; COND - Condenser; WP - Water Pumps; FWH - Feed Water Heater.

Fig. 10.1 Nuclear MHD Power Plant Without Regeneration

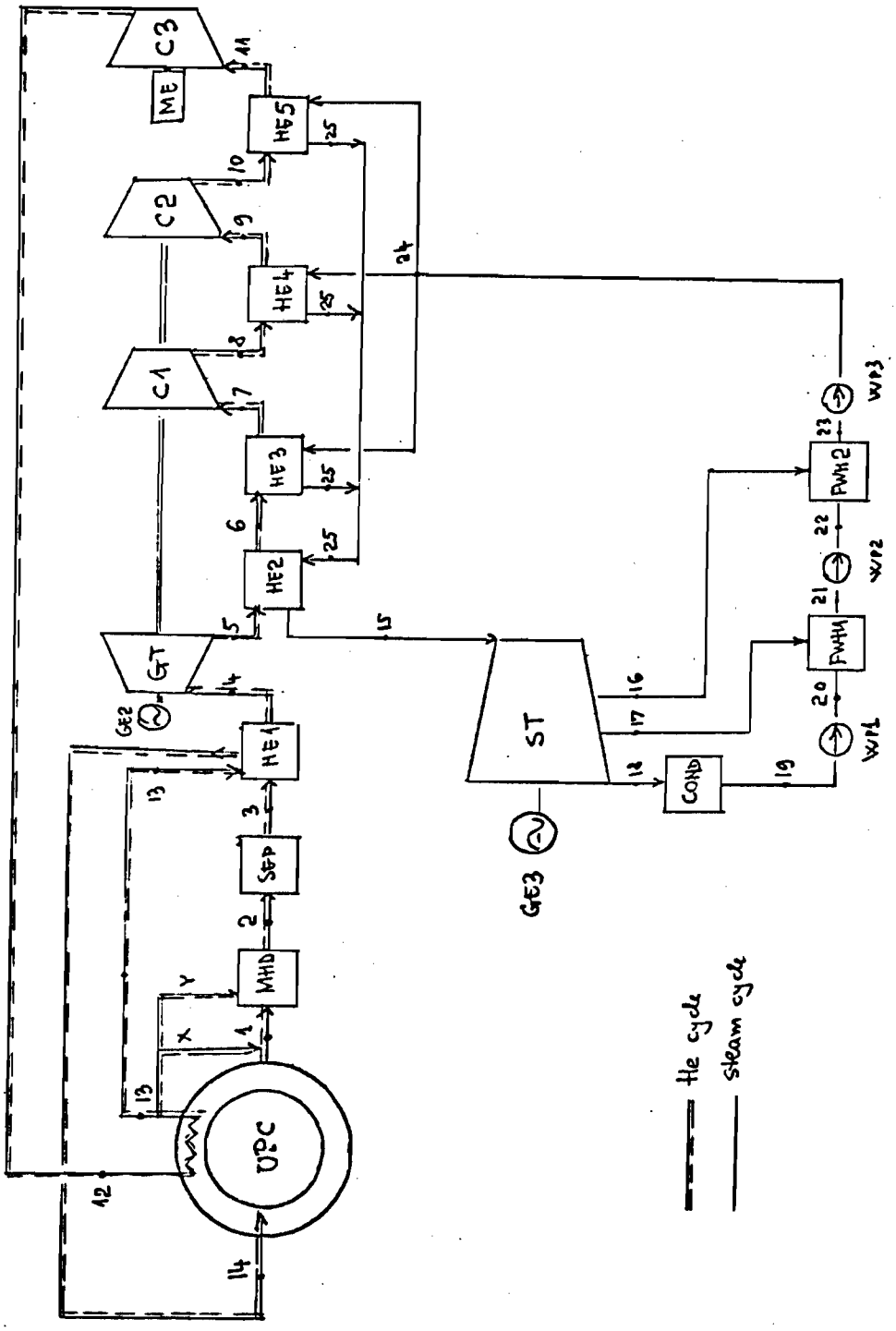

UPC - Uranium Plasma Core; MHD - MHD Generator; SEP - Diffuser and Separator; HE1 - Regenerative Heat Exchanger; HE2,3,4 and 5 - Heat Exchangers; GE - Electric Generator; GT - Gas Turbine; C - Compressor; ME - Electric Motor; ST - Steam Turbine; COND - Condenser; WP - Water Pump; FWH - Feed Water Heater.

Fig. 10.2 Nuclear MHD Power Plant With Regeneration

then split into two loops. The inner loop is provided to feed the mixing tank. The outer loop is to cool the reactor and for this purpose the helium needs two more compression stages (C2 and C3). The intercoolers (HE3 and HE4) transfers heat to the steam cycle. Before entering the reactor, two fractions, x and y, are taken for cooling the nozzle and MHD duct. Since the MHD pressure ratio is greater than that of the gas turbine, and to maintain a functional unity for the components with the same mass flow rate of gas, compressor (C1) is on the same axis with the gas turbine and electric generator (GE2), while compressors (C2) and (C3) are powered by electric motors.

The nuclear MHD power plant with regeneration (Fig. 10.2) is similar to the previous system in the heat source region (reactor, MHD, and SEP). After the separator, helium passes through a regenerative heat enchanger (HE1) and enters the gas turbine. Between states 5 (exit GT) and 12 (inlet breeding zone of the reactor), helium is compressed in three stages and transfers a part of its heat to the steam cycle in heat exchangers HE2, HE3, HE4, and HE5. Unlike the previous system, helium passes through only one loop and transfers a major part of its heat through regeneration.

For both systems the steam cycle is the same. Water heated in one or two stages of feedwater heaters (or directly from the condenser) goes to a boiler. Superheated steam enters a steam turbine (ST) and then passes through a condenser (COND).

All studies used values for input data according to current commercial technology (i.e. efficiencies for steam cycle components, gas turbine, and compressors) or with current use in MHD research. For the

isentropic efficiency of the MHD generator we assumed values of 75% - 80%.[1,2] The electric efficiency of the MHD generator was provided by Fig. 10.3.

The modeling of the MHD cycle consisted of defining a pseudo - Brayton cycle and treating the expansion within the MHD generator in a similar manner as in a gas turbine. In order to analyze the two systems it was necessary to write two computer codes:

(1) NMHD-1 — code to analyze the nuclear MHD power plant without regeneration in the helium loop

(2) NMHD-2 — code to analyze the nuclear MHD power plant with regeneration in the helium loop.

The basic logic followed in the computer codes is presented in Fig. 10.4. Table 10.1 lists input parameters for each system.

The codes are general in that they permit any changes in input data. From the input data, using special subroutines (TSAT, SUPER and SATL), the program STEAM evaluates all necessary parameters for the steam cycle and calculates the net power produced within the cycle. In addition, the code prepares the enthalpy values for determining the mass flow rate ratio between the helium cycle and steam cycle. For evaluation of state parameters characteristic to the top cycles the codes have implemented a subprogram MHD (different for the two codes). Taking information from calculations done by STEAM and MHD the codes evaluate the power distribution for each energy conversion unit and calculates the plant overall efficiencies.

For a pair of selected parameters by the user, the codes permit a parametric study of the whole system yielding information for evaluating power distributions and overall efficiencies. The first parameter

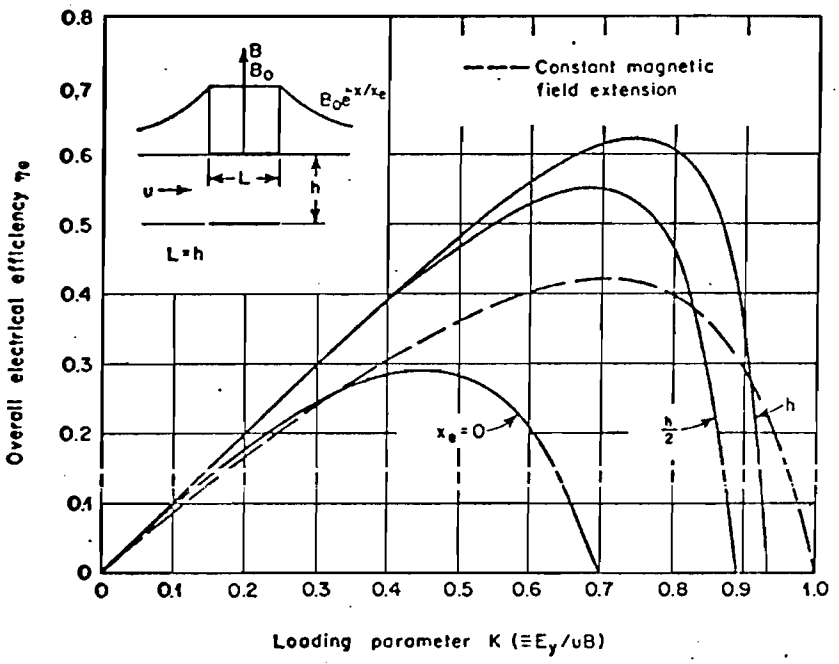

Fig. 10.3 Overall Electrical Efficiency Versus Load Parameter K for a Faraday MHD Generator(3).

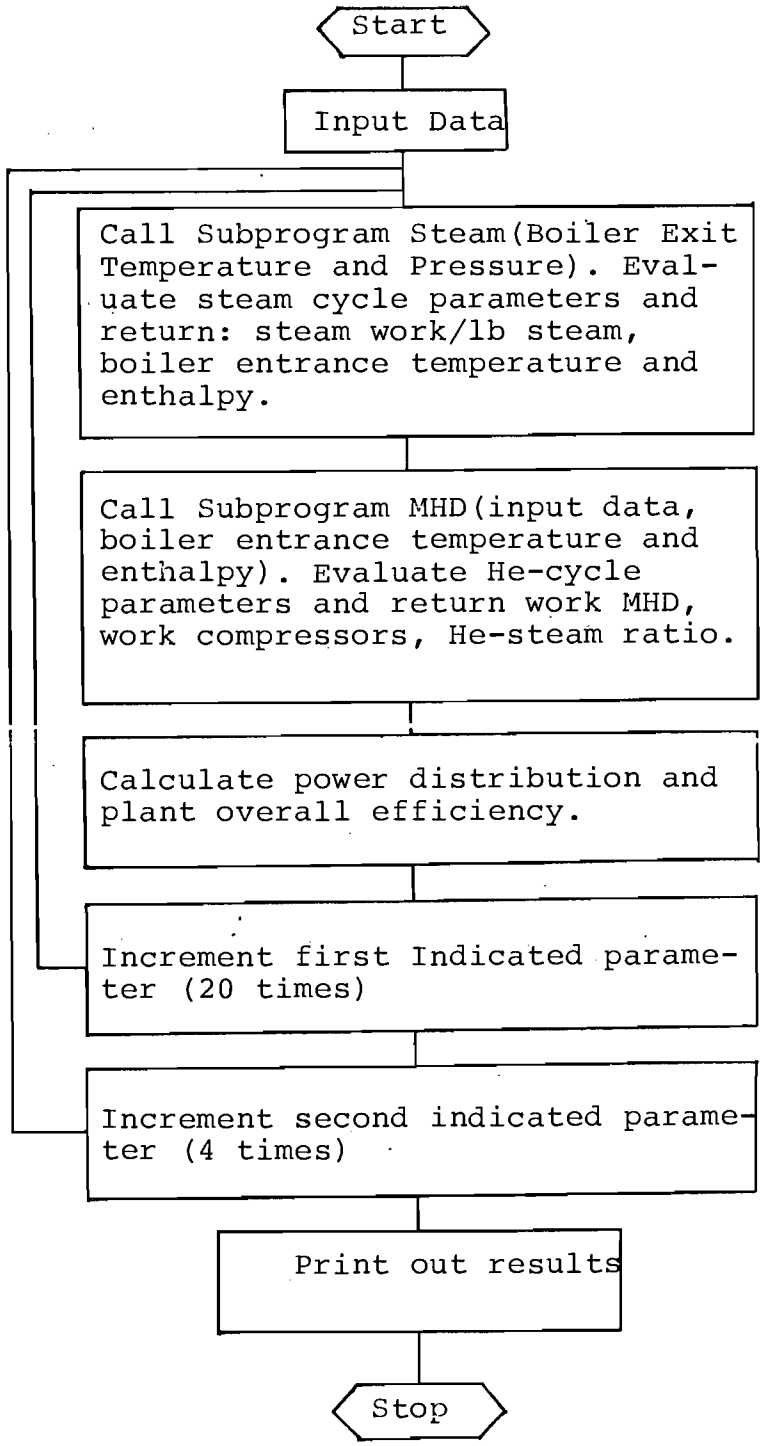

Fig. 10.4 NMHD Program Flow Chart

Table 10.1 Input Data for NMHD-1 and NMHD-2

Index	NMHD-1		NMHD-2	
1	Boiler Temperature ----	1000°F	Boiler Temperature ----	1000.°F
2	Boiler Pressure -------	1600 psia	Boiler Pressure -------	1600 psia
3	Condenser Pressure ----	1.0 psia	Condenser Pressure ----	1.0 psia
4	Steam Turbine Efficiency	81%	Steam Turbine Efficiency	81%
5	Pump Efficiency -------	80%	Number of Feed Heaters	0,1 or 2
6	Number of Feed Heaters	0,1 or 2	Reactor Temp Difference	200°K
7	Compressor Efficiency -	85%	Compressor Efficiency -	85%
8	MHD Inlet Temp --------	3000°K	MHD Inlet Temp --------	3000°K
9	MHD Inlet Press -------	200 bar	MHD Inlet Press -------	200 bar
10	MHD Pressure Ratio ----	5.0	MHD Pressure Ratio ----	3.0
11	Gas Turbine Pressure Ratio	2.0	Gas Turbine Press. ratio	3.0
12	Feed Heater 1 Pressure	12. psia	Feed Heater 1 press. --	12. psia
13	Feed Heater 2 Pressure -	4. psia	Feed Heater 2 press. --	4.0 psia
14	Bottom Temp Difference -	150°K	Bottom Temp Diff. ----	150°K
15	MHD Inlet Mach No. ----	0.5	MHD Inlet Mach No. ----	0.5
16	Sep Outlet Mach No. ----	0.1	Sep Outlet Mach No. ---	0.1
17	Gas Turbine Inlet Temp -	1500°K	Gas Turbine Inlet Temp	1500°K
18	MHD Efficiency ---------	49%	MHD Efficiency --------	49%
19	Gas Turbine Efficiency -	85%	Gas Turbine Efficiency	85%
20	Number of Compress Stages	3.0	Number of Compress Stages	3.0

is incremented twenty times; for each step of this variation, the second parameter is incremented four times.

The objectives of the parametric studies were to establish the influence of different parameters on overall efficiencies for each system and to determine power distribution. For a suitable comparison of the influence of each parameter on the overall efficiency, a new parameter called "sensitivity" was defined.

The sensitivity of the plant overall efficiency is defined as the ratio

$$\text{sensitivity (\%)} = \frac{\eta_i}{\eta_o} \times 100 \qquad (10.1)$$

where: η_o is the reference value efficiency obtained in the first step of calculation;

η_i is the efficiency obtained in the ith step of the parametric study.

The results obtained in this study provide valuable information concerning the behaviour of overall efficiencies. Results are presented in Fig. 5. The most important parameters affecting overall efficiency are as follows:

1. MHD inlet temperature.
2. MHD pressure ratio.
3. Temperature drop across the regenerative heat exchanger (for NMHD2).
4. Gas turbine pressure ratio
5. MHD inlet pressure.
6. Boiler temperature
7. Boiler pressure

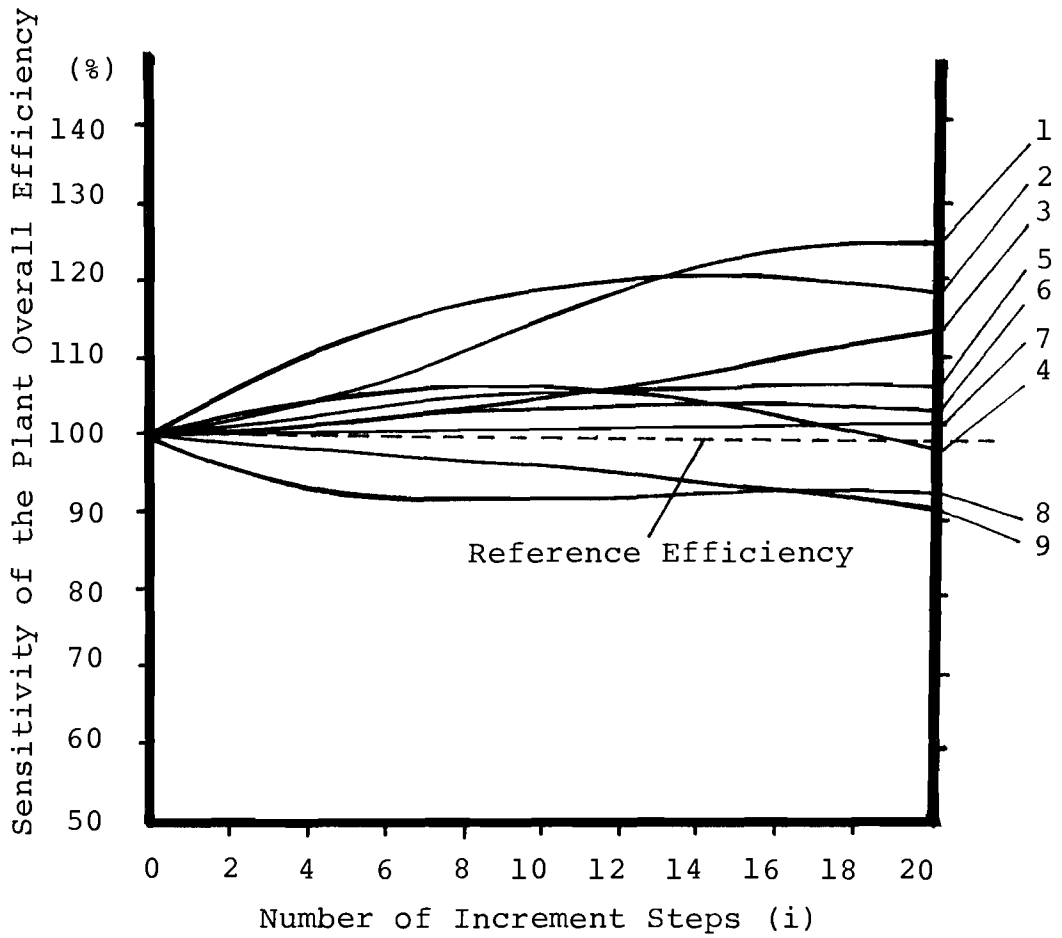

1 MHD Inlet Temperature (3000-5000°K, η_o=62.75%)
2 MHD Pressure Ratio (1.5-11.5, η_o=59.65%)
3 Temp Drop Regenerator (300-1000°K, η_o=60.13%)
4 Gas Turbine Press. Ratio(1.5-11.5, η_o=61.45%)
5 MHD Inlet Pressure (100-200bar, η_o=58.64%)
6 Boiler Temperature (1000-2000°F, η_o=62.75%)
7 Boiler Pressure (1000-2000psia, η_o=62.42%)
8 Number of Comp. Stages(1.0-10.0, η_o=67.5]%)
9 Bottom Temp. Difference(100-300°F, η_o=65.10%)

Fig. 10.5 Sensitivity of the Plant Net Overall Efficiency to the Variation of the Main Parameters

8. Number of compression stages

9. Bottom temperature difference.

Results from the sensitivity study are shown in Fig. 10.5.

After performing the sensitivity analysis a study was made of the effect on overall efficiency of varying the reactor coolant outlet temperature from 3000°K to 4000°K for the two systems. Tables 10.2 and 10.3 list the output works for each energy conversion device and plant overall efficiencies for systems without and with regeneration on the helium loop, respectively. The effect of reactor outlet temperature is more substantial on the system with regeneration. The effect of reactor outlet temperature on plant overall efficiency is shown graphically in Fig. 10.6.

For Nuclear MHD Power Plants without regeneration, the major contribution of electric power is due to the steam turbine subsystem (36.03% - 36.36% from 100 % heat produced by the reactor). Due to a significant fraction of the electric power being produced by the steam cycle with a low efficiency (40%), it is desirable to shift the power production toward the top of the cycle to improve the overall efficiency. This can be achieved by reducing the mass flow rate of helium within the inner loop and increasing the pressure ratio of the MHD generator. This system produced overall efficiencies that are 15-20% higher than actual power plants in use and that are 5-10% higher than the expected coal-fired MHD power plant. Due to the relatively low temperatures within the helium loop, this type of power plant could be considered as a first step in a national program of implementation of MHD power plants with a nuclear heat source.

Table 10.2 Plant Net Overall Efficiencies For MHD Inlet Temperature Variation

MHD Inlet Temperature	3000°K		3250°K		3500°K		3750°K		4000°K	
Gas Flow Rate Through the GT.	2.33 kg/sec		2.60 kg/sec		2.88 kg/sec		3.15 kg/sec		3.42 kg/sec	
Q_R	12265.71	100.0%	13563.96	100.0%	14862.21	100.0%	16160.46	100.0%	17458.71	100.0%
W_{MHD}	1777.71	14.49%	2077.87	15.32%	2378.55	16.0%	2679.22	16.58%	2929.90	17.07%
W_{GT}	456.46	3.72%	510.00	3.76%	563.54	3.79%	617.68	3.82%	670.62	3.84%
W_{ST}	4419.73	36.03%	4901.75	36.14%	5383.76	36.22%	5865.78	36.30%	6347.80	36.36%
η_{PLANT}	54.24%		55.22%		56.01%		56.70%		57.27%	

Q_R = REACTOR HEAT RATE

W_{MHD} = MHD NET ELECTRIC POWER : $W_{MHD} = W_{MHD}$ OUTPUT $- 2W_{COMPRESSOR}$

W_{GT} = GAS TURBINE ELECTRIC POWER : $W_{GT} = W_{GT}$ OUTPUT $- W_{COMPRESSOR}$

W_{ST} = STEAM TURBINE ELECTRIC POWER: $W_{ST} = W_{ST}$ OUTPUT $- W_{PUMP}$

$$\eta_{PLANT} = \left(\frac{W_{MHD}}{Q_R} + \frac{W_{GT}}{Q_R} + \frac{W_{ST}}{Q_R}\right) \times 100 = \left(\frac{W_{MHD}}{Q_R}\,100\right) + \left(\frac{W_{GT}}{Q_R}\,100\right) + \left(\frac{W_{ST}}{Q_R}\,100\right) \quad [\%]$$

Table 10.3 Plant Net Overall Efficiencies For MHD Inlet Temperature Variation

MHD Inlet Temperature	3000°K		3250°K		3500°K		3750°K		4000°K	
Q_R	4973.45	100.0%	5138.94	100.00%	5299.94	100.00%	5458.27	100.0%	5693.55	100.0%
W_{MHD}	1689.52	33.97%	1914.65	37.26%	2139.78	40.37%	2139.78	43.44%	2590.04	45.49%
W_{GT}	319.12	6.42%	319.12	6.21%	319.12	6.02%	319.12	5.85%	319.12	5.60%
W_{ST}	1112.20	22.36%	1112.20	21.64%	1112.20	20.99%	1112.20	20.38%	1112.20	19.53%
η_{PLANT}	62.75%		65.11%		67.38%		69.56%		70.62%	

Q_R = REACTOR HEAT RATE

W_{MHD} = MHD NET ELECTRIC POWER: $W_{MHD} = W_{MHD}$ OUTPUT $- W_{COMPRESSOR}$

W_{GT} = GAS TURBINE ELECTRIC POWER: $W_{GT} = W_{GT}$ OUTPUT $- 2 \times W_{COMPRESSOR}$

W_{ST} = STEAM TURBINE ELECTRIC POWER: $W_{ST} = W_{ST}$ OUTPUT $- W_{PUMP}$

$$\eta_{PLANT} = \left(\frac{W_{MHD}}{Q_R} + \frac{W_{GT}}{G_R} + \frac{W_{ST}}{Q_R}\right) \times 100 = \left(\frac{W_{MHD}}{Q_R}\,100\right) + \left(\frac{W_{GT}}{Q_R}\,100\right) + \left(\frac{W_{ST}}{Q_R}\,100\right) \quad [\%]$$

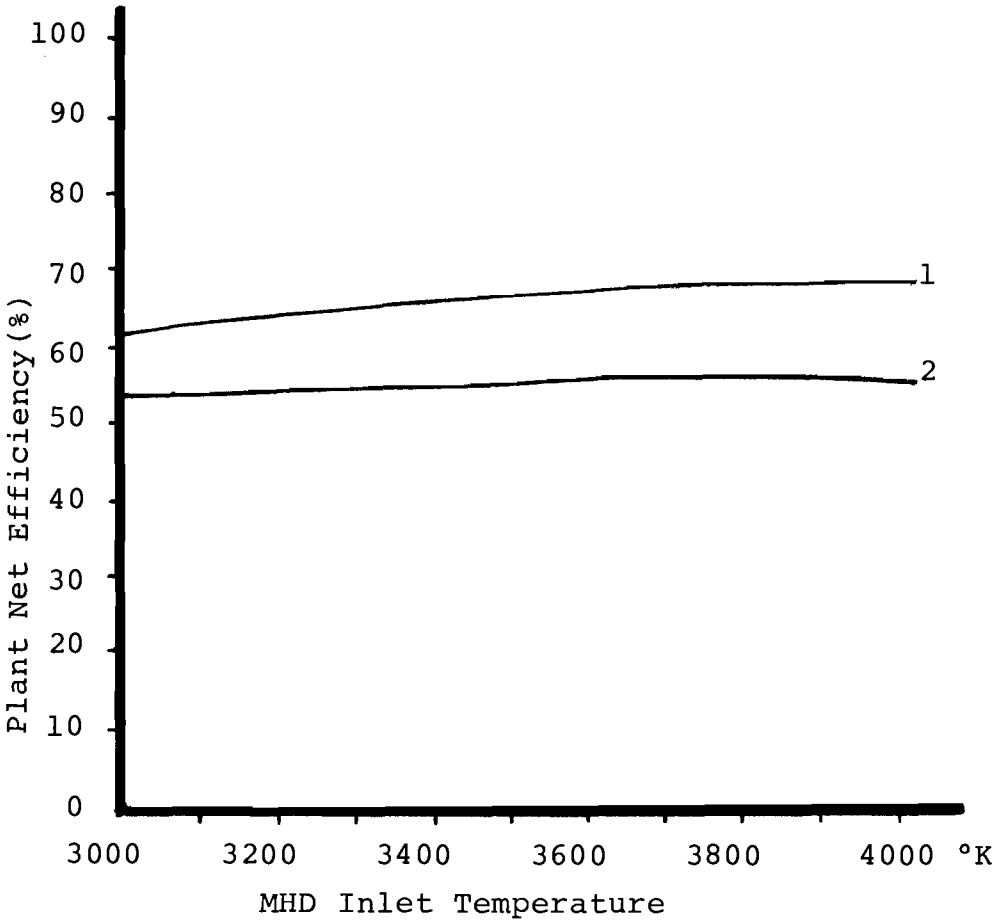

1 Nuclear MHD Power Plant - 1 (with Heat Exchanger)
2 Nuclear MHD Power Plant - 2 (with Mixing Tank)

Fig. 10.6 Plant Net Efficiencies vs MHD Inlet Temperature

For Nuclear MHD Power Plant with regeneration, the major contribution of the electric power is produced in the top of the power cycle by the MHD subsystem (33.97% - 45.49% from 100% heat produced by the reactor). The power production has been shifted toward the top of the ternary cycle with a positive effect on overall efficiency. This system produces overall efficiencies that are 25-35% higher than actual power plants in use and that are 15-20% higher than the expected coal-fired MHD power plants.

REFERENCES FOR CHAPTER 10

1. HOLMAN, R. R. and T. E. LIPPERT, "Liquid-Metal Magnetohydrodynamic System Evaluation," Eleventh Intersociety Energy Conversion Engineers Conference Proceedings, Nevada, Sept. 12-17 (1976).

2. ZAUDER, B., "System Studies for Coal Fired Closed-Cycle MHD for Central Station Power Plant," Eleventh Intersociety Energy Conversion Engineering Conference Proceedings, Nevada, Sept. 12-17 (1976).

3. ROSA, R. J., Magnetohydrodynamic Energy Conversion, McGraw-Hill (1968).

PROGRESS REPORT

NASA GRANT NSG-1288

GAS CORE REACTORS FOR ACTINIDE TRANSMUTATION AND BREEDER APPLICATIONS

J. D. Clement and J. H. Rust

NASA Program Manager, F. Hohl

Prepared for the

National Aeronautics and Space Administration

by the

School of Nuclear Engineering
Georgia Institute of Technology
Atlanta, Georgia 30332

August 31, 1978

PROGRESS REPORT

NASA GRANT NSG-1288

GAS CORE REACTORS FOR ACTINIDE TRANSMUTATION AND BREEDER APPLICATIONS

J. D. Clement and J. H. Rust

NASA Program Manager, F. Hohl

Prepared for the

National Aeronautics and Space Administration

by the

School of Nuclear Engineering
Georgia Institute of Technology
Atlanta, Georgia 30332

August 31, 1978

ACKNOWLEDGEMENTS

This work was supported by NASA Grant NSG-1288, Supplement No. 2. The authors wish to express their appreciation to the program manager, Dr. Frank Hohl, for helpful suggestions during the performance of the research.

The following graduate students, supported by the grant, made significant contributions to the research project: Stanley Chow and Pak Tai Wan.

TABLE OF CONTENTS

LIST OF FIGURES

LIST OF TABLES

I. INTRODUCTION

The Georgia Institute of Technology, under the sponsorship of the National Aeronautics and Space Administration, has performed research studies on gas core nuclear reactors for the past ten years. The objective of this semi-annual report is to put the Georgia Tech work on actinide transmutation in perspective, so a brief survey of literature in this area is included. The report also indicates the nature of the on-going work at Georgia Tech, but does not include results. Complete results will be included in the Final Report, due February 1979.

II. REVIEW OF ACTINIDE TRANSMUTATION STUDIES

Actinide elements are formed from neutron capture reactions of uranium or thorium which always accompanies the fission process. Together with the fission products, they constitute high-level radioactive waste. Satisfactory treatment of these wastes must be developed before nuclear power is to become a major supplier of our future energy needs. The radioactivity and toxicity of one metric ton of LWR-UO_2 spent fuels are shown in Figs. 1 and 2, respectively. See Appendix A for the definition of toxicity. Up to 300 years after irradiation, the fission product component of the wastes dominates the toxicity; but from then onwards, the actinide component is dominant. Most of the actinide toxicity is due to uranium and plutonium. If plutonium is recycled in LWRs or LMFBRs, it does not have to be considered in the waste management strategy. If reprocessing is carried out, uranium will most likely be recycled through the enrichment plant. The nature of the actinide portion of the high-level waste is shown in Table 1. The reprocessing was assumed carried out after ten years of storage, and it was also assumed that 0.5% of the uranium and plutonium remain in the waste after chemical reprocessing.

The ultimate method for disposal of high-level radioactive wastes in the U.S. is still being evolved. For the short-lived component it seems that storage in deep geologic formations of known characteristics (such as salt mines) remains the best method since less than thousand years is required to reduce the activity to an innocuous level. Assurance of tectonic stability for thousands of years with a very high degree of confidence is quite possible in some geologic formations. For

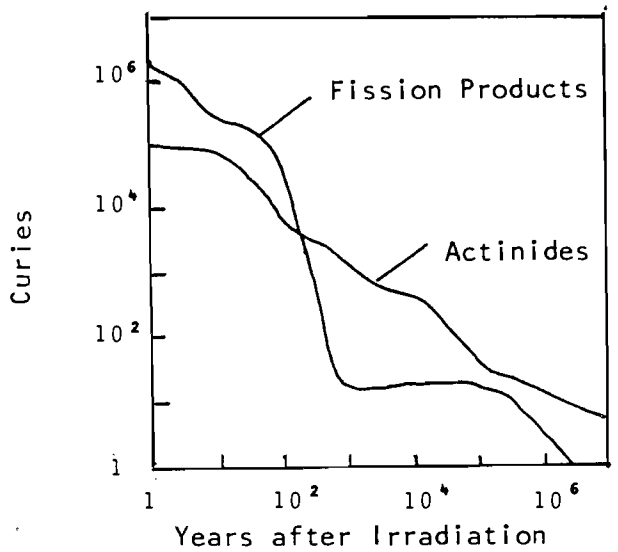

Fig. 1. Radioactivity of 1 MT of LWR UO_2 Spent Fuel (24)

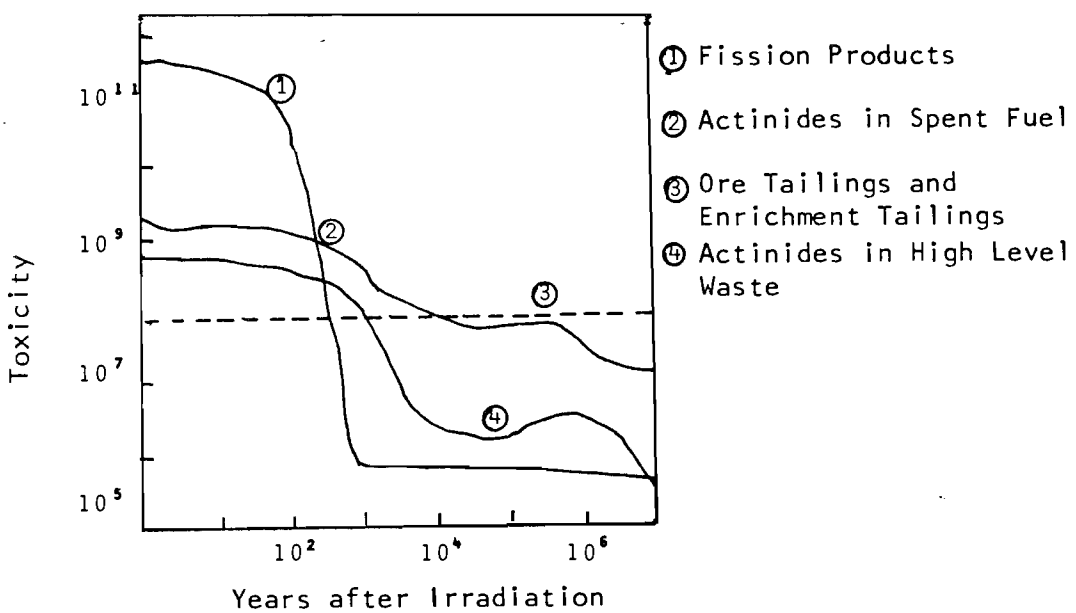

Fig. 2. Toxicity of 1 MT of LWR-UO_2 Spent Fuel (24)

TABLE 1. LWR Waste Concentrations (Separate @ 10 yr. 99.5% Removal of U and Pu; per MT of Fuel) (24)

Isotope	Grams	Curies	Toxicity, M^3 of Water
^{234}U	1.10	-	- - -
^{235}U	39.5	-	- - -
^{236}U	20.7	-	- - -
^{238}U	4730	-	- - -
^{237}Np	532	-	1.25 + 5
^{239}Np	-*	13.6	1.36 + 5
^{234}Pu	0.709	12.0	2.39 + 6
^{239}Pu	23.8	1.46	2.92 + 5
^{240}Pu	10.4	2.30	4.61 + 5
^{241}Pu	3.58	359	1.79 + 6
^{242}Pu	2.07	-	- - -
^{241}Am	456	1560	3.91 + 8
^{242m}Am	1.12	10.9	2.73 + 6
^{242}Am	-	10.9	1.09 + 5
^{243}Am	70.9	13.6	3.41 + 6
^{242}Cm	0.00271	3.31	6.62 + 5
^{243}Cm	0.0720	8.98	4.49 + 5
^{244}Cm	10.7	864	1.23 + 8
^{245}Cm	0.928	-	4.1 + 4
^{246}Cm	0.099	-	- - -
TOTAL	5910	2870	5.27 + 8

*A blank space denotes that contribution of the particular isotope is negligible.

the treatment of the long-lived component, much uncertainity exists because effects of geologic, climatic, and other natural phenomena cannot be reliably extrapolated in the time span of thousands to millions of years. This study deals with one alternative, the neutron-induced transmutation of actinide wastes.

A technical hurdle that must be overcome before actinide transmutation can become a reality is their chemical extraction at high efficiencies from the bulk waste. Numerous studies have been performed on the chemical removal of actinides from high-level wastes (2-5). Studies to date have not been able to determine the feasibility (or infeasibility) of chemical processes for the satisfactory removal of actinides from actinide wastes. The Oak Ridge National Laboratory is currently conducting an extensive study in this area (5).

Many research organizations have performed studies on transmutation using different reactor systems. A chronological list of (1) the principal investigator(s), (2) the investigator's affiliation(s), and (3) a brief description of the transmutation studies conducted is given in Table 2. The list has been restricted mainly to studies with fission and fusion reactor systems. Those interested in other systems, such as accelerators or nuclear explosive transmutation, are referred to Ref. 1 which gives a discussion of these transmutation devices and an extensive list of references.

TABLE 2. Summary of Past Actinide Transmutation Studies

Investigator(s) (Organization)	Description	Reference (Date)
M. Steinberg G. Wotzak B. Manowitz (BNL)	Physics and economics of transmuting Kr-85, Sr-90, and Cs-137	6 (1964)
M. Steinberg M. V. Gregory (BNL)	Transmutation of fission product in a spallation reactor	7 (1967)
H. C. Claiborne (ORNL)	Discussion of fission product transmutation; investigation of actinide recycling in a PWR	8 (1972)
W. C. Wolkenhauer (PNL)	Physics of transmuting Sr-90 and Cs-137 in CTR	9 (1972)
W. C. Wolkenhauer B. R. Leonard, Jr. B. E. Gore (PNL)	Evaluation of potential of a CTR for transmuting fission products and actinides	10 (1973)
B. E. Gore B. R. Leonard, Jr. (PNL)	Physics of transmuting massive amounts Cs-137 in a CTR blanket	11 (1974)
K. J. Schneider A. M. Platt (PNL)	Comprehensive overview of waste management alternatives including actinide transmutation	1 (1974)
R. R. Paternoster (U. of Florida)	Calculation of actinide transmutation with a UF_6 Gas Core reactor	12 (1974)
R. J. Breen (WARD)	Actinide transmutation rates in oxide and carbide fueled LMFBR	13 (1975)
S. Raman (ORNL)	Review of actinide transmutation in many devices	14 (1975)
S. Raman C. W. Nestor, Jr. J. W. T. Dabbs (ORNL)	Actinide transmutation in a U^{233}-Th^{232} reactor	15 (1975)
A. G. Croff (ORNL)	Review of actinide transmutation studies	16 (1975)
A. G. Croff (ORNL)	Parametric survey of actinide transmutation	17 (1976)
S. L. Beaman E. A. Aitken (GE)	Physics of recycling wastes from 3 BWRs and 1 LMFBR in an LMFBR	18 (1976)

TABLE 2. Summary of Past Actinide Transmutation Studies (cont'd)

J. J. Prabulos (CE)	Calculation of actinide transmutation in a 1500 MWe carbide fueled LMFBR	19 (1976)
W. Bocola L. Frittell G. Grossi A. Moccia L. Tondinelli (CNEN-CSN, Italy)	Calculation of sensitivities of actinide buildup to cross section changes comparison of risks from nuclear transmutation and geologic disposal	20 (1976)
T. A. Parish E. L. Draper, Jr. (U. of Texas)	Engineering and physics design of a CTR for long-lived fission product transmutation	21 (1976)
R. H. Clarke G. A. Harte (GEGB,UK)	Actinide production and transmutation in MAGNOX and sodium cooled fast reactors	22 (1976)
R. P. Rose (EPRI)	Engineering and physics design of a tokamak fusion actinide transmuter	23 (1976)
U. P. Jenquin B. R. Leonard, Jr. (PNL)	Physics of transmuting actinides in CTR blankets	24 (1976)
D. H. Berwald (U. of Michigan)	Engineering and physics design of a laser driven fusion actinide transmuter	25 (1977)
T. H. Pigford J. Choi (U. C. Berkeley)	Calculation of approach-to-equilibrium times for PWR and LMFBR as actinide transmuter	26 (1978)
J. D. Clement J. H. Rust (Ga. Tech)	Analysis of gas core actinide transmutation reactor	27 (1977)
G. Oliva G. Palmiotti M. Salvatores L. Tondinelli (Italy)	Comparison of actinide transmutation in LWRs and LMFBRs	28 (1978)
J. D. Clement J. H. Rust (Ga. Tech)	Design of plasma core reactors for actinide transmutation	29 (1978)

The most important parameter affecting actinide transmutation rates is the neutron flux in the actinide region. All studies strive to maintain as high a flux as possible. Studies using commercial power reactors as transmuters are hampered by low fluxes because the flux level is already determined by power production considerations. Typical LWR thermal fluxes are on the order of 10^{13} to 10^{14} n/cm^2-sec. Typical LMFBR fast fluxes are on the order of 10^{15} to 10^{16} n/cm^2-sec. For fusion reactors, Rose (23) indicated that a high neutron wall loading (about 10 MW/m^2) will be required for effective transmutation rates. However, tokamak fusion reactors probably cannot achieve such high wall loadings due to high plasma beta stability considerations (23) and laser driven fusion reactors will be required.

The energy spectrum of neutrons irradiating the actinides is a significant factor. Many authors (8,14,18) have stated that fast reactors are superior to thermal reactors because the fission-to-capture ratio is generally higher for fast reactor neutron spectra. Rose found that thermal spectrum actinide burner concepts will have difficulty achieving a high neutron multiplication constant in the blanket region, whereas fast burners can attain k_{eff} as high as 0.85-0.95. However, on the basis of reaction rates, a study by Oliva et al. (28) showed that LWRs are better than LMFBRs. This is because the fast neutron fluxes of present day LMFBRs are not high enough to compensate for the drop in neutron cross sections at fast energies so that their product, i.e. the reaction rate, is less than that of the LWR case. One clear advantage that fast reactors have over thermal reactors is that their criticality is less sensitive to the introduction of foreign materials in the core. This means that for the

same reactivity penalty, larger quantities of actinides can be inserted in fast reactors. For fusion reactors the mean energy of neutrons emerging from fusion reactions is very high (14 MeV for the deuterium-tritium reaction). Theoretically a greater number of neutron reactions, e.g. (n,2n), (n,3n), (n,p), is available as transmutation channels. In practice the cross sections of these high energy reactions are small and they are found to contribute insignificantly to overall reaction rates. In fact, many fusion transmutation studies utilize well-moderated actinide blankets to maximize the transmutation reaction rates.

Another major factor affecting the overall effectiveness of actinide transmutation is the logistics of the transmutation strategy. Some studies make the simplifying assumption that the actinides are loaded into the transmuter once and for all and they are irradiated continuously for long periods of time (typically 30 years) with no reprocessing. Under such a strategy, the actinide inventory in the transmuter will decrease almost exponentially. Other studies utilize the concept of actinide recycling. The irradiated actinides are discharged for reprocessing after one cycle of irradiation. At reprocessing, a fresh batch of actinides are added to the unfissioned actinides. Together, they are extracted, made into forms suitable for irradiation and inserted back into the transmuter. After many cycles, an equilibrium will be reached. From then onwards the quantity of actinides removed in one cycle is equal to the quantity of fresh actinides added during reprocessing. For actinide recycling schemes, the actinide extraction efficiency is of vital importance. Since each time the actinides pass through the reprocessing step, a fraction will be lost to waste storage together with the fission products, these actinides will not be

transmuted and will then contribute to the long-term hazard of the storage wastes. If all the actinides are kept within the transmutation system, they will eventually be beneficially transmuted. A subtle but important point is whether converted uranium and plutonium are removed during reprocessing. During reprocessing, the fission products are removed. In the studies of Claiborne (8) and Beaman (18), the converted uranium and plutonium are also removed. The nuclides removed are mostly Pu^{238}, formed from the neutron capture of Np^{237} and the decay of americium and curium isotopes. For such a transmutation strategy, there will be two main pathways for the removal of actinides. One is via direct fission during irradiation, and the other is via reprocessing as converted uranium and plutonium. Claiborne's data (8) showed that in one equilibrium cycle, about 35% of the in-core actinides are removed: 12% is fissioned directly, 24% is removed in reprocessing. The extracted Pu^{238} can be used as a breeding material for Pu^{239}. From the point of view of ultimate waste disposal, the removal of Pu^{238} constitutes a postponement since Pu^{238} is a highly hazardous nuclide with toxic decay daughters. Thus, a proper disposal strategy must be developed for the extracted Pu^{238}.

Complications may arise due to the changing characteristics of the actinide region. As the actinides are irradiated, they are either fissioned or converted to higher actinides by neutron capture. Hence, the composition of the actinide mix is gradually changing with time. Initially, it consists mostly of Np^{237} , Am^{241}, and Am^{243}. Upon irradiation, they are converted to nuclides with large fission cross sections. This may cause problems because the neutron flux is usually set at the maximum

permissible value, consistent with fuel heat transfer, and thermal-hydraulic constraints. As the actinide mix becomes more fissile, the neutron flux will have to be lowered to maintain a constant volumetric heat generation rate. Upon further irradiation, the fission product poisons become dominant and the flux may have to be re-adjusted again.

The validity of actinide transmutation calculations are very dependent upon the accuracy of the actinide neutron cross sections. A large number of reactor concepts, including LWRs (8), LMFBRs (13,18,19, 22,28), CTRs (9-11, 23-25), have been studied as transmutation candidates. Therefore, the range over which the capture and fission cross sections of the actinides need to be known extends from below thermal to about 18 MeV neutron energy (30-35). There are 16 transactinium elements with 200 isotopes known to date. For many of these actinides, experimental cross section data may not exist. This is due to short half lives, an inability to obtain samples of sufficient isotopic purity and the difficulty of obtaining higher energy (about 14 MeV monoenergetic neutron sources for differential cross section measurement. Consequently, for many actinides the necessary data has been obtained by application of nuclear systematics and model calculations (36). Generally, the main isotopes of Th, Pa, U, Np, Pu have been evaluated extensively. There is an urgent need for the evaluation of americium and curium isotopic cross sections, and to a lesser extent, those of berkelium and californium. For the higher actinide isotopes, they usually are very short lived and exist in such minute quantities that they are insignificant for most applications. The thermal cross sections of actinides have been found to yield computational results in agreement with experimental data from the

transplutonium production programs (37-41). As one moves away from the thermal region into the fast energy region, greater uncertainty persists.

There is a need for the study of fission reactors specifically designed to burn actinides. As actinide transmuters, commercial power reactors have two shortcomings. The flux level is limited by power production considerations. The number of reactors serviced by one power reactor is small; consequently, many power reactors would have to be used as transmuters. Fusion reactors do produce an abundant supply of high-energy neutrons. However, considerable amount of basic research and developmental work will be required before fusion reactors can be expected to be commercially available. Hence, there is motivation to use near-term technology to design fission reactors especially suited for the burnup of actinide elements. The present study is concerned about the design of a uranium hexafluoride gas core reactor for such an application.

III. SUMMARY OF PAST GEORGIA TECH WORK ON GAS CORE REACTORS

The Georgia Institute of Technology has participated in the research and development efforts of gas core reactors from the 1960s. Table 3 below summarizes the Georgia Tech work to date.

TABLE 3. Summary of Georgia Tech Gas Core Studies

Investigator(s)	Description	Reference (Date)
A. S. Shenoy J. R. Williams J. D. Clement	The attenuation of radiant energy in hot seeded hydrogen	52,53 (1968,1969)
W. L. Partain J. R. Williams J. D. Clement	The attenuation of radiant energy in hot seeded hydrogen at high pressure	54,55 (1969,1970)
J. R. Williams J. D. Clement	Review of gas core technology	47 (1970)
K. R. Turner J. D. Clement	A dynamic model of coaxial flow gaseous core nuclear rocket system	56,57 (1971)
R. A. Benns	Generation of induction heated seeded hydrogen plasmas at one atmosphere	58 (1972)
J. R. Williams J. D. Clement	Exploratory of several advanced nuclear - MHD power plant systems	48 (1973)
S. D. Thompson	Theoretical and experimental study of radial temperature profiles in an RF plasma over a wide range of applied magnetic flux intensities	59 (1974)
J. D. Clement J. R. Rust	Analysis of a UF_6 breeder power plants	49 (1976)
J. D. Clement J. R. Rust	Analysis of the gas core actinide transmutation reactor (GCATR)	50 (1977)
J. D. Clement J. R. Rust	Gas core reactors for actinide transmutation and breeder applications	51 (1978)

Early Georgia Tech work was concerned mainly with the heat transfer problems of the hydrogen propellant gas. Shenoy et al. (52,53) measured the mass attenuation coefficient of hydrogen, seeded with submicron-sized particles of carbon, silicon and tungsten over the wavelength range of 1200Å to 6000Å for temperatures up to 3500°F. It was found that the mass absorption coefficient was essentially independent of wavelength over the range of wavelengths and temperatures investigated. The experimentally measured values were not in direct agreement with theoretical values calculated using Mie's theory. The discrepancy was attributed to the highly irregular shape and different sizes of the seed particles. Since the pressure inside the gaseous core rocket engine would probably be in the range of 100-500 atmospheres, Partain et al. (54,55) extended the previous work to high pressures. The extinction parameter of a tungsten-hydrogen aerosol was measured as a function of wavelength from 2500Å to 5800Å at pressures up to 115 atmospheres and temperatures to 2500°K. The measured extinction parameter at room temperature for all pressures to 115 atmospheres was found to compare well with the theoretical value calculated using the Mie theory. The extinction parameter was observed to increase with pressure at temperatures above about 1000°K. Several physical processes that might be expected to enhance proton extinction beyond that predicted by the Mie theory were discussed. In order to study the behavior of the extinction parameter at higher temperatures, a new heating technique had to be used. Benns (58) designed and constructed a radio frequency induction heater to produce tungsten seeded hydrogen plasmas, corresponding to an actual plasma temperature of about 8000°K. The opacity of the plasma was measured with a helium-neon laser.

His measurements indicated that the tungsten-hydrogen opacity window was not as transparent as had been expected. Hence, the heat transfer in the propellant gas may not suffer much due to the seed-hydrogen opacity window. Thompson (59) performed an analytical and experimental study of the radial temperature profiles in a RF plasma over magnetic field intensities ranging from 20 amp turns/cm to 80 amp turns/cm. A one-dimensional numerical treatment of the energy balance equation, Maxwell's equations, and Ohm's law was used. It was found that the average measured temperature in the plasma compared well with the numerical treatment, though the experimental profile showed less of an off center temperature peak than predicted by theory.

Turner et al. (56,57) modeled the neutronic dynamic behavior of a coaxial flow gas core reactor. Six reactivity feedback mechanisms were involved--fuel mass, fuel temperature, moderator temperature, buffer gas temperature and density, and fuel cloud radius. The shape of the fuel cloud was assumed to remain spherical but was allowed to alter its radius. Results indicated that the fuel volume was the dominant reactivity feedback mechanism. Numerical results showed that the idealized coaxial flow reactor could be controlled by conventional means.

Williams et al. (48) analyzed several gas core nuclear-MHD power plant systems. Most energy-conversion devices, such as turbines and thermoelectric elements, cannot operate with source temperatures above ~ 2500°F. However, with a MHD generator, power is extracted from the volume of a fluid moving in a duct where the fluid can be much hotter than the walls of the duct. Hence, by combining an MHD generator with a plasma core reactor, the top temperature limit of the thermodynamic cycle is raised considerably. Three types of closed cycle nuclear MHD power

plant systems were analyzed to determine the operating characteristics, critical parameters, and performance of these power plant systems. Overall thermal efficiencies as high as 80% were projected using an MHD turbine-compressor cycle with steam bottoming, and slightly lower efficiencies were projected for a simple MHD.

Despite the potential benefits associated with a plasma core reactor, this concept requires substantial funding for basic research and developmental work. Subsequent research efforts on gas core reactors was shifted to UF_6 gas core reactors. In fact, several UF_6 reactors have been constructed and successfully operated (45,60).

Clement and Rust (49) performed a design study of a $^{233}UF_6$ gas core breeder reactor. Using present technology the UF_6 temperature was limited to less than $1660^{o}R$ ($922^{o}K$). A Rankine cycle was used to extract the power. With reheating, a maximum plant efficiency of 41.4% was obtained. The reactor consisted of $^{233}UF_6$ gas surrounded by a molten salt (Li^7F, BeF_2, ThF_6) blanket. The core diameter was approximately one meter. The blanket thickness ranged from 60 to 130 cm. A breeding ratio of approximately 1.18 and a critical mass about 379 kg were found.

It was recognized early (42-44) that due to the low density of the fuel, gas core reactors are suitable as irradiators since high flux levels can be maintained with a low critical mass. These neutrons can be used to transmute hazardous actinide wastes. Clement and Rust (50,51) performed a design study on gas core actinide transmutation reactors. The heat transfer property of UF_6 was greatly improved with the addition of helium in the circulating fuel. This led to much more compact heat exchangers. A 577 MWt UF_6 actinide transmutation reactor power plant was designed to

operate with 39.3% efficiency and 102 kg of U^{233} in the core and heat exchangers for beginning-of-life conditions. Even though the UF_6 reactor is capable of maintaining high neutron fluxes, the build-up of fissile isotopes in the actinide region posed severe heat transfer problems. One solution was to decrease the flux with time; however, the effectiveness of the transmuter was substantially reduced.

IV. CONCLUDING GEORGIA TECH WORK

Future research efforts will be directed at the completion of the design of a UF_6 gas core actinide transmutation reactor. Four tasks will be involved:

(1) Task I consists of up-dating the actinide cross sections. Reference (61) gives a list of the transactinium nuclides in the main evaluated neutron data files. These cross section data will be processed into a consistent format ready for input into neutron transport calculations.

(2) Task II consists of the design of the UF_6 irradiator. Neutronics, heat transfer, fluid mechanics, and material considerations will enter into the design of a realistic UF_6 irradiator. One candidate is the externally moderated concept suggested by Safonov (44). A central UF_6 gas core is surrounded by a moderator, with the actinide region located outside the moderator. Safonov calculated that for such a design about one neutron per fission leak from the outer reflector surface. These neutrons are ~ 99% thermal and are clearly available for irradiation without decreasing reactor criticality. Another candidate is an internally moderated UF_6 reactor. One design (57) consists of a UF_6-He mixture flowing through a beryllium matrix. This heterogeneous design may have smaller critical masses, and lower power peaking factors.

(3) Task III consists of the design of the actinide region. One design criterion is for a design using present technology. Of major importance is the question of whether the converted plutonium should be removed during reprocessing. If removal of Pu is carried out, a fuel

management scheme similar to that used in CANDU reactors can be employed. The fuel pellets are moved slowly through the core. The ejected fuel pellets are sent to reprocessing to remove the uranium and plutonium. If it is decided that the converted plutonium is to be fissioned in situ, severe heat transfer problems may arise. One solution is to mix a dummy element (e.g. Zr) in the actinide rods so as to maintain an acceptable volumetric heat generation rate.

(4) Task IV consists of integration of the preceding tasks. Once the design for the UF_6 irradiator and the actinide blanket region is reached, detailed neutronic calculations can be carried out following the growth and decay of the actinide nuclides in the UF_6 transmuter. Close coupling of the actinide region and core region is expected. The effectiveness of the transmuter is evaluated by analyzing the short term hazard increase and the long term hazard decrease.

REFERENCES

1. Schneider, K. J. and Platt, A. M., "High-Level Radioactive Waste Management Alternatives," BNWL-1900, Battelle Pacific Northwest Laboratories (May, 1974).

2. Bond, W. D., Clairborne, H. C., and Leuze, R. E., "Methods for Removal of Actinides from High-Level Wastes," Nuclear Technology, 24, 362 (December, 1974).

3. Bond, W. D., and Leuze, R. E., "Feasibility Studies of the Partitioning of Commercial High-Level Wastes Generated in Spent Fuel Reprocessing: Annual Progress Report for FY-1974," ORNL-5012 (January, 1975).

4. Bond, W. D., and Leuze, R. E., "Removal of Actinides from High Level Wastes Generated in the Reprocessing of Commercial Fuels," Transplutonium Elements, 423 (1976).

5. Blomeke, J. O., and Tedder, D. W., "Actinide Partitioning and Transmutation Program Progress Report for Period October 1, 1976 to March 31, 1977," ORNL-TM-5888 (June, 1977).

6. Steinberg, M., Wotzak, G., and Manowitz, B., "Neutron Burning of Long-Lived Fission Products for Waste Disposal," BNL-8558 (September, 1964).

7. Gregory, M. V., and Steinberg, M., "A Nuclear Transformation System for Disposal of Long-Lived Fission-Product Waste in an Expanding Nuclear Power Economy," BNL-11915 (November, 1967).

8. Claiborne, H. C., "Neutron-Induced Transmutation of High-Level Radioactive Waste," ORNL-TM-3984 (December, 1972).

9. Wolkenhauer, W. C., "The Controlled Thermonuclear Reactor as a Fission Product Burner," BNWL-SA-4232 (1972).

10. Wolkenhauer, W. C., Gore, B. R., Leonard, B. R., Jr., "Transmutation of High-Level Radioactive Waste With a Controlled Thermonuclear Reactor," BNWL-1772 (1973).

11. Gore, B. E., Leonard, B. R., Jr., Nuclear Science Engineering, 53, 319-323 (1974).

12. Paternoster, R. R., "Radioactive Waste Disposal by Nuclear Transmutation in a UF_6 Gaseous-Core Reactor," M.S. Thesis, U. of Florida (1974).

13. Breen, R. J., "Elimination of Actinides with LMFBR Recycle," Trans. Am. Nucl. Soc., 21, 262 (June, 1975).

14. Raman, S., "Some Activities in the United States Concerning the Physics Aspects of Actinide Waste Recycling," Proc. IAEA Advisory Group Mtg. Transactinium Isotope Nuclear Data, CONF-751104-4 (1975).

15. Croff, A. G., "Actinide Transmutation Studies: A Review," Trans. Am. Nucl. Soc., 23, 545 (June, 1976).

16. Croff, A. G., "Parametric Studies Concerning Actinide Transmutation in Power Reactors," Trans. Am. Nucl. Soc., 22, 345 (1975).

17. Raman, S., Nestor, C. W., Jr., Dabbs, J. W., T., "The U^{233}-Th^{232} Reactor as a Burner for Actinide Wastes," CONF-750303-36 (1975).

18. Beaman, S. L., Aitken, E. A., "Feasibility Studies of Actinide Recycling in LMFBRs as a Waste Management Alternative," CONF-760622-48 (1976).

19. Prabulos, J. J., "Actinide Destruction in a 1500 MWe Carbide Fueled LMFBR," Trans. Am. Nucl. Soc., 23, 548-549 (June, 1976).

20. Bocola, W., Frittell, L., Gera, F., Grossi, G., Moccia, A., Tondinelli, L., "Considerations on Nuclear Transmutation for Elimination of Actinides," IAEA-SM-207/86 (1976).

21. Parish, T. A., Draper, E. L., Jr., "Determination of Procedures for Transmutation of Fission Product Wastes by Fusion Neutrons," UTNRL-FU101, U. of Texas (1976).

22. Harte, G. A., Clarke, R. H., "Investigation into the Use of a Fast Breeder Reactor to Incinerate Actinide Waste from the U.K. Nuclear Power Programme," CEGB-RD/B/N-3903 (1976).

23. Rose, R. P., "Fusion-Driven Actinide Burner Design Study," EPRI-ER-451 (1976).

24. Jenquin, U. P., Leonard, B. R., Jr., "Evaluations of Fusion-Fission (Hybrid) Concepts: Transmutation of High-Level Actinide Waste in Hybrids," Part B, EPRI-ER-469 (1976).

25. Berwald, D. H., "Preliminary Design and Neutronic Analysis of a Laser, Fusion Driven Actinide Waste Burning Hybrid Reactor," Ph.D. Thesis, Dept. of Nuclear Engineering, U. of Michigan (1977).

26. Pigford, T. H., Choi, J., "Actinide Transmutation in Fission Reactors," Trans. Am. Nucl. Soc., 27, 450-451 (1977).

27. Clement, J. D.,, Rust, J. H., "Analysis of the Gas Core Actinide Transmutation Reactor (GCATR)," NASA Grant NSG-1288, Georgia Institute of Technology (1977).

28. Oliva, G., Palmiotti, G., Salvatores, M., Tondinelli, L., "Elimination of Transuranium Elements by Burnup in a Power Fast Breeder Reactor," Nuclear Technology, 37 (March, 1978).

29. Clement, J. D., Rust, J. H., "Gas Core Reactors for Actinide Transmutation and Breeder Applications," NASA Grant NSG-1288, Georgia Institute of Technology (1978).

30. Mann, F. M., Schenter, R. E., "Actinide Cross-Section Calculations and Evaluations," Trans. Am. Nucl. Soc., 23, 546-547 (1976).

31. Morrison, G. W., Burns, T. J., Weisbin, C. R., "Actinide Transmutation: Cross Sections Methods, and Reactor Sensitivity Analysis," Trans. Am. Nucl. Soc., Vol. 23, 552 (1976).

32. Raman, S., "General Survey of Applications which Require Actinide Nuclear Data," Proc. IAEA Advisory Group Mtg. Transactinium Isotope Nuclear Data, CONF-751104-4, Review Paper A1 (1975).

33. Kusters, H., Lalovic, M., "Review of Transactinium Isotope Build-Up and Decay in Reactor Fuel and Related Sensitivities to Cross-Section Changes and Results and Main Conclusions of the IAEA-Advisory Group Meeting on Transactinium Nuclear Data Held at Karisruhe, November, 1975," KFK-2283 (1976).

34. Yiftah, S., Gur, Y., Caner, M., "Status of Transactinium Isotope Evaluated Neutron Data in the Energy Range 10-3 eV to 15 MeV," IAEA-186, 165-194 (1976).

35. Dabbs, J. W. T., "The Nuclear Fuel Cycle and Actinide Wastes: Cross Section Needs and Recent Measurements," ORNL/TM-5530 (1976).

36. Mann, F. M., Schenter, R. E., "Actinide Cross Section Calculations and Evaluations," HEDL-SA-814 (1976).

37. Graves, W. E., Benjamin, R. W., "Predicting Production Rates of Heavy Actinides," CONF-720901, 97-107 (1972).

38. Hennelly, E. J., "The Heavy Actinide Cross Section Story," CONF-710301, Vol. 2, 494-501.

39. Benjamin, R. W., McCrosson, F. J., Gorrell, T. C., Vandervelde, V. D., "A Consistent Set of Heavy Actinide Multigroup Cross Sections," DP-1394 (1975).

40. Benjamin, R. W., "Status of Measured Neutron Cross Sections of Transactinium Isotopes for Thermal Reactors," DP-MS-75-87 (1975).

41 Hennelly, E. J., "Nuclear Data for Actinide Recycle," Natl. Bur. Stands. Spec. Publ. (CONF-750303-P1) (October, 1975).

42. Bell, G. I., "Calculations of the Critical Mass of UF_6 as a Gaseous Core with Reflectors of D_2O, Be and C," Los Alamos Report LA-1874 (February, 1955).

43. Safonov, G., "The Criticality and some Potentialities of Cavity Reactors," The RAND Corporation, Research Memorandum RM-1835 (July, 1955).

44. Safonov, G., "Externally Moderated Reactors," Proc. Intern. Conf. Peaceful Uses Atomic Energy, Geneva, Vol. 12, 705 (1958).

45. Kikoin, I. K., Dmitrievsky, V. A., Glazkov, Y. Y., Grigoriev, I. S., Bubovsky, B. G., Kersnovsky, S. V., "Experimental Reactor with Gaseous Fissionable Substance (UF_6)," Proc. 2nd Int. Conf. Peaceful Uses of Atomic Energy, Geneva (1958).

46. Dmitrievski, V. A., Voinov, E. M., Tetel'baum, S. D., "Use of Uranium Hexafluoride in Nuclear Power Plants," Atomnaya Energiya, 29, No. 4, 251-255 (October, 1970).

47. Clement, J. D., and Williams, J. R., "Gas-Core Reactor Technology," Reactor Technology, 13, No. 3, 226-251 (1970).

48. Williams, J. R., and Clement, J. D., "Exploratory Study of Several Advanced Nuclear-MHD Power Plant Systems," NASA Grant NGR-11-002-145 (March, 1973).

49. Clement, J. D., and Rust, J. H., "Analysis of a UF_6 Breeder Reactor Power Plants," NASA Grant NSG-1168 (February, 1976).

50. Clement, J. D., and Rust, J. H., "Analysis of the Gas Core Actinide Transmutation Reactor," NASA Grant NSG-1288 (February, 1977).

51. Clement, J. D., and Rust, J. H., "Gas Core Reactors for Actinide Transmutation and Breeder Applications," NASA Grant NSG-1288 (April, 1978).

52. Shenoy, A. S., Williams, J. R., Clement, J. D., "The Attenuation of Radiant Energy in Hot Seeded Hydrogen—An Experimental Study Related to the Gaseous Core Nuclear Rocket," NASA Grant NGR-11-002-068, Semi-annual report (1968).

53. Shenoy, A. S., "The Attenuation of Radiant Energy in Hot Seeded Hydrogen," Ph.D. Thesis, Dept. of Nuclear Engineering, Georgia Institute of Technology (1969).

54. Williams, J. R., Clement, J. D., and Partain, W. L., "The Attenuation of Radiant Energy in Hot Seeded Hydrogen at High Pressure—An Experimental Study Related to the Gaseous Core Nuclear Rocket," NASA Grant NGR-11-002-068 Final Report (1970).

55. Partain, W. L., "Interactions of Radiant Energy with Small Particles in Hot, High Pressure Gases," Ph.D. Thesis, Dept. of Nuclear Engineering, Georgia Institute of Technology (1970).

56. Turner, K. H., "A Dynamic Model of Coaxial Flow Gaseous Core Nuclear Rocket System," Ph.D. Thesis, Dept. of Nuclear Engineering, Georgia Institue of Technology (1971).

57. Turner, K. H., and Clement, J. D., "A Model of the Dynamic Behavior of the Coaxial-Flow Gaseous-Core Nuclear Reactor," Nuclear Technology, 20, 5-15 (October, 1973).

58. Benns, R. A., "Generation of Induction Heated, Seeded Hydrogen Plasmas at One Atmosphere Pressure," Ph.D. Thesis, Department of Nuclear Engineering, Georgia Institue of Technology (1972).

59. Thompson, S. D., "Radial Temperature Profiles in a RF Plasma Over a Wide Range of Magnetic Flux Intensities; Theory and Experiment," Ph.D. Thesis, Department of Nuclear Engineering, Georgia Institute of Technology (1974).

60. Lofthouse, J. H., and Kunze, J. F., "Spherical Gas Core Reactor Critical Experiment," NASA CR-72781 (February, 1971).

61. "The Transactinides in the Main Evaluated Neutron Data Files," IAEA-186, 195-200, contributed paper from the NEA Neutron Data Compilation Centre (February, 1975).

APPENDIX A

Definitions of Hazard Measure, Hazard Index, and Hazard Criterion

A measure of the toxicity that radioactive waste represents is expressed as the quantity of air or water that would be required to dilute the waste to a level considered acceptable for inhalation or ingestion. This level is set by the U.S. Government's Radioactive Concentration Guide (1), and is known as the "RCG" level. The hazard measure (HM) of radioisotope i is given by

$$HM_i = \frac{\lambda_i N_i}{(3.7 \times 10^{10})(RCG_i)}$$

where HM_i (cubic meter of water or air) is the hazard measure of radioisotope i, $\lambda_i N_i$ (disintegrations/sec) is the decay activity of radioisotope i, and RCG_i (Ci/m^3 water or air) is the recommended concentration value for radioisotope i for unrestricted use.

The hazard index (HI) of a body of waste is the hazard measure of the body per unit volume. For example, pitchblende has an ingestion hazard index of 10^8 m^3 of water/m^3 pitchblende (2). Pitchblende is the most radioactive mineral with about 70% uranium content. High grade uranium ore (0.2% U) has an ingestion hazard index of about 10^5 m^3 of water/m^3 ore (2).

The hazard criterion (HC) is the ratio of the hazard measure due to a volume of waste to the hazard measure due to an equal volume of naturally radioactive substance. Typically, the latter is chosen to be pitchblende. Therefore,

$$HC = \frac{HI}{10^8} \times 100\%$$

where HC(%) is the waste hazard criterion, HI(m^3 of water or air/m^3 of waste) is the hazard index of the waste body.

REFERENCES

1. Code of Federal Regulations, Title 10, Part 20, Col. 2.

2. Claiborne, H. C., "Effect of Actinide Removal on the Long-Term Hazard of High-Level Waste," ORNL-TM-4724 (January, 1975).